Boundary layer flashback prevention by active control

Combining process and control engineering knowledge

T.H.M. van der Laan

Master of Science Thesis

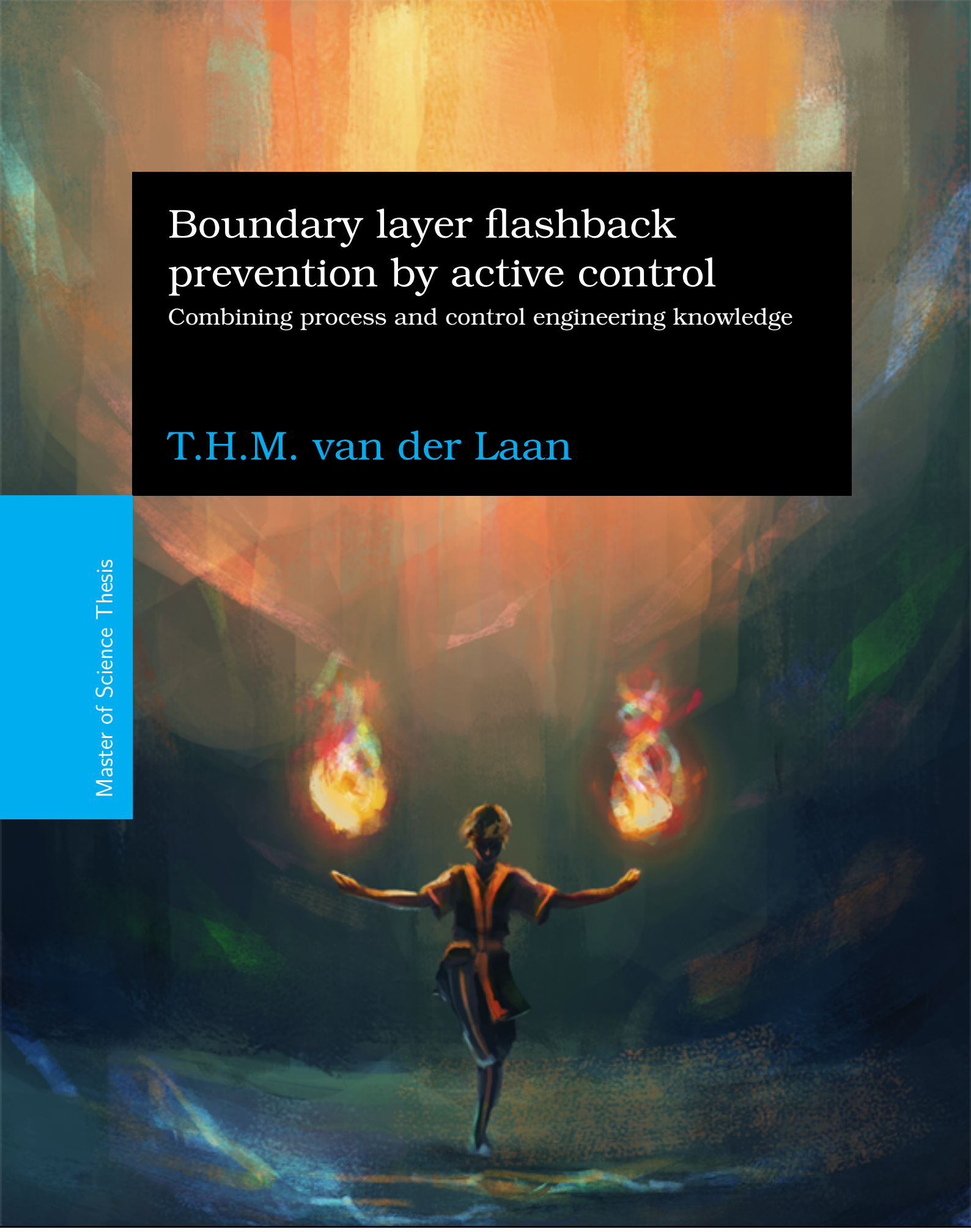

TU Delft Delft University of Technology

Process & Energy Delft||Delft Center for Systems and Control

Cover art by Ang Hui Qing

Boundary layer flashback prevention by active control

Combining process and control engineering knowledge

Master of Science Thesis

by

T.H.M. van der Laan

For the double degree of master of science in:
Mechanical Engineering
&
Systems and Control
at Delft University of Technology

August 11, 2022

Student number:	4496663	
Thesis duration:	December, 2020 - Augustus, 2022	
Mechanical engineering		
MSc track:	Process and Energy	
Thesis committee:	Prof. dr. ir. S.A. Klein	, TU Delft, EPT, supervisor, chair
	Dr. ir. M.J. Tummers	, TU Delft, EPT, external
System and Control		
Thesis committee:	Dr. R.M.G. Ferrari	, TU Delft, SC, supervisor
	Ir. J. Gonzalez-Silva	, TU Delft, SC, mentor
	Dr. N.J. Myers	, TU Delft, SC, external

An electronic version of this thesis is available at http://repository.tudelft.nl

Faculty of Mechanical, Maritime and Materials Engineering (3mE)
○
Delft University of Technology

Abstract

Hydrogen is a promising fuel for both reducing greenhouse gas emissions and being used as an energy carrier for renewable energy sources. The adaption of hydrogen instead of natural gas as a fuel in gas turbine combustors introduces additional challenges regarding flame stability. One instabilities is boundary layer flashback. This phenomenon occurs if the flame speed exceeds the local flow velocity. Then the flame can propagate upstream, which can result in equipment failure. Lean premixed hydrogen mixtures are more prone to boundary layer flashback because hydrogen flames have both a smaller quenching distance and higher flame speed compared to natural gas. Therefore, operating at 100% hydrogen fuel content is an enormous challenge. Active control strategies are a promising strategy to prevent and withstand possible occurrences of boundary layer flashback in gas turbine combustors. In this work, the detection, prevention, and counteraction of flashback are investigated in unconfined Bunsen burners. After an experimental analysis of suitable sensors, a tracking controller is therefore designed and different control design approaches evaluated.

Both the increase in flame fluctuations and in flame angle are reasonable as indicators for a flame moving towards flashback as the flow velocity is reduced. However, the complex nature of a flame makes it challenging to measure these effects in a flame. Four types of sensors, i.e. an ion sensor, a thermocouple, a photo-detector and a microphone, were investigated for their ability to detect flashback and to find precursors that indicate the onset of flashback. A Bunsen burner equipped with the different types of sensors was used in an experiment to determine the most suitable sensor type. Of the investigated sensors, the thermocouple is the most promising sensor for both flashback detection and use the temperature signal as a control variable. The temperature is a precursor for the onset of flashback since the temperature increases with increasing flame angle. Also, by placing multiple thermocouples in 360^oC configuration on the burner rim, it is possible to estimate the position, where the flame entered the burner.

A complete fault-tolerant framework to control a flashback event is proposed. This framework increases the flashback resistance of the system and it counteracts possible flashback events, which is considered as a fault in the system. A supervisor block has two functions. Firstly, the supervisor uses a fault detection method, known as trend checking, to detect flashback. Secondly, it decides which strategy should be applied, based on the temperature measurements. The fault-tolerant control strategy is threefold. First, the prevention controller closes the loop, so it can steer away from flashback conditions by rejecting disturbances and tracking a desired reference path using the temperature data. Different tuning methodologies based on the traditional proportional and integral (PI), linear-quadratic-integral (LQI) and pole placement regulator (PPR) are explored for this purpose. The robustness of the proposed controller was verified through loop shaping interpretation. However, flashback could be consider as an stochastic process that still could be triggered. Therefore, the second task is to detect present flashback events and apply counteraction to oppose the fault. A design is pro-

posed by the injection of pressurized air upstream of the burner rim to push back the flame by diluting the boundary layer and increasing the flow speed. A proof-of-concept is validated in the experimental set-up as a possible and feasible counteraction. The third task is a final safety measure. A safety switch would be applied to shut off the fuel supply to fail safe after a potential unsuccessful counteraction attempt. The fault-tolerant control framework was simulated in Simulink for a demonstration purpose, where the models were identified from experimental data.

The proposed fault tolerant control framework is intended to increases the flashback resistance of the system by being more robust towards disturbances and flashback events that would normally require a restart of the system. Its potential to do so has been confirmed by simulations. However, further research on the prediction of flashback and controller implementation are still required to run burners on 100% hydrogen without flashback.

Acknowledgements

Shortcuts are not the easiest path, so combining two masters in one thesis project is a challenging task. It is a path with ups and downs, but along the road you learn a lot. Since the start many things has changed and I could not have done it alone. Luckily, I met many new awesome people. Therefore, I would like to thank my supervisors professor Sikke Klein and professor Riccardo Ferrari for this graduation project opportunity. I especially appreciated Sikke's weekly visits to the lab and his help to get me back on track. Also, the assistance of Luuk in the lab was very useful. Furthermore, I would like to thank Bart with the practical support and for providing coffee (Actually, I often choose the thee or hot chocolate options). For my system and control questions, I have talked many times with Jean. Thank you for your tips and ideas to tackle the problems. Thanks to the people of DEMO for helping with building my setups and Jan Graafland for providing the microphone. Also, it was pleasant to work together in the lab with Gersom and exchange ideas on the topic. A special thanks to Raymond for reading my report and giving useful feedback. Also, I would like to thank Robbert and Fokko for providing suggestions on my report. Last but not least thanks to Floor, my family, kartboys, 35ste, theeleuten and my student debt for their support and fun adventures along the road.

Delft, University of Technology — T.H.M. van der Laan
August 11, 2022

"The more you know, the more you realize you don't know."
— *Aristotle*

Table of Contents

List of Figures

List of Tables

Glossary

List of Acronyms

CIVB	Combustion Induced Vortex Breakdown
BLF	Boundary Layer Flashback
DNS	Direct Numerical Simulations
DL	Darrieus Landau
IR	Infrared
UV	Ultraviolet
MSIR	Multi-Spectrum Infrared Flame Detector
LQR	Linear Quadratic Regulator
IPCC	Intergovernmental Panel for Climate Change
EC	European Commission
SISO	single-input and single-output
LQR	Linear-Quadratic Regulator
LQI	Linear-Quadratic Integrator
PPR	Pole Polacement Regulator
LQ	Linear-Quadratic
UV	Ultraviolet

Chapter 1

Introduction

The global energy demand is expected to grow 50% in the period from 2020 to 2050, as stated during the International Energy Outlook 2020 [1]. However, the energy required for power generation is currently mainly produced by the combustion of fossil fuels, like coal, natural gas, and oil. The Intergovernmental Panel for Climate Change (IPCC) [17] states that 78% of the total amount of emitted greenhouse gasses is produced by industrial processes and combustion of fossil fuels. Fossil fuel combustion mainly results in the emitting of the greenhouse gas CO_2. Power production is therefore related to an increase in global greenhouse gas concentrations. These increased gas concentrations are likely the main driver for the increase in global temperature. In 2020, the average global temperature has increased by approximately $1.2°C$ compared to the 19^{th} century [18]. To limit the effects of global warming, the goal has been defined to keep this average global temperature increase below 2^oC, negotiated in the international treaty of the Paris Agreement [19]. Therefore, the European Commission (EC) targets in its long-term strategy to achieve net-zero greenhouse gas emissions by 2050 [20].

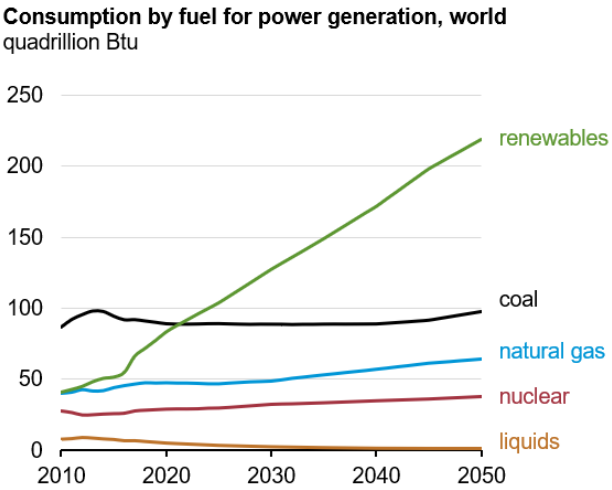

Figure 1-1: The expected worldwide consumption trend of different fuels for power generation. The global energy demand increase is covered by utilizing renewable energy sources. The worldwide use of fossil fuels, except for liquid fuels, still has a large role. Image from Capuano [1].

To realize this goal, energy from renewable sources will become the primary contributor. The share of renewable energy sources, like wind, solar photovoltaic, biomass, and hydro-power, is predicted to grow substantially over the years, as seen in Figure 1-1. The challenge of using renewable energy as a primary energy source is its fluctuating nature. The availability of wind power and solar radiation is both daytime and seasonal-dependent. This results in a

mismatch between the energy production and demand. Therefore, the electricity grid requires flexible power plants to balance the grid [2].

Gas turbine power plants could fulfill this task as a balancing system for the future. These generators have three main advantages [21]. Firstly, they can handle frequent startups. Secondly, they can quickly adapt the output to the current demand on the grid. Thirdly, they are efficient, as state-of-the-art combined-cycle gas turbines have efficiencies of around 60% [22]. At the moment, natural gas is the most used fuel in gas turbines for power production [17]. The combustion reaction of natural gas is much cleaner than the combustion reaction of for example coal. It is both more efficient and produces fewer pollutants, such as CO_2 and soot [23]. To achieve low NO_x emissions, lean premixed combustion is employed [24]. Here, fuel and an abundant amount of air are premixed upstream to control the adiabatic flame temperature .

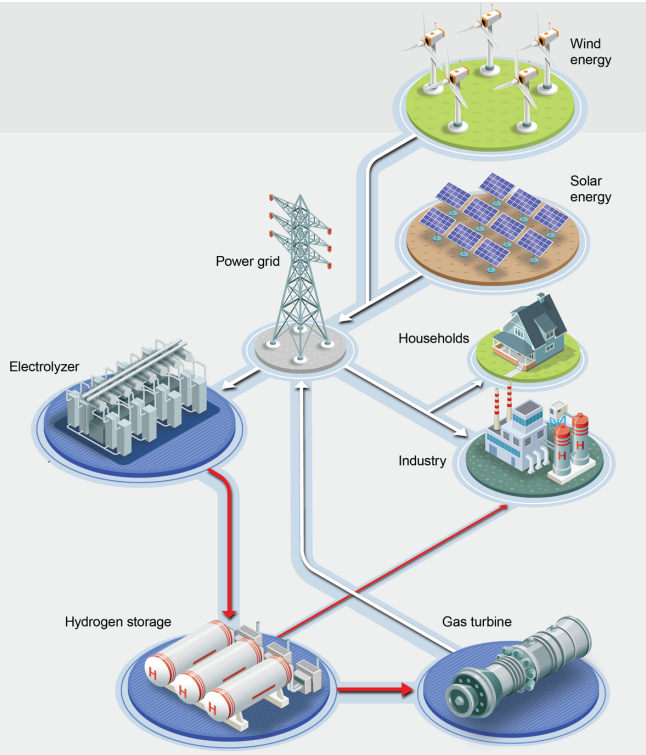

Figure 1-2: Power grid of the future where renewable energy is stored in hydrogen. Adopted from Fairley [2].

However, the use carbon-free fuels is necessary to reach net-zero greenhouse gas emissions. Work is done on utilizing different fuel blends in gas turbines. A promising fuel is hydrogen since the combustion of hydrogen does not produce carbon dioxide [25]. Furthermore, hydrogen can also be used as an energy carrier in a hydrogen ecosystem. This concept is illustrated in Figure 1-2. If the production of renewable energy sources is higher than the current demand, the excess energy is used for the production of hydrogen. Via electrolysis, water is converted into hydrogen and oxygen. The produced hydrogen can be stored. If the energy demand is higher than the current production, the hydrogen can be converted back again. Hydrogen can be either be combusted in gas turbines to generate electricity or be

directly consumed by the industry.

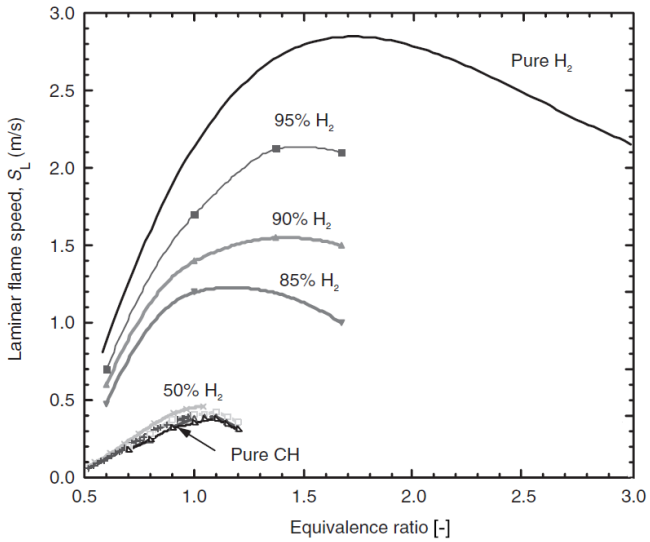

Figure 1-3: Laminar flame speed as function of equivalence ratio for H2/Air flames, CH4/Air flames and flames with fuel blends of H2/CH4/Air. Adopted from Dunn-Rankin [3].

The use of hydrogen introduces stability challenges for the design of gas turbines. According to Dunn-Rankin et al. [3], the flame velocity of hydrogen is much faster compared to natural gas flames for two reasons. Firstly, the reaction rate is faster and secondly, the diffusion coefficient is larger. Figure 1-3 shows the laminar burning velocity for different fuel blends. The laminar flame speed is a measure of the reactivity and diffusivity of a flame, which indicates the flame front propagation velocity. Fuel blends with high hydrogen contents have a substantially higher laminar flame speed. This property results in a higher risk for the upstream propagation of the flame from the desired flame location into the premixing zone [26] . In this zone, the fuel and oxidizer are mixed. This phenomenon is known as flashback and it is a safety issue. Furthermore, hydrogen has a low quenching distance, so the flame sustains itself close to a cold wall. Due to the non-slip boundary, the flow velocity reduces to zero at the wall. In this low velocity region close the wall, the hydrogen flame is more likely to propagate upstream. This phenomenon is called boundary layer flashback and is the main flashback mechanism for lean premixed combustors, like open air or unconfined Bunsen burners. When the flashback event is triggered, the operator should quickly switch off the gas turbine to prevent equipment failure. The components upstream are not designed to withstand the high flame temperatures.

This elevated risk for flashback sets a limit on the usage of 100% hydrogen as fuel. Existing gas turbines can handle fuel blends with up to 20% hydrogen content without major modifications. This results in a reduction of 9% in CO_2 emission [27]. The world's largest gas turbine manufacturers committed to contribute to the energy transition by developing gas turbines that can handle renewable fuels [21]. They target to gradually increase the goal for the hydrogen-burning capability of the gas turbines. Starting with fuels with at least 20% hydrogen content by 2020 towards 100% hydrogen content by 2030. The industry is developing methods to achieve this goal. The current state-of-the-art combustion systems with diffu-

sion flames and nitrogen or steam dilution injection methods operate at 100%. Nevertheless, those gas turbines have even higher NO_x emissions than conventional gas turbines because the peak flame temperature is higher due to diffusion effects [28]. Diluting the mixture with steam has energy and environmental disadvantages and nitrogen cannot lower the flame temperature enough to reach low NO_x levels [21]. Therefore, lean premixed combustion is a more promising solution as lower emissions can be achieved. Currently, fuel blends with up to 60% hydrogen are possible, but more developments are required to achieve 100%.

Active control strategies are a promising strategy to prevent and withstand possible occurrences of boundary layer flashback for high hydrogen content fuels in gas turbine combustors. The use of these fuels concerns safety and stability issue as the upstream propagation of the flame can be considered as a fault. Blanke et al.[4] described a fault as the cause of a change in the system behavior. It leads to degraded system performance or can eventually result in system failure. A failure is a permanent system interruption to perform the required function [29]. This is different from a malfunction, where there is an intermittent irregularity in the system's function fulfillment. The flashback fault can have damage the equipment but is also a risk for human operators and bystanders. To avoid the effect of flashback, it should be detected early on to take counteractive measures. Therefore, a systems safety can be improved by aiming for a fault-tolerant system. By making the burner system fault-tolerant to flashback, it can prevent flashback events and counteract the occurrence of flashback. A typical architecture of a fault-tolerant controller is shown in Figure 1-4. It adds a supervision level to a typical control schematic. In this layer, the system behavior is analyzed to diagnose a fault. If a fault is detected, it changes the control law to reject the faulty behavior and steer the plant performance to an acceptable region. This structure can be used to deal with high flashback propensity systems. This will be the focus of this work.

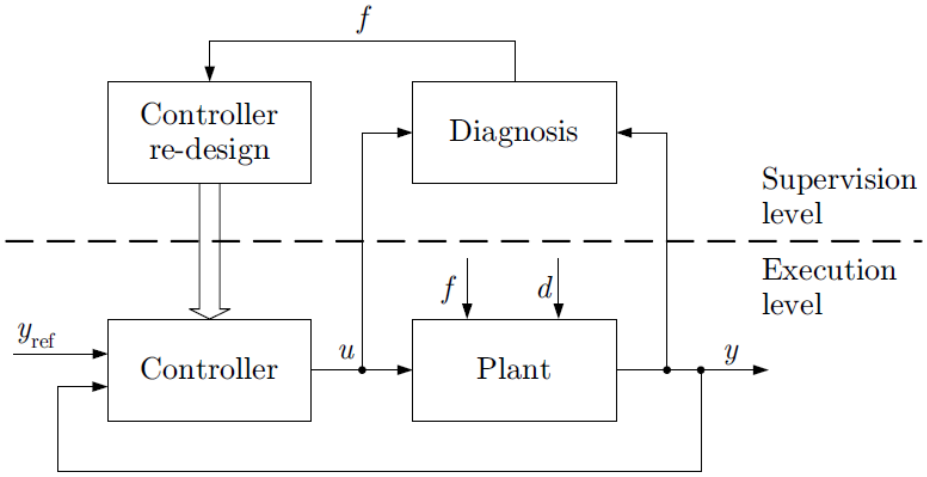

Figure 1-4: Architecture of fault-tolerant controller. Adopted from Blanke et al. [4].

A literature review on boundary layer flashback research has been conducted by Kalentari et al. [30]. Many numerical and experimental studies have been conducted to understand the mechanism behind the flashback phenomenon. However, research on controlling this problem is limited. The focus of this work will therefore be on applying the control principles to deal with flashback.

Research objective

This master thesis aims to design a fault-tolerant control framework as a solution for the problem sketched above. Process engineering knowledge is combined with theories from the field of control engineering. Both experiments and simulations are employed to discuss the feasibility of a possible active controller. As a guidance, the following main research question is formulated:

Can boundary layer flashback be prevented by active control?

This question is subdivided into four sub-questions:

- *What causes boundary layer flashback?*
- *How to detect the occurrence of flashback?*
- *How to find precursors for the onset of boundary layer flashback?*
- *How to use control to prevent boundary layer flashback in unconfined Bunsen burners?*

Report structure

The report is divided in three parts. In the first part, the theoretical fundamentals of the problem are studied. Chapter 2 describes the fundamental concepts for a lean premixed combustion Bunsen burner. In Chapter 3, the flashback phenomena and indicators of the onset of flashback are explained, according to the relevant experiments, simulations and theories found in the literature.

After the fundamentals, the second part focuses on the detection of flashback and precursors, indicating the onset of flashback. Measurements are required to get state information of the burner. Therefore in Chapter 4, different sensors are tested. Afterwards, the sensors are compared against each other to choose an appropriate sensor.

In the third part, the chosen sensor and the findings from the previous chapters are integrated to construct a controller framework. This framework has multiple functions to both prevent and counteract flashback. In Chapter 5, different counteracting systems are investigated. A prototype is constructed for the most promising solution to proof the concept. The performance of this design is evaluated by a performing lab test. In Chapter 6, the design of a fault-tolerant control framework is explained. The framework has multiple tasks. A supervisory system decides, which task to execute. By performing simulations, the switching controller behavior is evaluated.

Finally in Chapter 7, the thesis is summarized and concluded. Several recommendations are proposed for future research.

Part I

Fundamentals of boundary layer flashback

Chapter 2

Lean premixed combustion in Bunsen burners

Flashback prevention is investigated in a unconfined Bunsen burner, where the fuel and oxidizer are premixed upstream. Therefore, the fundamentals of the lean premixed combustion in these burners is discussed, which are relevant to get a better understanding of the physics behind the problem. This chapter covers the function of premixed combustion, the laminar premixed flame, the flame configurations and the definition of the Bunsen flame angle.

2-1 Premixed combustion

When the fuel and oxidizer mixture is premixed upstream of the flame front, it results in a homogeneous mixture. If this mixture is stoichiometric, it contains the exact amount of air needed to let all oxidizers in the air react with the fuel. The richness of the mixture is expressed by the equivalence ratio ϕ [31]. The equivalence ratio is displayed in equation 2-1, where $\dot{m}$ is the mass flux. It is defined as the relation between the fuel/air ratio of the mixture to the fuel/air ratio of a stoichiometric mixture. The mixture is called lean if $\phi < 1$, so more air is present than needed to combust all the fuel. If $\phi = 1$, the combustion is stoichiometric and when $\phi > 1$ the conditions are rich. The equivalence ratio determines the flame properties of the combustion.

$$\phi = \frac{\dot{m}_{fuel}/\dot{m}_{air}}{(\dot{m}_{fuel}/\dot{m}_{air})_{st}} \tag{2-1}$$

The primary drive to operate at fuel-lean conditions is to reduce NO_x emissions [3]. The remaining air absorbs heat to reduce the adiabatic flame temperature and material hot spots in the combustion chamber. This has a positive effect on emissions and complete combustion. A typical hydrocarbon profile can be seen in Figure 2-1. Two elements in this graph stand out. Firstly, the concentration of unburned hydrocarbons and soot increases again at too lean conditions. Secondly, the maximum adiabatic temperature is reached at richer conditions. Endothermic molecular reactions reach their maximum reaction rate at strict stoichiometric conditions, resulting in a lower temperature. The thermal efficiency of the process is also improved at leaner conditions due to better thermodynamic equilibrium properties [3].

Dependent on the nature of the flow, it can interact with the reaction chemistry in the flame. A flow is considered laminar if the ratio between momentum and viscous forces is dominated by viscous forces. This ratio is also known as the Reynolds number. It is defined in equation 2-2, where l is the characteristic length, U is the flow velocity and ν is the kinematic viscosity. The flow in a pipe is laminar when $Re < 2300$ [32]. For flows with Reynolds higher than 4000, the momentum forces dominate. These flows are called turbulent. Compared to laminar flows,

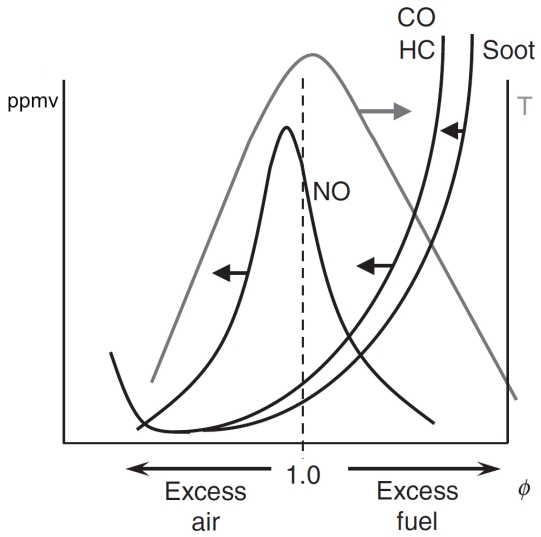

Figure 2-1: Temperature and relative emissions as a function of the fuel-air equivalence ratio. Adopted from Dunn-Rankin [3].

the turbulent flow interacts with the flame. The chaotic fluctuations in a turbulent flow can alter the shape of the flame front. In turbulent premixed combustion, the flame can locally behave as a laminar flame, which is the topic of the next section.

$$Re = \frac{lU}{\nu} \tag{2-2}$$

2-2 Laminar premixed flame model

The simplest way to describe laminar flames is with the plain laminar flame model [33]. This model is illustrated in Figure 2-2. Several assumptions are made [24]. The flame is one-dimensional and the Mach number is low. Mechanical energies, viscous dissipation, and the pressure difference across the flame front are negligible. Furthermore, the specific heat capacity, thermal conductivity and diffusivity have constant values. Also, the flame is thin, unity Lewis number and the reaction is single-step irreversible. Additionally, the unburned mixture is continuously heated to the point where the ignition takes place during the sustained combustion [34]. At the left unburned side, the oxidizer Y_{O_2} and fuel Y_F mixture enter the reaction region with unstretched laminar flame speed $s_{l,0}$ and temperature T_u. The laminar flame speed is dependent on the equivalence ratio. Since the mixture is lean, there is more oxygen in the form of air present than fuel.

The flame thickness δ_f is composed of the preheat region with thickness δ_{ph} and the reaction zone with thickness δ_r. The preheat zone is assumed to be greater than the reaction zone, so $\delta_{ph} \cong \delta_f$. In the preheat zone, the convection-diffusion balance dominates. Whereas in the reaction zone, the diffusion-reaction balance is dominant. These balances are described with the Lewis number Le, given in equation 2-3, where α is the thermal diffusion, and D is the mass diffusion. For lean hydrogen-air mixtures, the Lewis number is smaller than one.

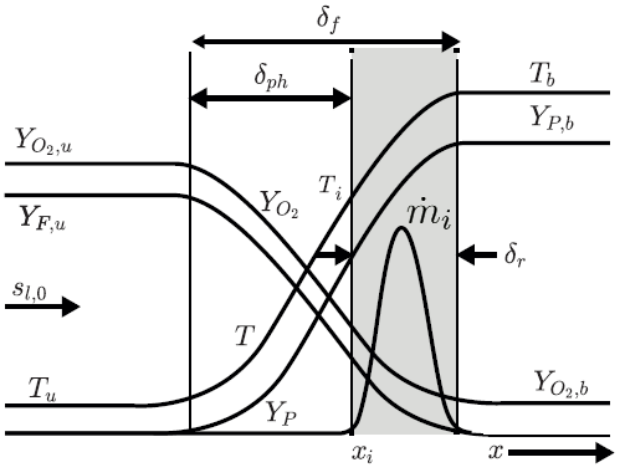

Figure 2-2: Schematic profiles of temperature and concentration for a simplified laminar flame front. Adopted from Peters [5].

This results in an instability between the heat and mass diffusivity. This thermal-diffusive instability increases flame front curvature.

$$Le = \frac{\alpha}{D} \tag{2-3}$$

As the unburned fuel and oxygen concentrations diffuse into the reaction zone, their concentrations in the preheat zone decrease. The combustion heat Y_P is dissipated in the opposite direction from the reaction zone into the preheat zone. If the unburned mixture reaches temperature T_i, the combustion reaction $\dot{m}_i$ will start. The exothermic reaction converts all fuel into heat. The temperature increases rapidly.

The gross combustion reaction of a typical natural gas can be seen in equation 2-4 [6]. However, the actual reaction consists of many chain reactions. A reduced mechanism is shown in Figure 2-3.

$$CH_4(g) + 2O_2(g) \rightarrow CO_2(g) + 2H_2O(g) \tag{2-4}$$

2-3 Flame configurations

Two different flame configurations can be identified, which are shown in Figure 2-4a [8]. In the confined situation, the flame is settled in the premix section and is enclosed by the walls. In the unconfined configuration, the flame is emitted in the free air and is stabilized at the burner rim. Eichler et al.[35] showed that the unconfined flames have a higher flashback resistance than flames in confined geometries. Baumgartner et al.[36] ascribed this observation to the insignificant interaction between flame and the flow for a stable unconfined flame, caused by outward deflected flame at the burner exit.

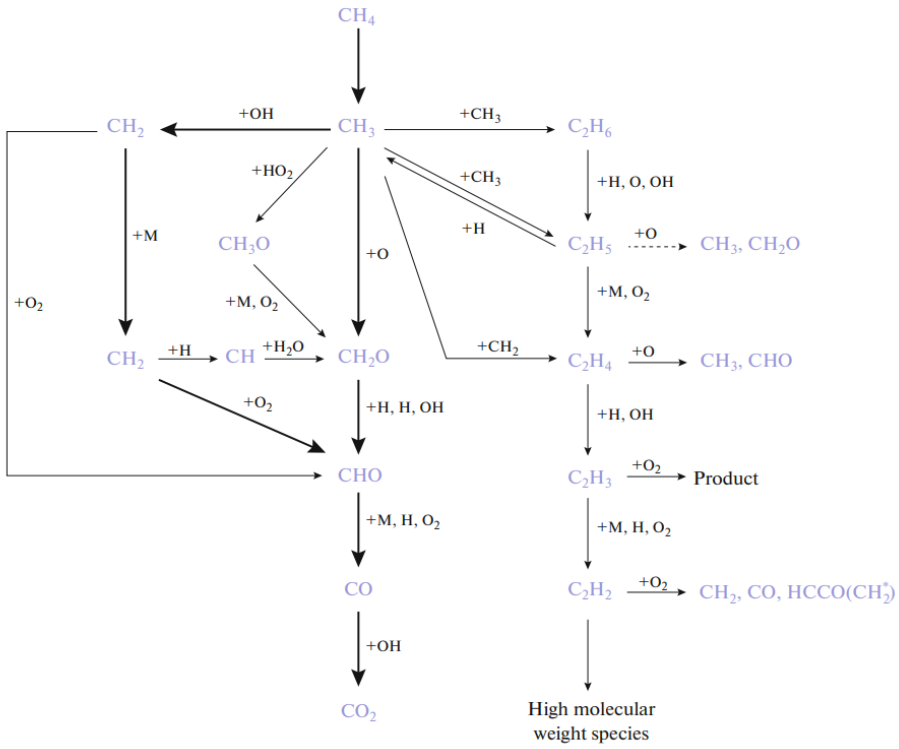

Figure 2-3: Reduced reaction mechanism for the methane-air mixtures. Adapted from Son [6].

2-4 Bunsen flame angle

The Bunsen burner produces an unconfined flame. Fuel and air are premixed upstream and ignited at the exit of the burner tube. The produced flame has a conical shape. In Figure 2-4b, the schematic of half of the conical shaped flame front is shown. The black solid line represents the flame front. The flame makes a flame angle α_f with the velocity of the approaching unburned mixture U_u. The normal and tangential components of the unburned mixture velocity are $U_{u,n}$ and $U_{u,t}$ respectively. The laminar flame speed is denoted by S_l and has a velocity component normal to the flame front. The combustion reaction accelerates the burned mixture, so the outgoing normal component $U_{b,n}$ is larger than the incoming flow [31]. Therefore, the velocity of the burned mixture U_b makes a different angle β with the flame front.

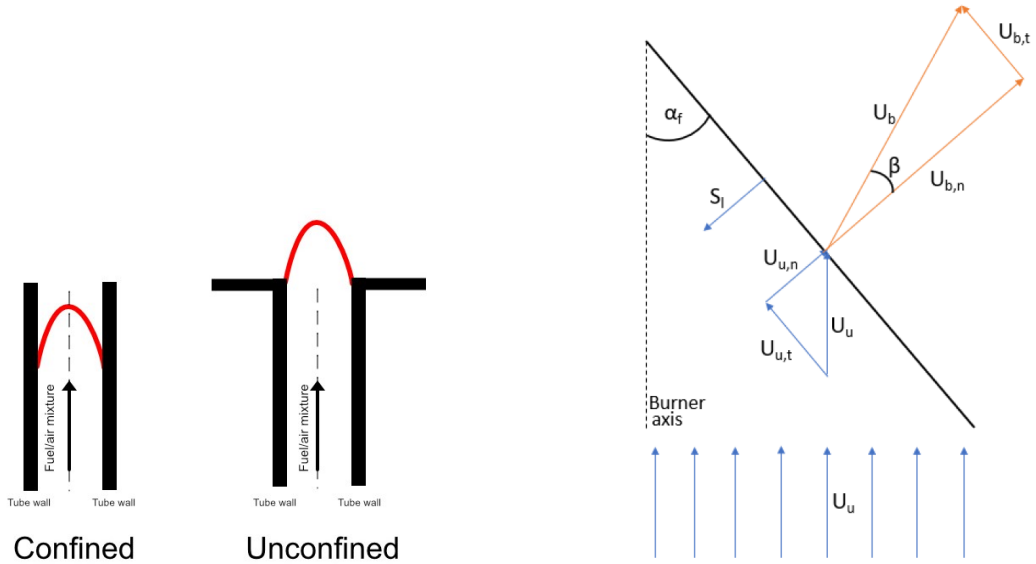

(a) At the left in the confined flame configuration, the flame is surrounded by walls. At the right in the unconfined flame configuration, the flame is emitted in the free air.

(b) The schematic of half of the conical shaped premixed laminar flame front. Adapted from Lambers [37].

Figure 2-4: Schematics describing flame configurations and definitions.

Chapter 3

Boundary layer flashback phenomenon

To prevent flashback, the understanding of the phenomenon is useful. Therefore, the first section explains the different flashback mechanisms. In the section thereafter, the boundary layer flashback phenomenon is described according to the main findings in the literature. In the remainder of this chapter, possible indicators for the onset of flashback are discussed.

3-1 Flashback mechanisms

During flashback, the flame burning speed locally exceeds the local flow velocity, which results in an upstream propagation of the flame into the premixing section. Four main mechanisms are identified to trigger flashback [8]:

Core flow flashback

If the turbulent burning velocity of the flame exceeds the local velocity of the flow in the core, the flame will flashback and propagate upstream. The magnitude of the turbulent burning velocity causes the initiation of flashback. This velocity is a relation between the turbulent-flame interaction and chemical kinetics. Hence, the fuel composition and turbulent flame structure are determinative of the flashback limit. The occurrence of core flashback is reduced by increasing the axial flow velocity, so the turbulent flame velocity cannot exceed the core flow velocity. However, flame stabilization techniques, such as swirl burners, decrease the velocity of the axial flow and consequently increase the risk of core flashback.

Combustion instability induced flashback

Different instabilities induce flow fluctuations. They are generated by the interaction of acoustic modes, unsteady heat release and flow structure. These instabilities cause velocity and pressure oscillations, which in turn induces flame movement and large vortices. This eventually will lead to flow reversal and is a potential risk for flashback.

Combustion Induced Vortex Breakdown (CIVB)

To stabilize a flame, a possible method is to use a swirl stabilized combustion chamber. The strength of the swirl is described by the swirl number. It relates the azimuthal velocity to the axial velocity. If the swirl number exceeds a critical value, a reverse flow region is created by an abrupt vortex breakdown. During this breakdown, the vortex structure is changed abruptly. It results in the formation of both a stagnation point and a recirculation zone downstream of the structure. On the one hand, the volumetric expansion of the gases in the flame front, generating positive vorticity, pushes the vortex bubble downstream to stabilize the flame. On the other hand, the produced baroclinic torque causes negative vorticity. This enhances the negative axial velocity and the vortex bubble propagates upstream. The unbalance between these two forces eventually leads to the occurrence of flashback.

Boundary Layer Flashback (BLF)

BLF is the typical flashback mechanism in premixed Bunsen burner flames, investigated in this work. During regular operations in these burners, the core flow exceeds the flame burning speed. Therefore, flashback cannot arise in the core region of the burner, but the no-slip boundary condition assumes zero velocity at the solid boundaries. This results in a reduction of the flow speed towards a boundary. Hence, the flashback risk shifts to regions closer to a wall. The burning velocity also decreases close to the wall because heat is lost to the wall and the flame stretches. Eventually, the flame cannot sustain itself and it quenches. This distance to the wall is described as the quenching distance. BLF will occur if the flame burning speed exceeds the flow velocity close to the wall but further than the quenching distance.

3-2 Describing boundary layer flashback

To get a better understanding of the BLF phenomenon and triggers, leading to the onset of the event, the fundamentals are investigated by using models and theories from the literature.

Capturing BLF events

Faldella [7] conducted experiments to visualize the boundary layer flashback events for both hydrogen-air and methane-air mixtures by using Mie-scattering and PIV techniques. This resulted in two series of eight time sequence snapshots. In Figure 3-1 and 3-2, the results are shown for the Mie-scattering experiment. Methane flashback events take place in about five milliseconds. However, hydrogen flashback events are five times faster. They occur in less than one milliseconds

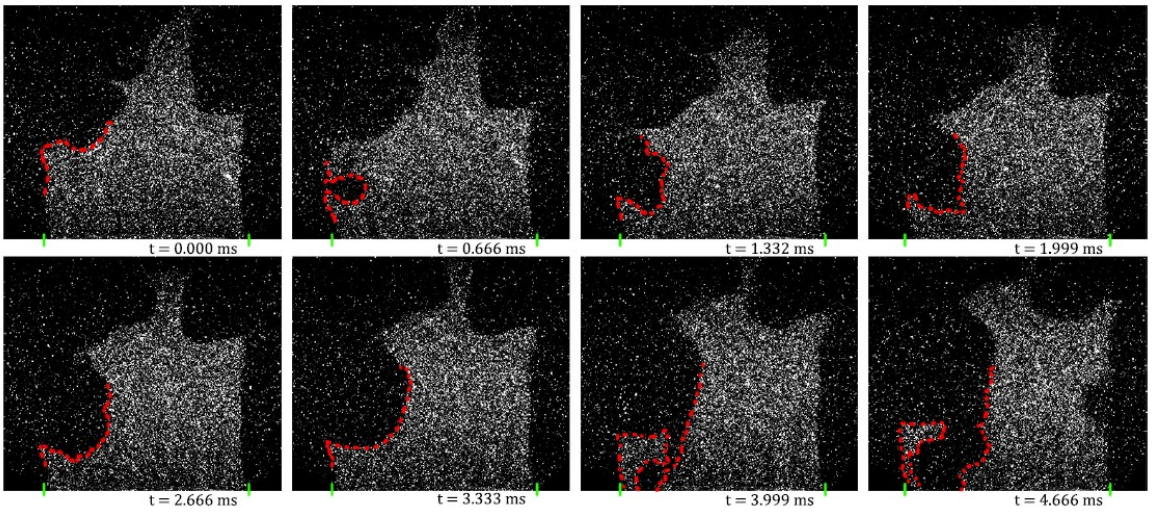

Figure 3-1: Time sequence of Mie-scattering experiment to capture BLF in METHANE-AIR flames at 100% CH_4 ($\phi = 0.9$) at $Re \approx 5000$. The time between each image is 0.666 ms. The inner wall of the tube burner is indicated with the green marks at the bottom of the frames. The part of the flame front that eventually flashes back is indicated by the red dashed line. Adopted from Faldella [7].

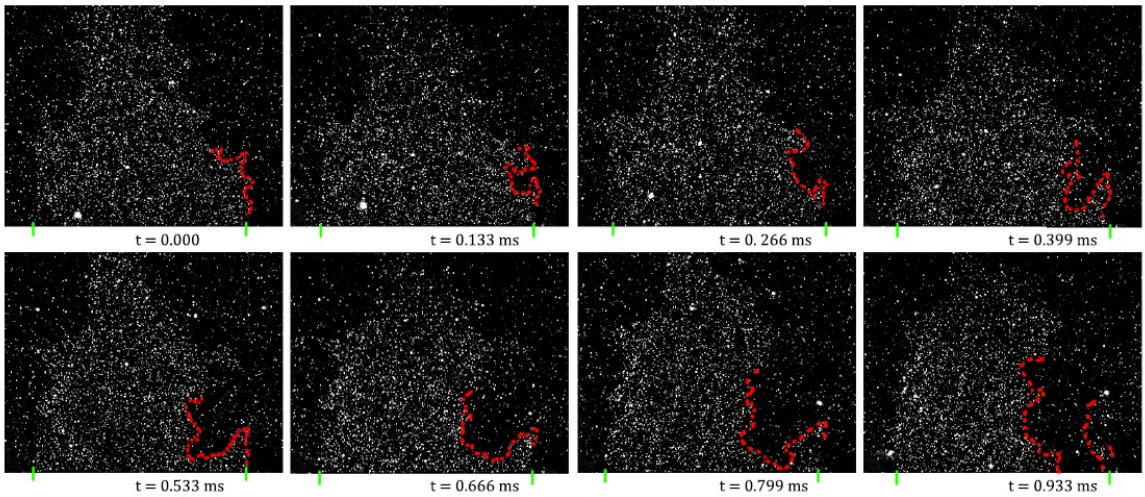

Figure 3-2: Time sequence of Mie-scattering experiment to capture BLF in HYDROGEN-AIR flames at 100% H_2 ($\phi = 0.6$) at $Re \approx 11800$. The time between each image is 0.133 ms. The inner wall of the tube burner is indicated with the two green marks at the bottom of the frames. The part of the flame front that eventually flashes back is indicated by the red dashed line. Adopted from Faldella [7].

Critical velocity gradient prediction model for BLF

In 1943, Lewis and Von Elbe [38] conducted experiments on BLF. They developed the first prediction model for BLF for a perfectly mixed mixture of natural gas and air at atmospheric pressure and temperature. This model is constructed for laminar confined burners and it is used to illustrate the mechanisms behind BLF. Two main assumptions are made. Firstly, the flow velocity is undisturbed and secondly, the flame-flow interaction are neglected.

The model schematic is illustrated in Figure 3-3a. The height y is measured from the wall at the bottom. The velocity profile of the incoming laminar unburned mixture is defined by $u(y)$ with a non-slip boundary condition, so the velocity is zero at the wall and has an approximately linearly increasing velocity profile. The burning flame speed is represented by $s_f(y)$. The quenching of the flame occurs at the quenching distance from the wall, denoted by δ_q. Flashback will take place if the flame burning velocity locally exceeds the flow velocity. The location from the wall, where this happens is denoted by penetration distance δ_p.

In Figure 3-3b, three flow velocity profiles and one burning velocity profile are drawn. At the quenching distance δ_q from the wall, the burning velocity is zero and from there it increases exponentially to the constant one-dimensional laminar flame velocity. For the flow velocity, the gradient of the velocity at the wall depends on both the shear stress and viscosity of the flow. For trajectory 2 there is a critical point where the two velocities meet. At this location, a risk for flashback is present. If the flow velocity is further reduced as for trajectory 1, the flow will flashback and propagate upstream. On the other hand, if the flow velocity is increased in trajectory 3 the flame will be pushed downstream.

The bulk velocity, at which flashback occurs, is determined by the critical velocity gradient g_c at the wall. The critical velocity gradient is defined in equation 3-1. The laminar flow is assumed to have a linear velocity gradient within the penetration distance close to the

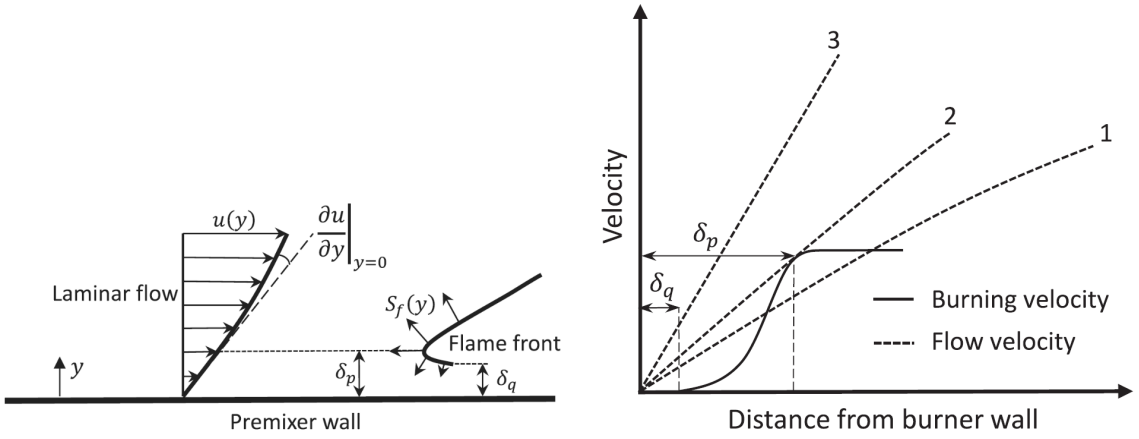

(a) Schematic overview of the critical boundary layer model in confined configuration.

(b) Three flow velocity and one burning velocity profiles for the critical boundary layer model.

Figure 3-3: Schematic drawings of the critical boundary layer model. Adopted from Kalentari [8]

wall. Therefore, the critical velocity gradient simplifies to be approximately equal to the ratio between the local velocity and the penetration distance. If the critical velocity gradient is considered for a fully developed pipe flow, the bulk flow can be related to the radius of the tube (For more details see [8]). For the flame speed, a comparable ratio is derived between the laminar flame speed s_l and the penetration distance δ_p in equation 3-2. The burning velocity is assumed to be close to the laminar flame speed. If equation 3-1 and 3-2 are equalized, the flashback bulk velocity can be determined.

$$g_c = |\frac{\partial u}{\partial y}|_{y=\delta_p} = \frac{u|_{y=\delta_p}}{\delta_p} = \frac{4\bar{U}}{R} \tag{3-1}$$

$$g_c = \frac{s_l}{\delta_p} \tag{3-2}$$

The assumptions made in the critical velocity gradient prediction model are not generally true. By doing measurements on BLF for laminar propane-air mixtures, Dugger [39] found that the penetration distance is smaller than the quenching distance. According to the model of Lewis and Von Elbe, this is not possible, since the flame would propagate below the quenching distance to the wall. He therefore suggests that the flame might influence the velocity profile of the approaching flow. Eichler et al. [9] investigated the flame in a confined configuration experimentally and numerically. Their simulations showed that the backflow region already was present before the occurrence of flashback. In the backflow region, the pressure reduces until stagnation or even becomes negative. This decelerates the flow velocity and reverses the flow. It eventually supports upstream flame propagation. Furthermore, laminar flames alter the backflow region upstream during flashback. The conclusion was that the flame-flow interaction is significant in the confined configuration, so the critical velocity gradient prediction model contains unmodelled effects to fully capture the phenomenon.

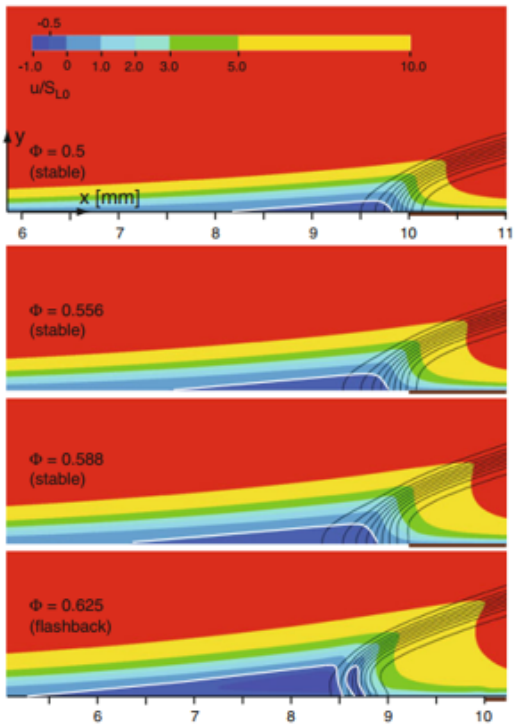

Figure 3-4: Numerical simulations showing the existence of backflow regions for the laminar premixed flame in both stable and flashback conditions. Adopted from Eichler [9].

Figure 3-4 shows that flow reversal is already present at the wall as the flame approaches flashback. Lieuwen [40] explained that the flame is accelerated and refracted across the flame front, caused by the expansion of the gas. The presence of a wall further amplifies the flow displacement. The deflection of the fluid results in an increased pressure gradient for the approaching reactant. This pressure provokes a backflow region close to the wall as is illustrated in Figure 3-5.

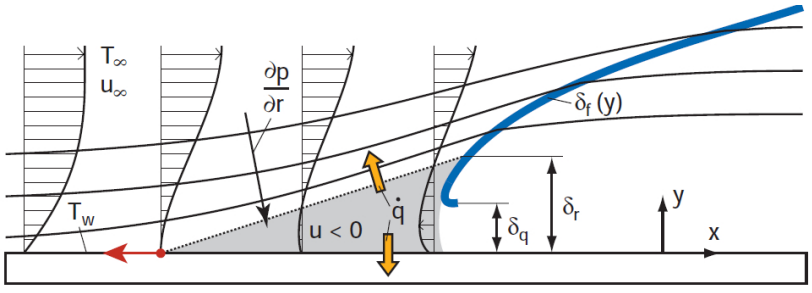

Figure 3-5: Schematic representation of the pressure increase upstream of the flame front, resulting in a back flow region. Adopted From Eichler [10]

Eichler et al. [35] showed that unconfined flames have a higher flashback resistance than flames in confined configurations. In Figure 3-6, the velocity gradient limit is shown for both confined and unconfined burners. Indeed the values for confined burners are larger than for unconfined burners. Baumgartner et al. [36] ascribe this observation to the insignificant interaction between flame and the flow for a stable unconfined flame, caused by outward deflected flame

at the burner exit. Again the critical velocity gradient model did not predict the flashback limit perfectly. Gruber et al. [41] did a Direct Numerical Simulations (DNS) study on the mechanisms of premixed unconfined hydrogen-air flame flashback in the turbulent boundary layer. They found that reversed flows are present ahead of the upstream propagating flame in the near-wall region ($y^+ < 20$). This flow is convex towards the reactant flow. Together with Darrieus Landau (DL) instabilities, the reverse flow region contributes to the upstream acceleration of the flame. DL affects both the pressure field and the turbulent motion with the wrinkled flame.

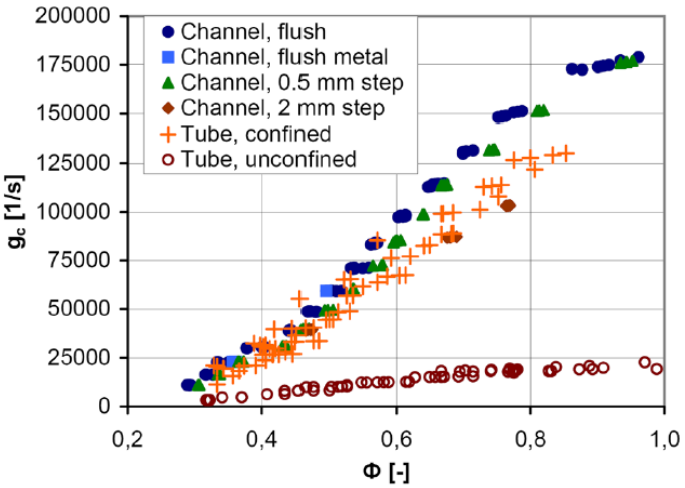

Figure 3-6: Boundary layer flashback limits for both confined and unconfined hydrogen-air flames. Adopted from Eichler [9].

Turbulent BLF prediction model from TU Münich for unconfined flames

Hoferichter et al. [42] developed an improved prediction model for boundary layer flashback limit for flames in confined ducts or Bunsen burners compared to the original BLF model. They included the strong coupling between the flame and the flow as observed by Eichler et al. [9] and Baumgartner et al. [36]. They added the Stratford criterion [43] to the model, which is used to predict boundary layer separation.

In another research of Hoferichter et al. [11], they developed an analytical prediction model for unconfined BLF limits in premixed hydrogen-air flames. According to Baumgartner et al. [36], the turbulent flame front forms a notch at the distance Δx_{FB} at flashback conditions. The flame starts to propagate upstream at a distance of $y_{FB} \approx 1mm$ from the burner wall. After the transient from the outside to the inside of the burner, as shown in Figure 3-7, the flame behaves as a confined flame. In essence flashback is an intermittent phenomenon, where the flame transitions from the stable position at the burner rim into the premixing zone.

The flashback mechanism arises when the local turbulent flame velocity exceeds the local flow velocity. The local velocities close to the wall are schematically illustrated in Figure 3-8a. At the flashback height y_{FB}, the x component of the local flow velocity $u(y_{FB})$ is equal to the local turbulent flame velocity S_t, calculated in equation 3-3. The local turbulent flame

velocity is determined using velocity fluctuations and stretched laminar burning velocities.

$$S_t(y_{FB}) = u(y_{FB})sin(\alpha_{FB}) \tag{3-3}$$

To determine the local flow speed at flashback, not only the local turbulent flame velocity is required but also the flame angle α_{FB}. The flame angle α_{FB} can be calculated in different ways. Hoferichter used a global analysis, as in Figure 3-8b. The flame angle, which is assumed constant, is determined from the mass conservation balance as given in equation 3-4. Here, A_B is the cross-sectional area of the burner, A_F is the cross-sectional area of the flame front, ρ_u is the density of the unburned mixture and $\bar{S}_t$ is the average turbulent burning velocity. The cross-sectional areas can be related to the flame angle, shown in equation 3-5. So the flame angle is determined by combining equation 3-5 and 3-4 into equation 3-6. Finally, this equation together are solved simultaneously since the local flow speed $u(y_{FB})$ is related to the average bulk flow velocity at flashback $\bar{U}_{FB}$.

$$\rho_u A_B \bar{U}_{FB} = \rho_u A_F \bar{S}_t \tag{3-4}$$

$$\frac{A_F}{A_B} = \frac{1}{sin(\alpha_{FB})} \tag{3-5}$$

$$sin(\alpha_{FB}) = \frac{\bar{S}_t}{\bar{U}_{FB}} \tag{3-6}$$

Flame transient behavior

At the TU Delft, Willems [13] conducted experiments with turbulent natural gas/hydrogen-air flames at stoichiometric and lean equivalence ratios. He visualized the onset of flashback and the transient from unconfined to confined flame in a burner Bunsen by performing Particle Image Velocimetry and Mie-scattering. The tube was made of quartz glass to measure the flow approaching the flame. One of the visualizations of the flashback process for a hydrogen flame is shown, at the end of this chapter, in Figure 3-12. Here, a positive velocity fluctuation pushes the flame outwards in the first three images. This positive velocity fluctuation is followed by a negative velocity fluctuation in image 4. The interaction between the flame and the negative velocity fluctuation results in a local convex flame front in image 5. As a result, the flame loses its anchoring point and propagates upstream in the remaining images.

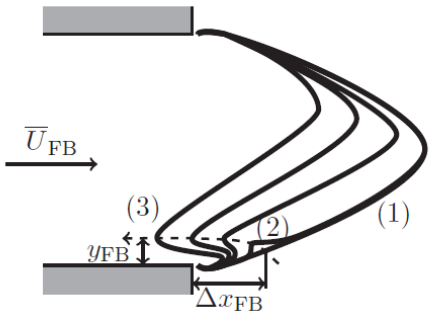

Figure 3-7: BLF mechanisms for an unconfined burner for timestamp (1) up to (3). Adopted from Hoferichter [11].

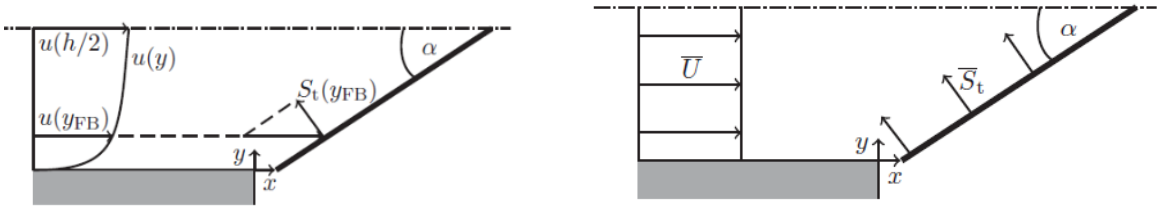

(a) Local analysis of the flame at flashback conditions. **(b)** Global analysis of the flame at flashback conditions.

Figure 3-8: Schematics for the local and global flame analysis to determine the flashback flow velocity limit. Adopted from Hoferichter [11]

By comparing the speed of the upstream propagating flame for both natural gas flames and hydrogen flames, the upstream propagation speed are $0.6ms^{-1}$ and $1.4ms^{-1}$ respectively. Hence, hydrogen propagates upstream considerably faster than natural gas flames.

When the Reynolds of a stable unconfined flame is reduced towards flashback conditions, the Reynolds stresses increase in magnitude and cover a larger area. The Reynolds stresses are a measure for the stress tensor due to turbulent fluctuations in the flow. For this behavior two reasons are proposed:

- By reducing the Reynolds number of the flow, thermal-diffusive instabilities have more time to develop. Therefore, the flame front becomes unstable and the flame tip location moves in a larger area, hence the spread of the Reynolds stresses is higher.
- By reducing the Reynolds number of the flow, the average flame angle increases. As a result, the flow has a higher acceleration across the flame front and hence the Reynolds stresses increase in magnitude.

Regions with negative velocity fluctuations in the approaching unburned gas mixture are the main factors for the onset of unconfined flashback. However, other boundary conditions are also influencing the onset of flashback. Such as the flow's bulk velocity, the position of flame front, the magnitude of fluctuations, and the presence of positive velocity fluctuations after the negative velocity fluctuation interacted with the flame front. As a result, unconfined flashback is a stochastic process, where the flashback chance increases for a decreasing bulk flow velocity.

3-3 Indicators of flashback onset

In the previous sections, the BLF phenomenon has been described. Flashback has a rapid and abrupt nature. Hence, indicators announcing the event provides extra time to interfere with the flame to stop further development of flashback. This section therefore discusses the average flame profile and transient phenomenon. These flame properties can be used as indicators for the onset of flashback.

Average flame profile

The flame angle might be an important parameter for indicating the onset of flashback [37]. This can be useful for inside a flashback prevention system. The prediction model for uncon-

fined flames, discussed in section 3-2, uses this flame angle to determine the flow velocity at flashback.

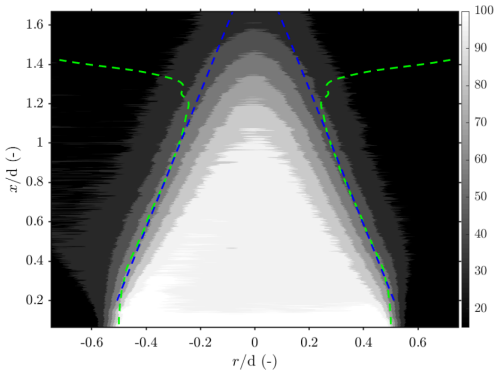

Figure 3-9: Average flame front surface indicated by the green lines and linearized average flame profile indicated by the blue line. Adopted from Faldella [7].

In the work of Faldella [7], Mie-scattering measurements were used to determine the flame front location and shape. An image of the determined average flame front can be seen in Figure 3-9. If the orientation of the flame front is perpendicular to the axial direction, the flow will experience the strongest acceleration through the flame front. The acceleration of the flow induces an adverse pressure gradient, affecting the incoming flow. As the flame condition moves towards flashback, the flame angle increases. The flame front is therefore on average closer to the burner exit. At this location, the flame-flow interaction is stronger and incoming flow is retarded even further. This increases the risk on flashback.

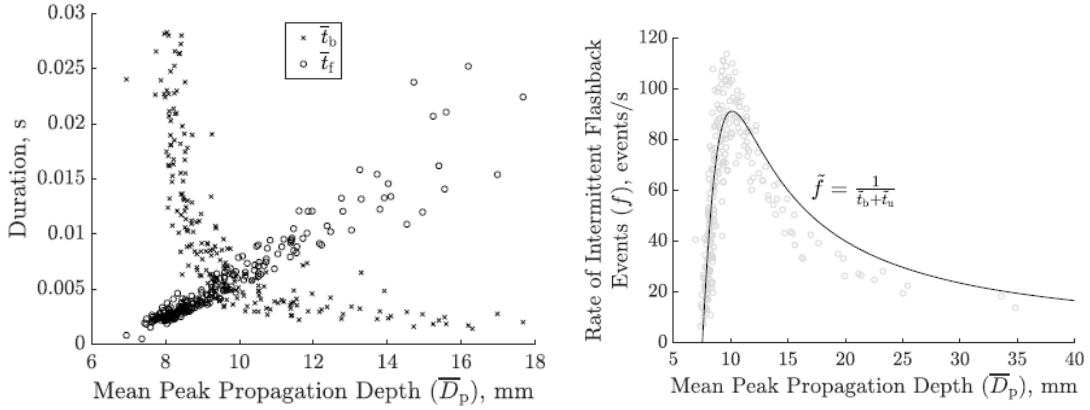

(a) Average time the flame spends inside $\bar{t}_f$ and outside $\bar{t}_b$ the premix area as a function of mean peak propagation depth $\bar{D}_p$.

(b) Rate of intermittent flashback events f as a function of mean peak propagation depth $\bar{D}_p$.

Figure 3-10: Link between intermittent flashback events and propagation depth. Adopted from Schneider [12].

Transient phenomenon

In the work of Schneider and Steinberg [12], they studied the flame behavior at conditions,

approaching flashback. For fuel-lean premixed swirl flames in a central bluff-body flame holder, they investigated the statistics of the flame dynamics. They captured the flame and flow development with high-speed OH^* chemiluminescent and PIV images for multiple flow configurations. The propagation depth and duration of the intermittent flashback event were offline statistically analyzed.

Figure 3-10a shows the two relations for the average time the flame spends in a certain section as a function of the mean peak propagation depth $\bar{D}_p$. One of the relations is for the average time spent in the premixing area $\bar{t}_f$ and the other relation is the average time spent outside the premixing area $\bar{t}_b$. It shows that the duration of an intermittent flashback event increases linearly with the depth of propagation. On the other hand, the time spends outside the premix zone between intermittent flashback events decreases hyperbolically with the propagation depth. These observations result in a general relation between the rate of intermittent flashback events f against the mean peak propagation depth $\bar{D}_p$. The relation is described by $\tilde{f} = (\tilde{t}_b + \tilde{t}_f)^{-1}$. In Figure 3-10b, this relation is plotted on top of the measurement data. A transition from fast shallow depth flashback events to slow deep flashback events is present at $D_p \approx 10mm$.

Apart from the characteristics of the intermittent flashback events they also took a closer look at the influence of operating conditions. In Figure 3-11a, the mean peak propagation depth $\bar{D}_p$ is plotted against the equivalence ratio of hydrogen ϕ_{H2} for different methane mixtures ϕ_{CH4}. The propagation depth remains small until complete flashback. In Figure 3-10b, the rate of intermittent flashback events f is also plotted against the equivalence ratio of hydrogen ϕ_{H2}. Interestingly, the maximum rate of intermittent flashback events is reached at lower equivalence ratios of hydrogen conditions than the complete flashback conditions. This may be a useful early warning sign for flashback.

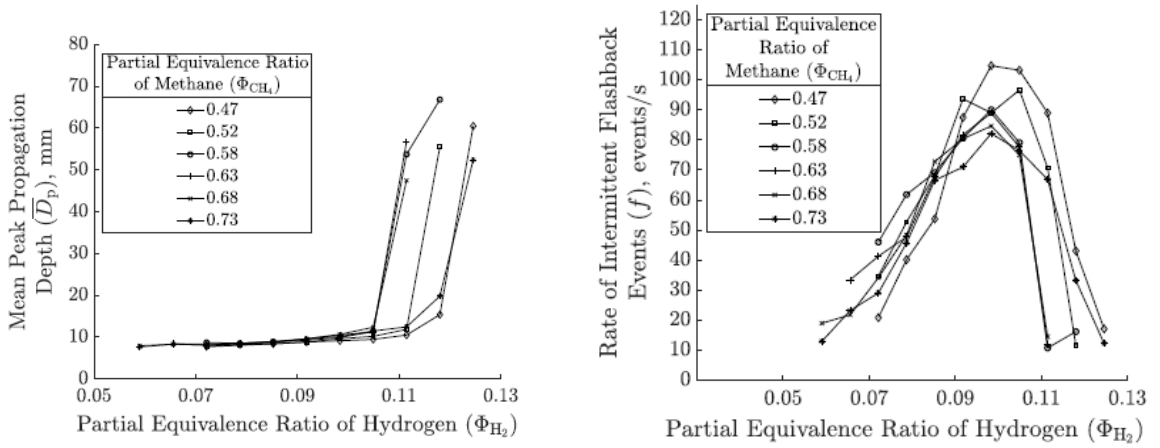

(a) Mean peak propagation depth $\bar{D}_p$ against the equivalence ratio of hydrogen ϕ_{H2}.

(b) Rate of intermittent flashback events f against the equivalence ratio of hydrogen ϕ_{H2}.

Figure 3-11: Effect of fuel composition on intermittent flashback properties. Adopted from Schneider [12].

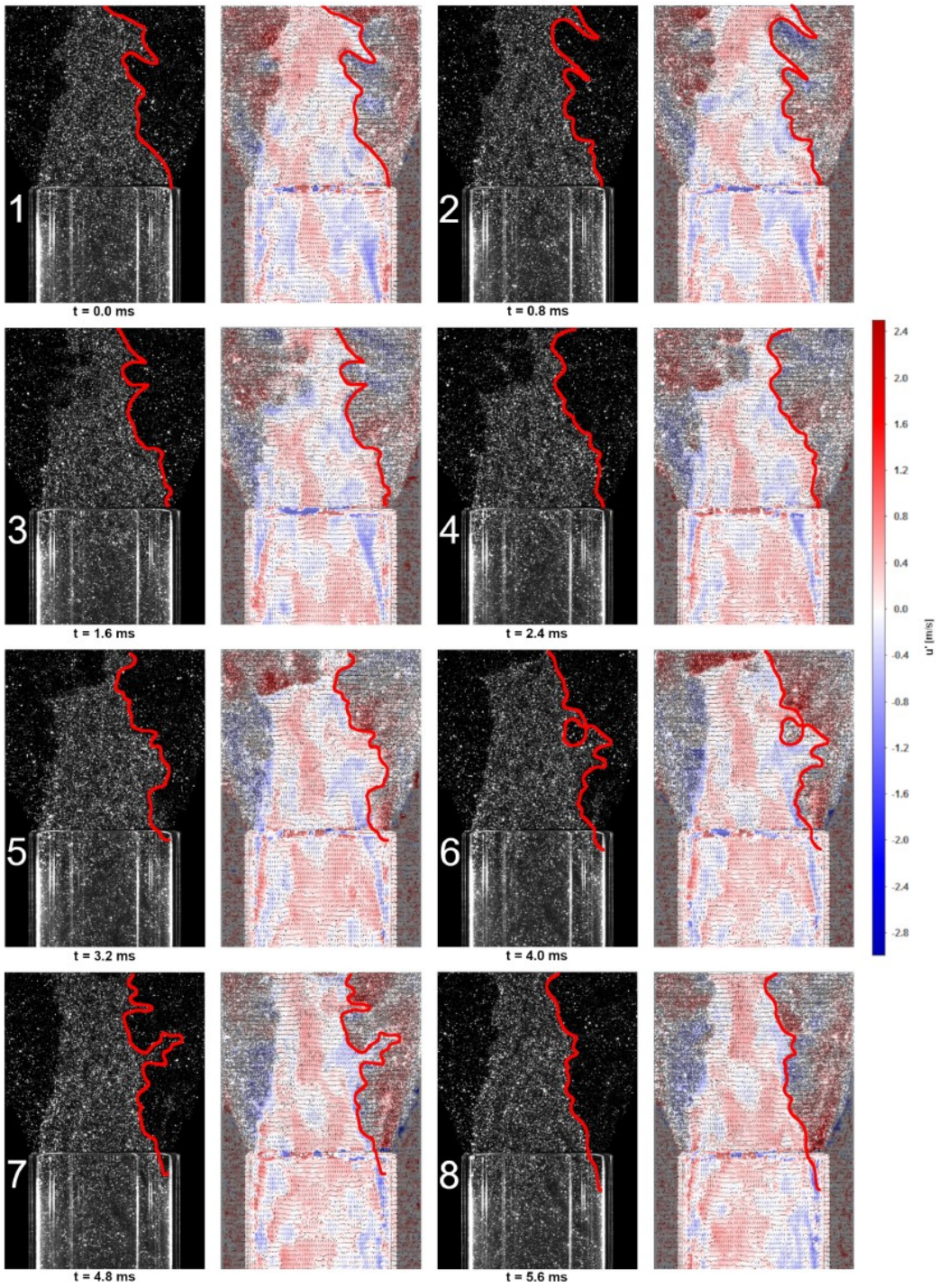

Figure 3-12: Time sequence of images visualization of the transient during the flashback process for an lean unconfined flame operating with 100% hydrogen and $\phi = 0.4$. The time interval between each image is 0.8 ms. The flame front at the side of flashback is highlighted in red. Each time frame consist of a pair of images, with a Mie-scattering on the left-hand side and the corresponding axial velocity fluctuations u' on the right-hand side. Adopted from Willems [13].

Part II

Measuring flashback: detection and precursors

Chapter 4

Flame analysis

In the previous section 3-3, discussed the potential of measuring the flame front continuously for flashback prevention. Both the flame location and fluctuations might provide indicators for the onset of flashback. Theretofore, sensors are required to collect data about the current state of the flame and/or the approaching flow. In this chapter, different sensors are evaluated for their abilities to detect and predict flashback. First, the different flame properties are described, which can be exploited to gather information about the undefined state of the flame. In the second section, the main test setup is described. Then for each sensor, the working principles, testing principles and data analysis are explained. In the last section, all sensors are compared to choose the most appropriate sensor.

4-1 Extracting data from flames

Fire is different from other matter in the universe. In the era of the agent Greeks, fire was considered as an element. Since fire consists of different chemicals in different states, this assumption is incorrect. The chemical combustion reaction between oxidizer and fuel results in a heavy reaction. This reaction is exothermic, so heat is released. The hot gasses in the reaction zone are visible as flames and emit light. The flame's heat is hot enough to ionize atoms, which is also the case in plasma [44].

The three basic ingredients for fire to exist are fuel, oxygen, and heat. Therefore, the flame ingredients should be sustained otherwise the flame extinguishes. For measurements, sensors cannot be attached directly to a flame because of the flame's abstract nature. Measurements can only be done indirectly. Multiple physical principles can be exploited to get information about the state, location, and presence of the flame and flow. Commonly used sensors for combustion monitoring in gas turbine are thermocouples, optical sensors, and dynamic pressure sensors [45]. Table 4-1 shows the different possible options for the physical and chemical properties of fire that can be measured with currently existing sensors. Four promising properties are identified.

Table 4-1: Morphological overview of the physical mechanism of the flame that can be exploited by sensors to gather information about the flame.

Mechanism	Free radials	Heat release	Pressure	Chemiluminescence
Sensor options	Ion sensor	Thermocouple	Microphone	Photodetector

The first mechanism in the table is free radials present during the reaction by the ionization of particles. As shown before in Figure 2-3, the reaction consists of many chain reactions and in this process hot gases are able to ionize atoms and the free electrons, that are shortly present, can be detected by ion sensors.

The second mechanism exploits the exothermic nature of the reaction. Heat is produced and is emitted in the form of radiation. The radiation heat can be sensed by heat-sensitive sensors, such as thermocouples.

The third mechanism is the acceleration of the hot gasses across the flame front. The heat accelerates the flow and this generates a pressure difference, which can be measured by a pressure transducers or microphones.

The final mechanism is the emitting of light, in the form of electromagnetic waves, by the chemical reaction. The fuel composition of the fire affects the electromagnetic radiation, emitted by the flame. If the frequency of the electromagnetic radiation is in a specific band, it is visible for the human eye. There exists a wide range of light-sensitive sensors, that capture different parts of the light spectrum. An array of these photosensitive sensor points form an imaging sensor. The image output of these photo-sensitive sensor can be analyzed to get information about flame position and angle.

4-2 Experimental setup

The sensors are tested on the setup located in a combustion lab at the TU Delft. A schematic overview can be seen in Figure 4-1. Further details can be found in Appendix A. The main setup was previously used in another master thesis project from [7], [37], [13]. The fuels, natural gas and hydrogen and oxidizer, air, are line supplied. The flow of these gasses are indivually controlled by three mass flow controllers. The fuel mixture and oxidizer are mixed upstream. The mixture flows through the burner pipes and it is ignited at the burner exit. The exit of the base burner is a simple copper tube with an outer diameter $d_o = 28mm$. To accommodate a collection of different sensor configuration and interchange them easily, a compression fitting is installed on top of the main setup.

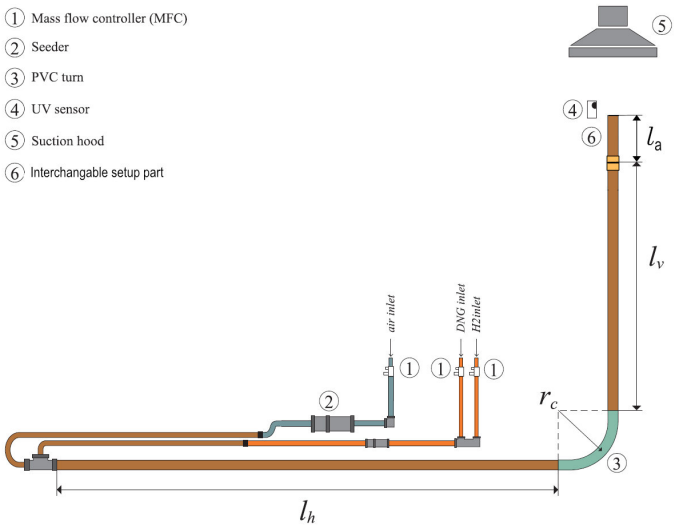

Figure 4-1: Schematic view of the burner setup in the experimental facility. Modified image of Faldella [7]

4-3 Sensors

The proposed sensors are evaluated for their abilities to detect and find precursors for indicating flashback onset by measuring the related property of the flame. The sensors are discussed with the following structure. Firstly, the working principle of each sensor is explained. Then a hypothesis is formulated on the expected use of the sensor. Next, the sensor setup design and test method are discussed. The test setup can run at different operating conditions. The system variables are the Reynolds, stoichiometric ratio of the fuel and air mixture, and the hydrogen content of the fuel. In previous experiments performed on this setup, the stoichiometric value and hydrogen fuel content was mainly constant, so only the Reynolds number was varied. As a starting point, the same procedure is used in this research by taking the Reynolds as the varying parameter and keeping the other variables fixed. The flame is operated at stoichiometric conditions ($\phi = 1$) and the fuel contains 100% natural gas.The combustion reaction of natural gas is less reactive than fuel mixtures containing hydrogen. Therefore, the use of nature gas makes it simpler to investigate the flame for precursors. In the case some indicator are found, their efficiency could be demonstrated under different conditions to support the claim.

4-3-1 Ion sensing sensor

Working principle

During the combustion process, the energy in the elementary reactions becomes large enough to ionize some molecules [46]. This ion production is called the chemi-ionization process. From the complex reaction schematic of methane, previously shown in Figure 2-3, not all reactions contribute equally to the production of ions. Calcote [47] showed that ionization occurs only in the thin reaction zone. This ionization cannot be explained by thermal ionization. After the reaction zone the temperature remains high, but the ion concentration drops. He proved that the mechanism in reaction equation in equation 4-1 is the key reaction for the presence of free ions in hydrocarbon flames. The high concentration of ions in the reaction zone is a useful property to locate the flame front by measuring the flame conductivity. Although the reaction in equation 4-1 is the main contributor to the ion production, the ion CHO^+ is not dominantly present. The ion is the ion is faster consumed by the reaction in equation 4-2 than produced [46]. For this reason, H_3O^+ is more abundantly present. This ion is in turn converted into the molecules via the recombination reaction in equation 4-3.

$$CO + O \rightarrow CHO^* \rightarrow CHO^+ + e^- \tag{4-1}$$

$$CHO^+ + H_2O \rightarrow CO + H_3O^+ \tag{4-2}$$

$$H_3O^+ + e^- \rightarrow H_2O + H \tag{4-3}$$

The property of flame ionization is already used as a safety measure in many central heating systems to detect if the fuel has been ignited. If the gas valve has opened, the flame rod should detect the flame conductivity within a couple of seconds. Otherwise, the gas valve closes again and the process repeats until the fuel has been ignited successfully [48].

In the work of Thornton et al.[49], they describe the basic working principle of a 360 degrees circumferential sensing sensor. An illustration of the sensor working principle can be seen in Figure 4-2a. Two isolated electrodes are placed in the premix area at the end of a central bluff-body. The electrode most upstream is called the *sense* electrode and the most downstream electrode is called the *guard* electrode. The cathode is connected to the electrodes and the anode is connect to the burner tube. If a voltage is applied to both electrodes, current can flow from the electrode through a flame to close the circuit. Signal data from their experiment can be seen in Figure 4-2b. The guard electrode measures the presence of the flame during stable conditions, whereas the sense electrode has only a significant ionization current output during intermittent flashback events. Since electric field lines do not cross, the presence of the guard electrode in front of the sense electrode block the excess of the potential gradient lines of the sense electrode to the combustion section. In the second part of the signal graph, a voltage is only applied to the sense electrode. The output signal of the sense electrode is significantly higher as the electrode can detect the flame in the combustion zone.

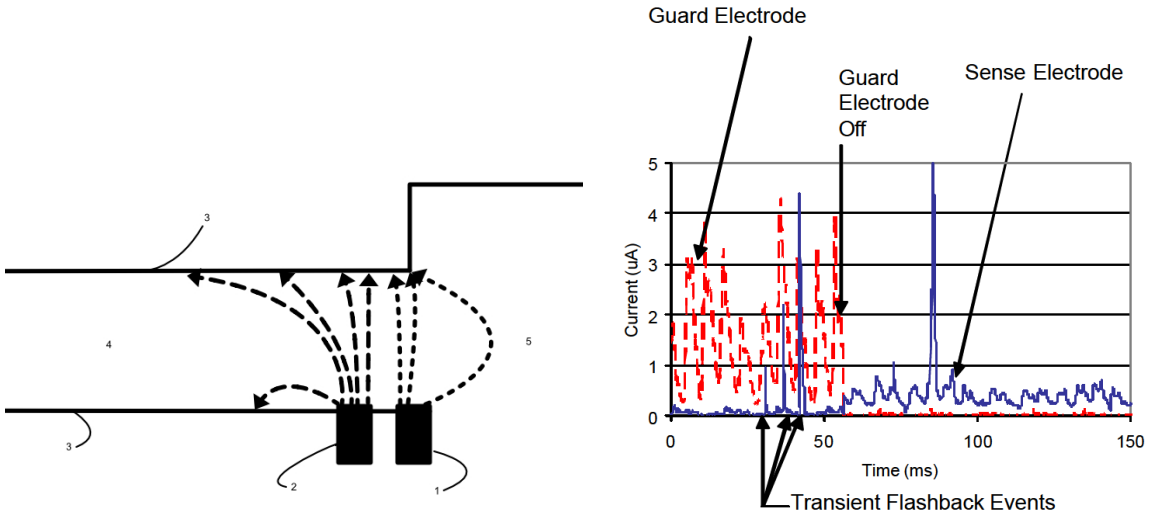

(a) Ion sensor, based on work of [49][50][51], where (1) is the guard electrode, (2) is the sensing electrode, (3) is the burner tube, (4) is the premixing section, and (5) is the desired flame region or combustion zone. The dotted lines represent the electrostatic field lines.

(b) Signal plot of both guard (red) and sense (blue) electrode. Adopted from [50].

Figure 4-2: The ion sensor

This sensor can fulfill three types of functions [51]:

1. The signal from the guard electrode can be used to determine if a flame is present in the main combustion. This is either useful during startup to detect the successful ignition or during operations to detect blown out under fuel-lean conditions.

2. The guard electrode can also detect the onset of dynamic pressure oscillations as the variation in flame ionization is proportional with pressure fluctuations.

3. The signal of the sense electrode detects flashback and intermittent flashback events.

A disadvantage of this sensor is the low signal magnitude. In [51], the magnitudes are in the order of 10^{-6} to 10^{-4} Ampere. Amplifying the signal with an operational amplifier can enhance the signal strength. In Cheng et al.[52], the ionization of hydrogen flames was almost negligible, but the signal became apparent with the addition of hydrocarbons. Ongkiehong [53] stated that the conductivity of hydrogen flames is very low in the order of $\kappa = 10^{-12}\Omega^{-1}$, but in addition of a small amount of organic material the conductivity increases. Holm [54] found that the signal strength of the sensor decreases by increasing the hydrogen content in the fuel mixture.

Hypothesis

In section 3-3, the rate of intermittent flashback events was an indicator for the onset of flashback. If these intermittent flashback events could be measured, the rate of the events can be related to the change of flashback. It might be a precursor for indicating the occurrence of flashback. The ion sensing sensor could fulfill task. The sense electrode detects flames entering the premixing section. Therefore, the hypothesis is that the ion sensor can detect intermittent flashback events in operation conditions to predict the onset of flashback.

Design

In Figure 4-2a, the guard and sensing electrodes were installed in the center body of a burner. However, the setup for this project, described in Section 4-2, does not have a central bluff-body. The electrodes are instead attached to the burner rim. An idea for the sensor design is sketched in Figure 4-3a. It is called a *spekkoek* configuration since the electrodes are stacked with layers of insulation in between. The two positive electrodes fulfill the task of the guard and sense sensor with a common ground. The electrodes are electrically insulated from each other to prevent a short circuit. A clamp connection holds the setup together. The construction is connected to the burner via a screw thread.

For testing, the design is simplified by using two electrodes. The ion sensor is built from a drilled-out compression fitting and was clamped on top of a piece of copper tube. The cathode is attached to a body ring and the anode is attached to the copper tube. To electrical insulate the two metals from each other, a single sheet of Novamica THERMEX is used [55]. The use of Mica has two main advantages. Firstly, it has a high electrical resistance and secondly, it can withstand heat up to 1000^oC. Silicon kit is used to glue the parts together. This glue has also high thermal resistance and it cannot conduct electricity. The final test sensor setup can be seen in Figure 4-3b. The wires diagram is shown in Figure 4-4. A direct voltage $U_b = 30V$ is applied to the circuit. When a flame enters the tube, electrons can conduct through the flame from the anode to the cathode. This generates a small current in the loop. This current is converted to a voltage as the data acquisition device (explained in Appendix A) reads out voltage data. Current is converted to a voltage signal by measuring the induced voltage drop over a resistor. Applying a voltage of 30V results in a current in the order of $I = 1\mu A$. If the voltage drop should be mapped to $U = 1V$, a resistor of $R = 1M\Omega$ is required, according to Ohm's law.

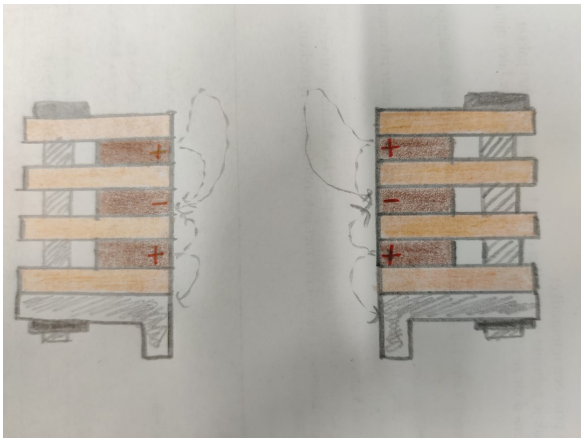

(a) Sketch of the cross-section of the "Spekkoek" configuration for the electrodes of the ion sensor. The brown parts are the electrodes, the orange are the insulating layers, the gray parts are the metal connections. The dotted lines are the potential gradient lines of the current. When an ionized flame front is present, negative charge can travel from negative to the positive electrode.

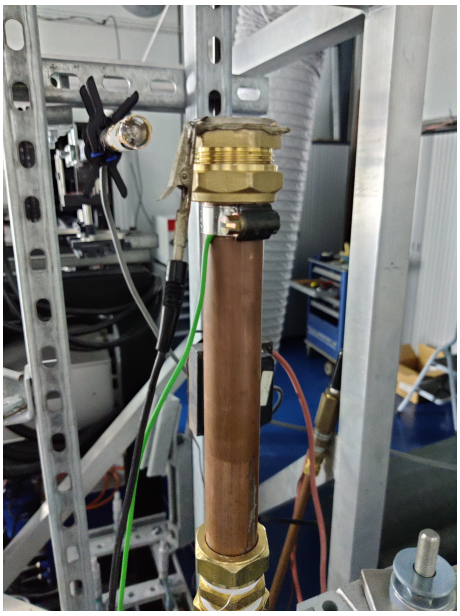

(b) Image of the ion sensor. The green cable connects the anode to the copper tube. The black cable connects the cathode to the body ring on top of the setup.

Figure 4-3: Ion sensor design and setup

Method

To test the ion sensor, flashback is triggered by reducing the Reynolds number from a stable region to critical conditions. The experiment is recorded to analyse the behavior of the sensor.

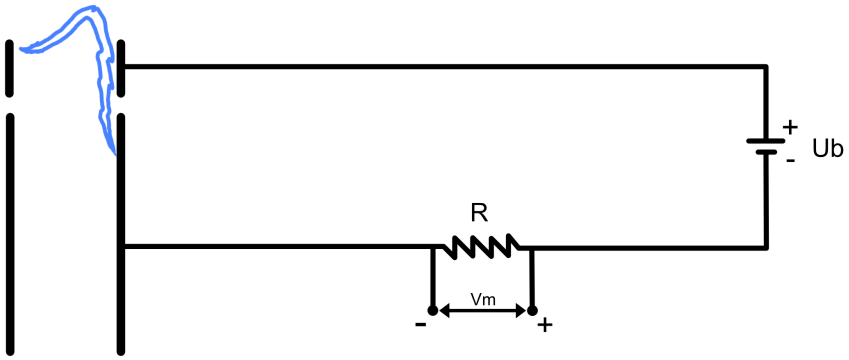

Figure 4-4: Wiring diagram of the electrical circuit of the ion sensor.

Results

The result of one of the ion sensor test is shown in Figure 4-5. At time $t = 14.5s$, a high peak is visible in the data, which indicates the flame passing the sensor. During the non-flashback conditions, a stationary sinusoidal noise of $0.2Hz$ is present in the data.

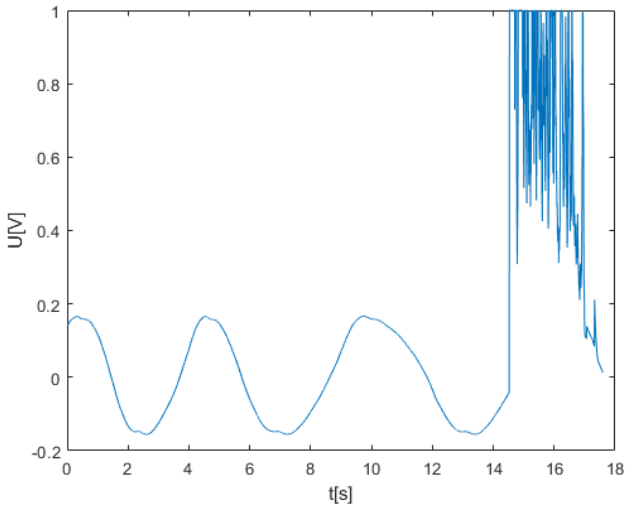

Figure 4-5: Result of testing the ion sensor with burner operating at 100% natural gas flame and $\phi = 1$.

Conclusions

The results show that the ion sensor can detect flashback. However, no intermittent flashback events are detected, so the hypothesis is not true. The flame only enters the tube during the full flashback event. As mentioned in the previous Chapter 3, the work of Schneider et al. [12], they used a swirl burner with a central bluff-body, where the flame is behaving differently. The flame behaves more like a confined flame as flame-flow interaction has a stronger effect, so the flame can move in the axial direction. Therefore, the ion sensor is probably more suitable for detecting the movement of confined flames. Also mentioned in that chapter, the quartz tube research of Willems [13] revealed that there are no transient flashback events observed for unconfined flames. The ion sensor cannot capture the instability of the flame, but it can detect flashback. Since one sensor detects the entire 360 degrees circumferential, it cannot distinguish the flashback location. For the sinusoidal noise is no clear explanation. It might be a disturbance in the measurement circuit or a slow oscillating motion in the approaching flow, but further research is required to pinpoint the real cause.

4-3-2 Thermocouples

Working principle

Thermocouples are heat-sensitive devices and are the most common method for measuring temperature [56]. In the industry, they are often applied for flashback detection [45]. However,

they have two disadvantages. Firstly, the sensor measures the temperature only at one specific point. Secondly, the sensor's mass takes time to heat up, so the response time has a delay. They consist of two different electrical conducting joined metals [57]. The connection between these two alloys is called the junction and can be made by different methods such as welding and soldering. Different types of junctions exist: insulated, grounded, and exposed as shown in Figure 4-6a [58]. The exposed junction offers the fastest response time, but the exposed tip limits the robustness. Therefore, a trade-off is made between response time and durability. The response time of an exposed junction is shown in Figure 4-6b, the smaller the tip the faster the response. The junction produces a temperature-dependent output voltage. The relation between these two is dependent on the materials and it is expressed by the Seebeck coefficient $\alpha_{AB} = \Delta U/\Delta T$ [56].

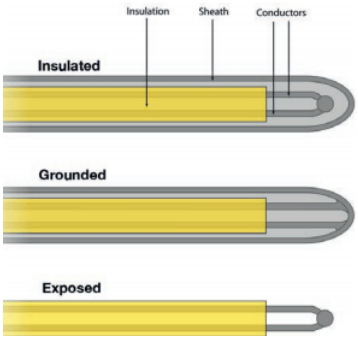

(a) Different types of thermocouple junctions. Adopted from [58].

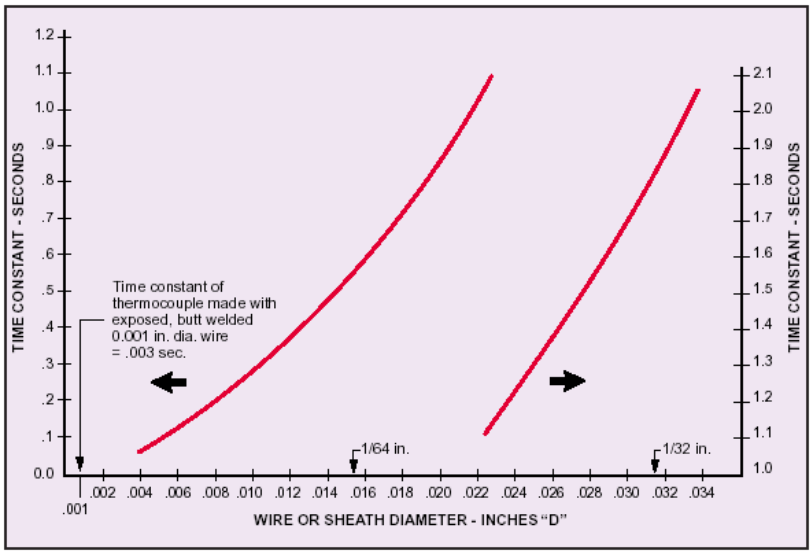

(b) Response time of a typical exposed junction at the left and grounded junction at the right for different diameters. It is defined as the time required to reach 63.2% of an instantaneous temperature change. The thickness 0.004 inches corresponds approximately to a thickness of 1 mm. Adopted from [59].

Figure 4-6: Thermocouples types of junctions and their response times.

Hypothesis

In section 3-3, different indicators for the onset of flashback are formulated. The effect of change in average flame shape and flame fluctuations might be detectable detected with thermocouples to indicate flashback onset. Therefore, two hypothesis are formulated:

- The thermocouples measure higher temperatures when the flow velocity is reduced. The increased temperatures can be related to the decrease in the average flame angle.
- The thermocouples can measure the flame's time constant because more fluctuations are observed as the flame approaches the flashback point.

Design

Multiple types of thermocouples are available, which differ in material composition, sensitivity, and temperature range. The K-type thermocouple is a combination of r-Nickel-10% chromium for the cathode and nickel-5% aluminum and silicon for the anode. This thermocouple is used in this research for three reasons. Firstly, it has a wide temperature range (-270^oC to 1260^oC). Secondly, it is reliable and thirdly, it is accurate [56]. If multiple thermocouples are used, they can be aligned in different configurations, for example:

- By placing the thermocouples in line along the tube, the position of the upstream propagating flame can be determined.
- By placing thermocouples in a 360^o configuration around the burner rim, the effect of the wiggling flame can be detected. If the flame tip moves from one side to another, one sensor will cool down as the other will heat up. Furthermore, the flashback location can be detected since at this location the sensor heats up first.

For this design, the 360^o configuration is chosen to test the hypotheses. The thermocouples used in this experiment are exposed K-type thin 0.3 mm thermowires isolated protected by an optical fiber sleeve, which sleeves can withstand temperatures up to 400^oC. According to Figure 4-6b, this thickness corresponds to a time response of $300ms$. Although, this time scale is slower than the flashback time scale, the temperature change is more relevant than the exact temperature. The built 360^o configuration is shown in Figure 4-7. Four small holes are drilled 2 mm below the burner rim approximately 90^o separated from each other. The holes are sealed with silicon kit. The tip of the thermocouples should stick out as little as possible because both the flow can be disturbed, and the flame can hatch to the thermocouple instead of the rim.

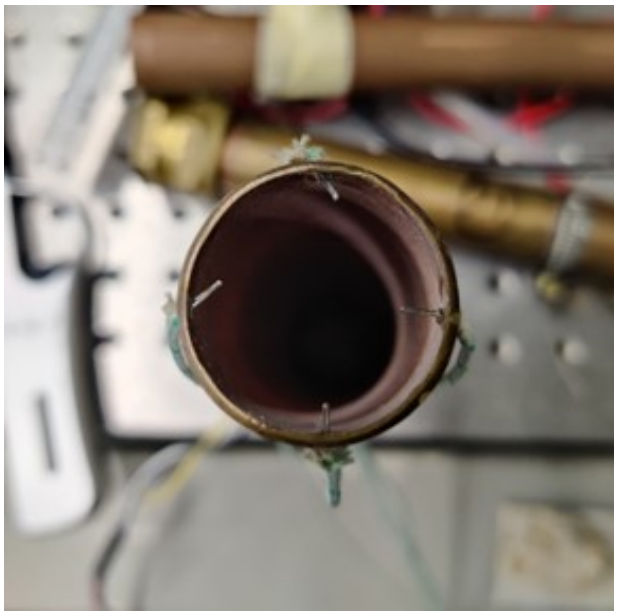

Figure 4-7: The built 360^o thermocouple configuration. The thermocouples are distinguished by their cardinal location on the tube. The northern thermocouple is at the top side of the image, the eastern thermocouple is at the right side of the image, etcetera.

Method

To obtain the required information to test the hypothesis, multiple experiments are conducted to collect the data. Two sets of experiments can be considered. During the first set, the flow speed is reduced in small steps of 100 Reynolds to bring the flow from stable to flashback conditions. Between each step, the flow got time to converge. During the second set, the Reynolds was set at different constant values for the Reynolds number for each experiment. This way measurements are less influenced by the transfer phenomena to limit disturbances. The sampling rate is set to 50 Hz for most experiments to achieve maximum sampling with four thermocouples. A couple of experiments are also conducted with fewer thermocouples to enable higher sampling rates.

Results

The experimental results are presented in this section. The measurements are both visualized and analyzed in the time and frequency domain to get different inside in the data.

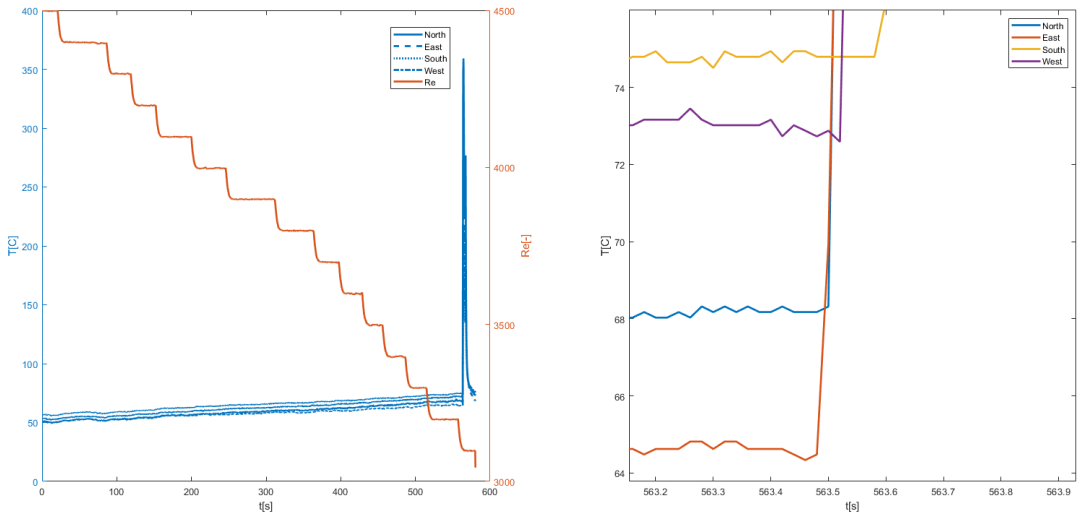

(a) The temperature profiles for the four thermocouples are shown in blue. They are indicated with cardinal points to indicate the position on the burner. The temperature is sampled with 50 Hz and is plotted as a function of Time for a 100% natural gas flame at stoichiometric conditions. The Reynolds is reduced in steps from 4500 to 3100, shown in red. The flashback peak is visible.

(b) Zoomed in on the temperature at the flashback time point. The flame flashed back at the eastern thermocouple since this sensor was the first to increase significant in temperature.

Figure 4-8: Temperature plots of a flashback experiment with thermocouples.

Time vs Temperature

Figure 4-8a shows a typical temperature profile behavior for the burner approaching flashback. All sensors measured an increased temperature as the Reynolds reduces. The flashback peak is visible at 563.5 seconds. If zoomed in on the temperature around the flashback time point

in Figure 4-8b, the thermocouple in the eastern position was the first to increase rapidly in temperature. Flashback, therefore, occurred probably at that side.

Reynolds vs Temperature

In Figure 4-9, the measured temperatures as a function of the Reynolds number are shown. If the flow's Reynolds number was reduced, the temperature increased slightly. A small spread in the temperature is present at each Reynolds point. This variance is investigated further in Figure 4-10. The variance is taken for a window size of 100 samples. The second-order curve fitted on this data shows a minor increasing trend for the variance as the Reynolds number was reduced. The flashback event is clearly visible as the variance speaks out of the domain. Furthermore, reducing the Reynolds number resulted in a temporarily increase of the variance.

When the variance is average at for a given Reynolds number set-point, it results in Figure 4-11. Here, a second-order fit on the data shows a parabolic trend with higher variance for Reynolds numbers far away and close to flashback conditions.

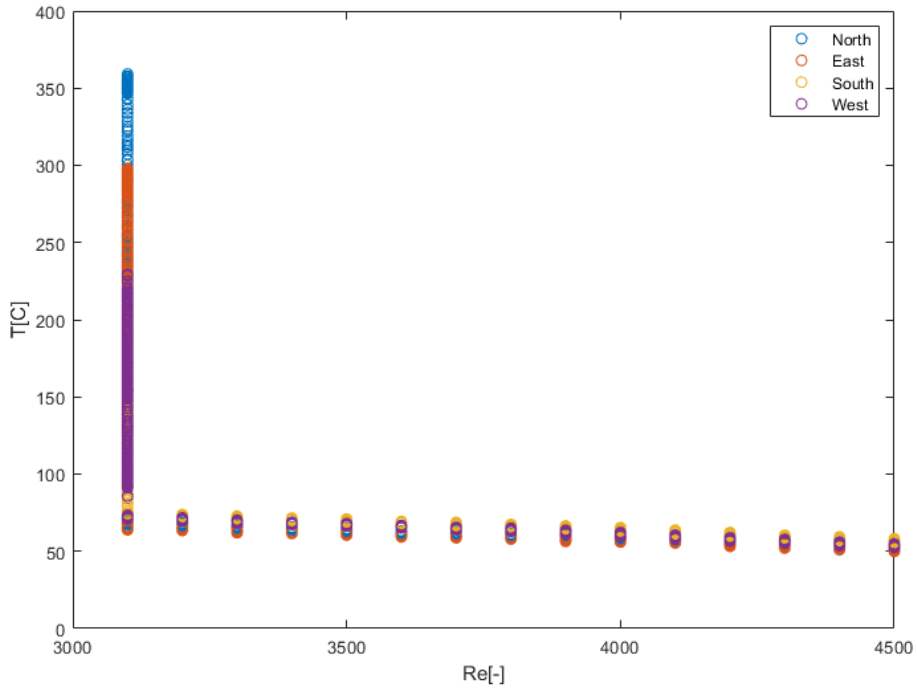

Figure 4-9: Temperature as function of Reynolds number for the four thermocouples.

Correlations

Apart from verifying this with the variance it is also interesting to look into the correlation of the sensors. The correlation indicates if there is a relation between the change of one variable compared to another. In Table 4-2 the determined correlations for one experiment are shown. All off-diagonal values are close to one, so the sensors are highly correlated.

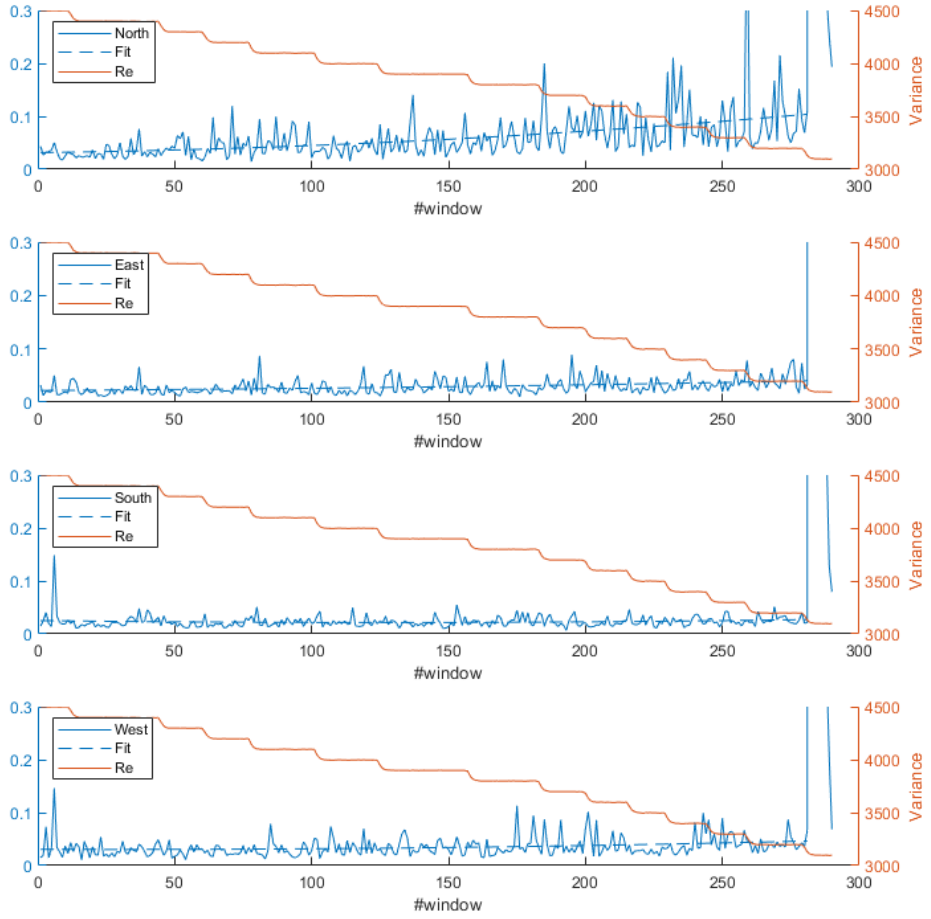

Figure 4-10: Variance of the temperature data for the four thermocouples with a window of 100 samples is plotted in blue. A second order curve fit is added on top of the variance. The Reynolds is plotted in red.

Reynolds vs Frequency

In the time domain, the signal change over time is analyzed, but the frequency domain might also give data inside. Figure 4-12a shows the frequency content in the data. This data is recorded from an experiment where the burner is operated at three different constant Reynolds numbers: far from flashback (Re=4500),closer to flashback (Re=4000), and critically close to

Table 4-2: Correlation of temperature data for an experiment up to flashback.

1.0000	0.9953	0.9971	0.9967
0.9953	1.0000	0.9954	0.9936
0.9971	0.9954	1.0000	0.9983
0.9967	0.9936	0.9983	1.0000

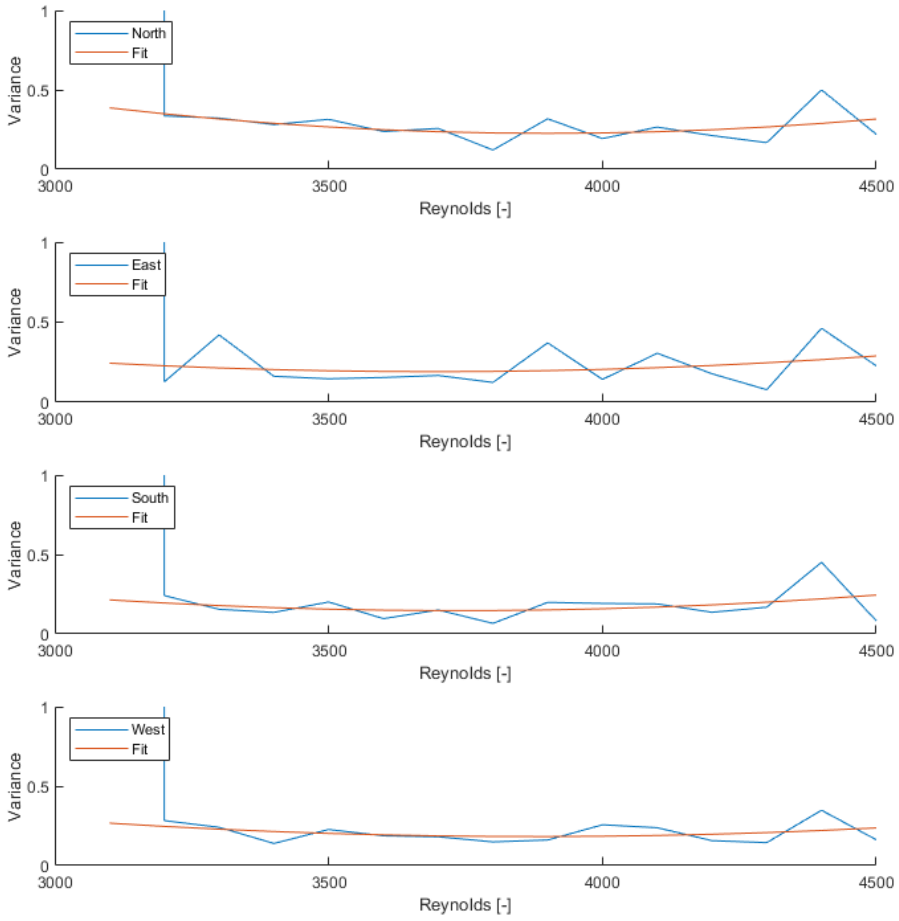

Figure 4-11: Variance of the temperature for all data with the same Reynolds number set point. A second order fit is added on top of the data. The flashback event occurred at Re=3200.

flashback (Re=3300). A 256-point symmetric Hamming window filter is applied to the data. The data is highly correlated, resulting in a large overlap. No significant frequencies popped up when comparing conditions far and close to flashback.

Spectrogram

A spectrogram is shown in Figure 4-12b. The window overlap is 50% and window size is $2^8 = 256$ samples. This graph visualizes the frequency content of the signal at each time step. The flashback event is clearly visible as the bright frequency band at the end of the experiment. Up to flashback, no particularity frequencies are present as the frequency signal is rather uniform.

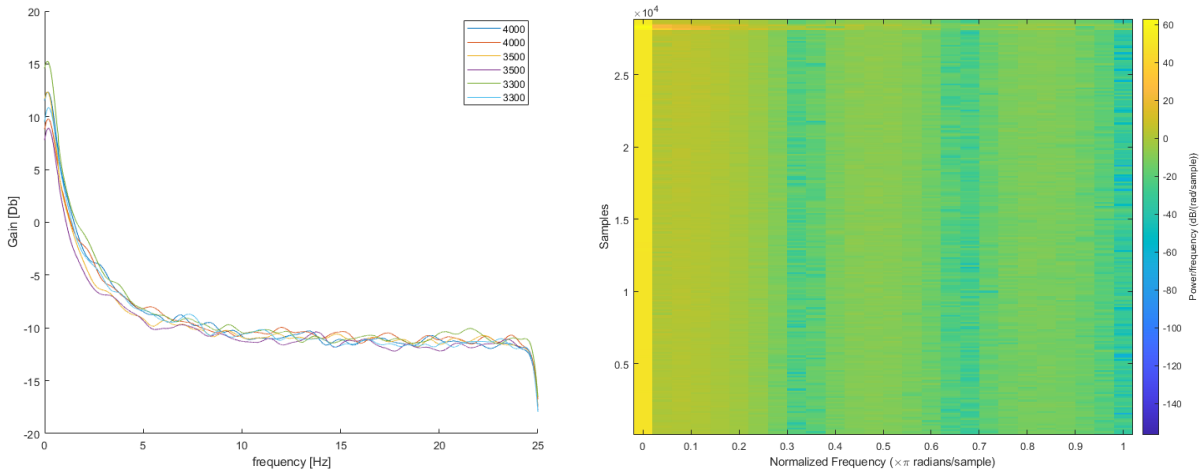

(a) Frequency plot of the thermocouple data. The experiment are repeated twice, where burner is operated under conditions far from flashback (Re=4500), closer to flashback (Re=4000) and close to flashback (Re=3300).

(b) Spectrogram with window size of $2^8 = 256$ samples and an overlap of 50%. The flashback event is clearly visible as brighter horizontal line. During this flashback experiment, the flow was reduced from 4500 to 3200 Re.

Figure 4-12: Frequency analysis of thermocouple data.

Reynolds vs flame angle

The relation between the flame cone angle and flow velocity is determined from a flashback experiment where the flow velocity was reduced step by step. From images at different time instants, the flame angle and the corresponding Reynolds number was determined. The findings are plotted in Figure 4-13. A linear fit can be fit through the data points. The closer the average flame front moves towards the rim, the more heat is sensed by the thermocouples.

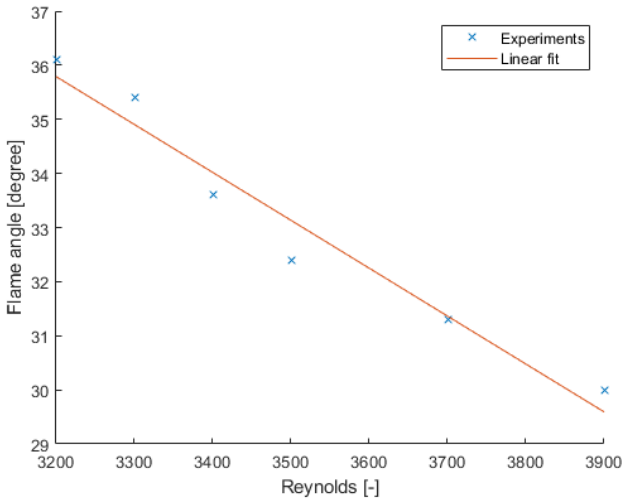

Figure 4-13: Reynolds vs flame angle shows a correlation between the decrease in flow velocity and increase in flame angle.

Conclusions

The thermocouple data have been interpreted in various ways to find indicators of flashback onset as proposed in the hypotheses. It has been observed that the measured temperature of each thermocouple is different. There are two possible reasons for this. Firstly, the thermocouples are not mounted at the same distance from the burner rim, and secondly, they could protrude differently among the different thermocouples. In the time domain, a clear sudden spike is visible, making it simple to distinguish from the burner in non-flashback conditions. Furthermore, the flashback location of the flame is determined with the four thermocouples in the 360^oC configuration. This can be useful for a local flashback prevention system, which requires the position of the tip of the upstream propagating flame front. The thermocouples are however highly correlated so extracting time constant of the flame wiggling is not possible.

A flame approaching flashback shows a slow temperature increase when the flow velocity was reduced. This can be explained by the relation between the flame angle and Reynolds number of the flow. If the flame angle increases, the flame front will move closer to the rim and more heat will be sensed by the thermocouples. By looking at the variance of the temperature data over time, a small but insignificant increase is observed. From the averaged variance at the same Reynolds number, it becomes apparent that the variance in the middle regime is the lowest and can be considered a stable region. Towards flashback and blow-off, however, the variance increases.

The frequency data did not show precursors indicating the onset of flashback. Thus, it is difficult to indicate exactly when flashback occurs.

4-3-3 Pressure microphone

Working principle

Pressure transducers and microphones can pick up the pressure fluctuations or change in static pressure. A pressure wave passing by the sensor deforms a pressure sensitive membrane. Pressure transducers are often piezoresistive strain gauges applied [60]. The pressure is measured as the resistance changes as a function of the applied strain.

According to Strahle [61], the noise in combustion systems noise arises from two effects. The first effect is the random motion of the turbulent working fluid in both time and space. This generates an unsteady pressure field. The second effect is caused by the temporal heat release fluctuations in the reaction zone, which generate pressure waves. These sounds are generally random in both frequency output and amplitude. However, it can be a phase-coherent fixed frequency oscillation in the case of combustion instabilities. The second effect is often the dominant factor. The noise product during the combustion of hydrocarbons is usually in the low frequency bands (20-200 Hz). These generated pressure waves can be picked up by a pressure microphone. The intensity of the pressure waves from the combustion noise is proportional to the surface fluctuations of the flame. It can therefore be a measure of the instability of the flame front [62].

To improve the signal bandwidth, the pressure pules can be guided through an infinity coil. This is a long thin tube damps out the pressure pulse, which prevents the reflection of the wave. Mounting a microphone inline of this tube reduces the influence of disturbances in

the signal to optimize the sensor's bandwidth [14]. A configuration used for combustion measurements in a gas turbine combustion chamber is shown in Figure 4-14.

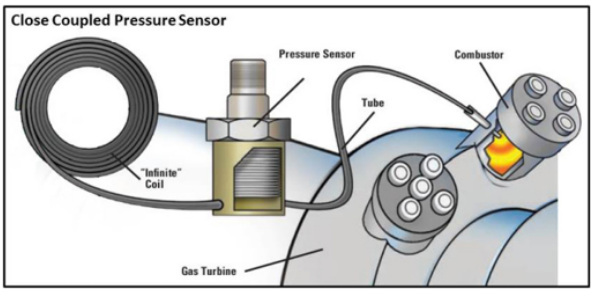

Figure 4-14: Concept of an infinity coil. Adopted from Christman [14].

Hypothesis

As previously discussed in section 3-2, backpressure is already found in confined flames before flashback occurs. The hypothesis is that the pressure sensor will measure a build-up of pressure. This pressure changes might indicate the onset of flashback. Furthermore, the noise of the signal might have different spectrum under different combustion conditions.

Design

Microphones are sensitive devices and care should be taken for their maximum allowable temperature. Flames passing the sensor can damage the sensor. Therefore, the microphone is mounted indirectly to the tube with an infinity coil configuration. The microphone is listens to all pressure waves entering this additional tube and pass along the sensor. The built setup is shown in Figure 4-15.

Figure 4-15: Infinity coil connected to the main burner with a microphone installed inline.

Method

To test the microphone multiple experiments are conducted with the described setup. The data acquisition device is operated at its maximum sampling frequency, 2000 Hz. The experiments are performed at different fixed Reynolds numbers from far away from flashback to close to flashback conditions. This done for conditions with and without flame to measure the background noise of the cold flow.

Results

The results of the experiments can be evaluated in both the time and frequency domain to get more insides.

Cold flow vs hot flow

The frequency spectrum for conditions with and without flame at a fixed Reynolds number are compared in Figure 4-16a. Here, the data is shown for $Re = 4200$. The signal peaks around 200 Hz. The hot condition has a higher signal strength for the low frequency region than the cold condition. This was also observed by Rajaram et al. [63].

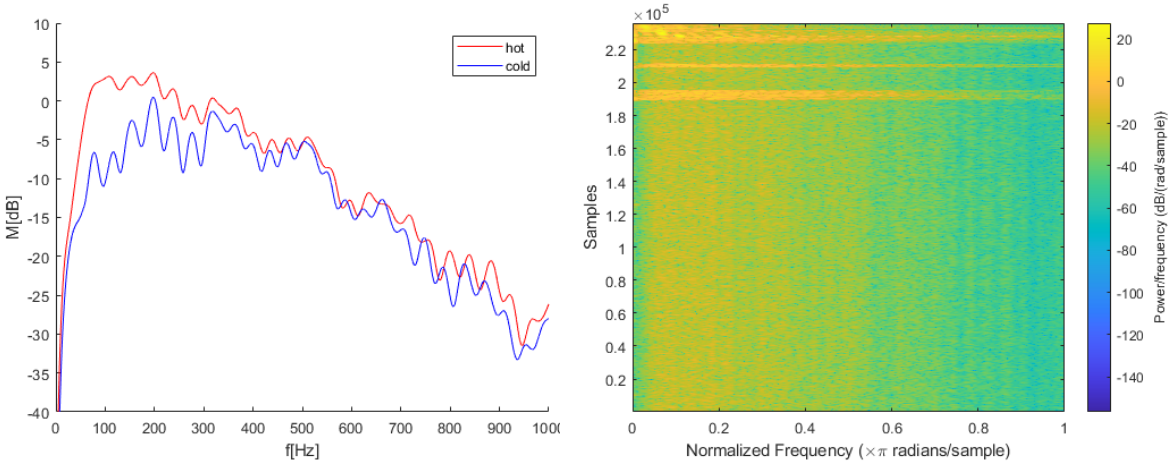

(a) Comparing the frequency spectrum of the microphone data for conditions with $Re = 4200$ for both conditions with and without flame (hot and cold). A hamming filter with a window size of 2048 is applied on the data after the FFT has been calculated.

(b) Spectrogram for conditions $Re = 3800$ and $\phi = 1$. The frequency is shown in normalized units and the samples is the window number. The window size is 2^8 and the overlap of each window is half a window.

Figure 4-16: Frequency analysis of microphone data.

Spectrogram

To analyze the frequency content of the signal at each time frame, the short-time Fourier transform of the signal is estimated. This estimate is visualized in a spectrogram and it shows an estimate of the frequency content for a certain time window. See Figure 4-16b.The flashback event is again clearly visible as the bright frequency bands at the end of the experiment. The frequencies developing towards flashback stays rather uniform so again no particular frequency band popped up.

Pressure signal

The signal from the microphone for conditions with flame far away from flashback and close to flashback are compared in Figures 4-17a and 4-17b respectively. The signal peak of the flashback event is clearly visible. The width of the sensor signal is wider in conditions far from flashback. This behavior is also shown in the average energy of the signals. The average energy is compared for multiple experiments at different Reynolds numbers with a hot flow, shown in Figure 4-18. The energy content of the signal reduces when the Reynolds number is reduced.

The experiments in conditions with and without flame in the time domain at the same Reynolds number, $Re = 3800$, are shown in Figures 4-17b and 4-17c respectively. It can be observed that at the same Reynolds number the flame has a wider signal strength. This indicates the flame produces more sound.

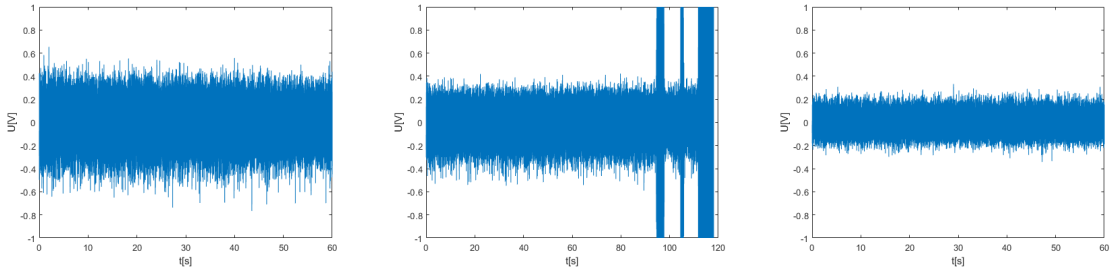

(a) Signal for experiment with flame far from flashback ($Re = 4500$, $\phi = 1$).

(b) Signal for experiment with flame at flashback conditions ($Re = 3800$, $\phi = 1$). The flashback peak is visible from time $t = 95s$.

(c) Signal for experiment with no flame ($Re = 3800$).

Figure 4-17: Signal from the microphone in three different conditions.

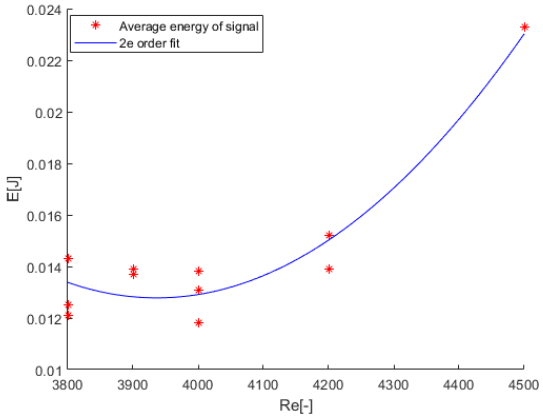

Figure 4-18: Average energy density for different experiments, where the Reynolds is varied between $Reynolds = 4500$ and $Reynolds = 3800$ under hot conditions. The average is taken over the signal up to flashback. A second order polynomial is plotted on top of the data.

Conclusions

The experimental results showed that the microphone can detect the flashback event. A clear peak is visible in the data. The power of the signal reduces for flames at lower Reynolds since the reduces flow speed produces less noise. The combustion reaction also produces noise since the signal power is higher for conditions with than without flame. Therefore, the average energy of the signal could be a measure for how far the flame is from flashback, since the average energy reduces towards flashback. However, the spectrogram did not contain indicators revealing the occurrence of flashbacks since no particular frequency pop-up right before the event occurred. The hypothesis is also invalid as the pressure build-up towards flashback was not detected.

4-3-4 Photodetector

Working principle

Optical sensors sense the presence of a flame in their directly observable surroundings. Daniele et al. [64] used a optical fiber in the premixing section to detect the flame. The advantages of optical sensors are the absence of direct contact with the flow and a fast response. However, measurements can only be done in a direct line of sight [49]. During the reaction, flames emit radiation in the form of Infrared (IR)($\lambda \approx 700$ to 10000 nm), Ultraviolet (UV) ($\lambda \approx 10$ to 400 nm) and visible light($\lambda \approx 380$ to 750 nm) [15]. The emission spectrum for hydrogen-air flames is shown in Figure 4-19. In the visible wavelength spectrum not much light is emitted. Most light is emitted in the UV or IR spectrum.

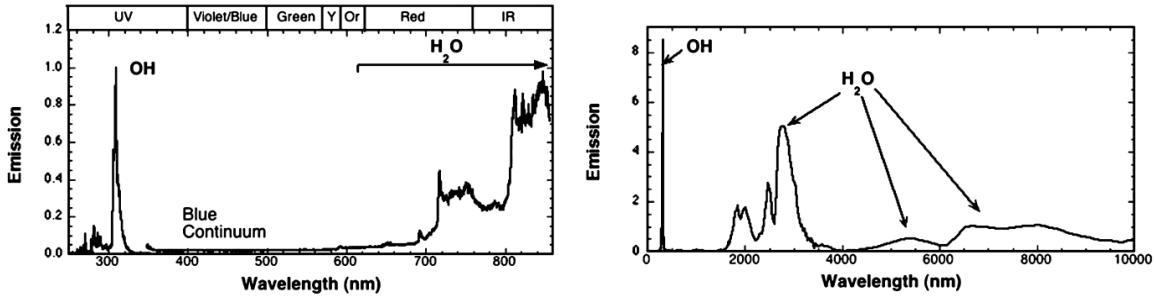

(a) Spectrum peaks for UV to near IR. It should be noted that the values in the near IR region are scaled by a factor 6.5 compared to the OH peak.

(b) Spectrum peaks for large infrared wavelengths.

Figure 4-19: The emission spectra of a typical premixed hydrogen-air flame. Adopted from Schefer et al. [15].

To measure the entire light spectrum, multiple sensors are required because a light-sensitive sensors are designed to measure only light in a specific bandwidth. MSA [65] recommend to combine multiple sensors to improve the performance of the optical sensor. For example by combining UV and IR sensitive detectors. This dual-band sensor can distinguish better between different types of flames and the reliability is improved against false alarms. This counteracts the degraded performance of a UV sensor in the presence of smoke, dirt or dust. Another advanced sensor is the Multi-Spectrum Infrared Flame Detector (MSIR), which is

sensitive to multiple frequencies in the IR domain. These sensors are tuned to detect a specific flame source and are immune to IR light patterns from other sources.

Design and method

If a light sensitive digital sensor array is used, such as a camera, the images from this sensor can deliver information about the flame. Algorithms can be developed to process the data to obtain information about the shape and location of the flame front. However, this requires post processing of the data. This requires computational time and can be slow in real time detection systems. Instead, a single light sensor was first tested with a single point measurement. This fire detection sensor is sensitive to light between $760nm$ to $1100nm$. This sensor is tested by mounting it close to the flame. The acquisition was done with an Arduino sensor.

Result

It was expected that with this sensor a light spectrum of the flame could be determined. However, the flame sensor's output is a binary value. It outputs one in the case a flame was present in the line of sight. Due to this binary nature, no precursors can be identified with this single sensor.

4-4 Sensor comparison

In the previous sections, the different sensors are tested in their capabilities to both detect flashback and find precursors, indicating flashback onset. The comparison is summarized in Table 4-3. All tested sensors can detect the flashback event. Since flashback occurs very abrupt and it has a high intensity, it is easily distinguishable from the non-flashback state.

Table 4-3: Comparison of the different sensors

Sensor	Features	Precursors		Detection		Remarks
Ion	Detects passing flame by electric conductivity	– –	No information prior to flashback	++	Clear detection	Can work well for CIVB flashback
Thermocouple	Measures temperature changes from heat by flame	+	Detect shift of flame angle	++	Clear detection	Relatively long time constant
Microphone	Sound spectrum	+/–	Change in spectrum intensity	+	Shift in spectrum	Better potential with advanced data processing
Photodetector	Light spectrum, only in line of sight	–	Binary signal	+	Detects if flame is at desired location	Better potential with advanced data processing and advanced sensors

The ion sensor cannot measure precursors, indicating the onset of flashback. The flame was expected to exhibit intermittent flashback events as in a swirl burner. Nonetheless, BLF occurs abruptly, so no information is available prior to a flashback event. A signal was only measured after the flame passing the sensor during a full flashback event. The flame produces an immediate signal response after flashback because electrons are rapidly conducted through a flame. This results in a short detection time of the fault. The sensor is also only sensitive to conducting flames, so it is insensitive to other heat sources in the environment.

Thus, the sensor is able to detect flashback, but cannot provide information about the onset of flashback. This detection may better work for CIVB flashback as the flame propagates less abrupt and has intermittent flashback behavior.

The thermocouple data reveals a clear sudden temperature spike in the case of flashback, making it simple to distinguish from the burner in non-flashback conditions. A flame approaching flashback showed a slow temperature increase when the flow velocity was reduced. This precursor is the result of the flow velocity decrease, increasing the flame angle. As a result the flame moves closer to the thermocouples.

By using multiple thermocouples, it is possible to estimate the start location of flashback. This can be useful for a local flashback prevention system, which requires the position of the tip of the upstream propagating flame front. The disadvantage, however, is the relatively long time response of the thermocouples because heating and cooling of mass require time. The effect can be reduced by using thin thermocouples.

A flashback event is clearly visible in the microphone data as it produces more noise than in non-flashback conditions. The microphone measured a change in signal power towards flashback. As the flow velocity is reduced, the intensity of the sound of the approaching flow also decreases. This can be used as an indicator of a flow approaching flashback conditions. Measures can be taken in time to prevent the occurrence. However, no precursors are found directly related to the onset of flashbacks. The expected build-up of pressure is not observed. More advanced processing tools are required to extract possible more information from the microphone data of the flame and flow.

The advantage of microphones is the fast response due to the high sampling rates, so flashback detection is quick. The disadvantage of this sensor is that the surroundings and approaching flow produce lots of noise. Therefore, it is hard to distinguish the flame from the flow sounds.

The photo-detector can measured if a flame is present at the desired location. The used sensor, however, had a binary signal as output, making it impossible to get information prior to flashback. If an array of these sensors or more advanced photo sensor were used together with advanced processing tools, the position of the flame front could be estimated. This information might reveal interesting insides in the behavior of the flame wiggling and flame angle close to flashback. This should done offline since calculation requires more computational time. There is is still an use case for this sensor as secondary sensor to measure the presence of a flame in the line of sight.

If the advantages and disadvantages of the sensors are weighed against each other, the thermocouple are the sensor of choice. This is because there is a precursor indicating the build-up towards flashback and the location of flashback along the rim can be determined. Although the heating and cooling effect of the thermocouple limits the reaction time, this is compensated by using thin thermocouples. Furthermore, thermocouples are already frequently used in the industry and the heat resistance of the sensor make it interesting to use as state estimator in the control design.

Part III

Control: prevent and counteract

Chapter 5

Counteracting flashback

As investigated in Chapter 4, no attribute was found in the measurement data directly related to the onset of flashback. Although the event is triggered abruptly, the temperature profile indicates the flame movement towards conditions with a higher likelihood of flashback. During a flashback event, the flame travels upstream and can damage vulnerable parts. This upstream movement of the flame should be opposed. In conventional burners, the fuel supply is shut off in the case of a detected flashback event. This blows off the flame and requires restart of the system. In this chapter, a proof-of-concept is designed to allow continuous operation of the burner even in the case of flashback. This flashback counteraction system will be integrated in a control system as is explained in the next chapter. After flashback detection, the counteraction system is activated to counteract the effect of flashback. Hence, a restart of the system is prevented and the burner remains operational.

This chapter starts by explaining the design requirements. Thereafter, the different options for counteracting flashback are discussed. A proof-of-concept is designed for the most feasible option. In the remainder of the chapter, this design is tested and evaluated.

5-1 Design requirements

A flashback counteraction system is required to put the flame back to the desired location on top of the rim to prevent a restart. This system is built into the setup in the lab facility, as explained in section 4-2. For the design of this system, a set of requirements is defined:

- Should have fast activation after flashback detection
- Should put flame back to desired location
- Minimal flow disturbance

After the detection of flashback, the counteraction should start as soon as possible to limit the upstream movement of the flame. This requires a fast responding actuator. Furthermore, the actuator should be able direct the flame back on top of the rim to continue operations. Also, disturbances can trigger the flashback event, so the actuator should not disturb the flow. Hoferichter et al. [66] the addition of the injection slots resulted in an initial penalty, due to the flow disturbance. Otherwise, the burner would be better of without additional flashback prevention measures.

The main setup has its mass-flow controllers placed far upstream of the burner exit. Therefore, changes to the settings of these devices take time before the new flow conditions arrive at the location of the flame and this could be too late to counteract flashback. By locally influencing both the flow and flame close to the burner exit, the reaction time is drastically reduced. Options for locally controlling the flame are discussed in the next section.

5-2 Actuator options

For the existence of a flame three ingredients are required to ignite the fuel and keep it burning: oxygen, heat and fuel. If one of these three elements is missing, the flame extinguishes. Therefore, quenching, starving and smothering of the flame can be used to take control. These effects provide different possibilities to counteract the effect of flashback. Three counteraction methods are identified: decreasing the flame speed, increasing the flow speed and locally blow-off the flame. These methods are explained in this section.

Decreasing flame speed

The flame speed can be reduced by diluent boundary layer injection to change the equivalence ratio, as this ratio is proportional to the flame speed. Daniele et al. [64] used nitrogen injecting into the boundary layer as passive control to suppress flashback. The nitrogen was injected into the premix zone upstream of the reaction zone. The nitrogen dilutes the reactive mixture in the boundary layer. This reduces the flashback propensity and it stops upstream propagation of a hydrogen-carbon monoxide flame.

Baumgartner and Sattelmayer [67] investigated the injection of air at different angles, axial upstream positions and mass flow rates.The further upstream the lower the positive effect on the flashback propensity because the injected air had more time to mix, reducing the diluting effect. Furthermore, adding flow rates up to 10% resulted in a reduction of the flashback propensity. Adding more air did not change the propensity. The importance of the injector angle is small.

Increasing flow speed

The flow speed can be increased by increasing the mass flow of the incoming mixture. By allowing more fluid flow through the mass flow controllers, the flow velocity is increased in the premixing section. During flashback, the flame can be pushed out of the premix section. As mentioned, the main setup has its mass-flow controllers placed far upstream of the burner exit, so by injecting additional air close to the burner exit, the reaction time is reduced.

Local flame blow-out

Completely blowing the flame off is not desirable because it discontinues the operation. However, by injecting a colder fluid into the boundary layer, the flame temperature is reduced. If the flame temperature is reduced below its ignition temperature, the flame will locally extinguished. Water absorbs the heat and use the energy to expand in volume [68]. In these conditions, the the flame can no longer withstand.

The development agency of the USA army [69] conducted research to different ways to blow off a flame. They investigated the use of acoustic waves. The blowout of a flame did not occur at a specific sound frequency nor pressure level. It was mainly dependent on the local air displacement at the flame body. The acoustic wave accelerates the flow speed above the blow-off limit. Parallel to the investigation of acoustic flame suppression, they also investigated flame blow-off with electric fields [70]. Flames of hydrocarbons produce ions during the intermittent reactions of the combustion. An oscillating electric field can generate flows by exerting momentum on the charged ions without using moving parts. This can be used to extinguish or guide the flame. The oscillating homogeneous electric field nudges a flow outwards away from the flame. The incoming mixture follows this path. It deflects from the

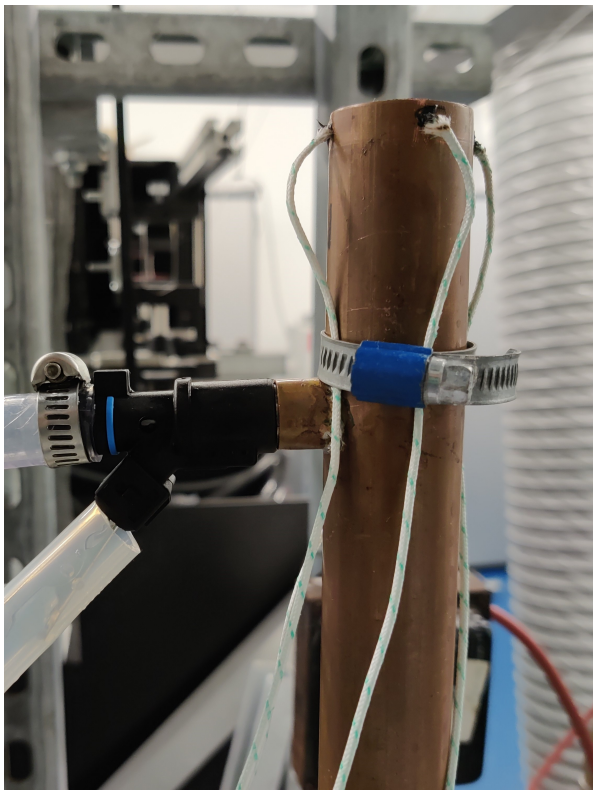

Figure 5-1: Tip of the burner with the injector system configuration installed, consisting of an injector and four thermocouples.

reaction zone. This can result in sufficient delay to prevent further upstream propagation of the flame.

5-3 Design of the counteraction system

As an initial design starting point, the injection of air is investigated to mitigate the flashback event. Air has less safety issues than using noble gasses or fuels to dilute the boundary layer. Furthermore, pressurized air lines are already present in the combustion lab. Local injection of air has two effects in the burner. Firstly, it reduces the equivalence ratio of the flame. The relation between equivalence ratio and flame speed was shown previously in Figure 1-3. Secondly, the injected air generates additional mass flow to push the flame downstream.

The designed and built injector setup is shown in Figure 5-1. The injector is mounted perpendicular to the burner tube as it easiest to solder. Four thermocouples are attached in the 360^oC to detect the presence of flashback. A supervisor analysis this temperature data and controls the valve of the actuator. This explained in more detail in Chapter 6. The amount of air injected depends on the time the valve is opened and on the pressure of the supply line. These are the control variables of the injector. As described in section 3-2, the flame travels upstream during flashback with speeds up to $1.4ms^{-1}$. To accommodate the time required for the detection and activation of the countermeasure, the air injector is located at 60 mm

from the burner tip. This reduces the chance that the flame has passed the actuator before it is activated.

5-4 Test method

The counteraction system design is tested by performing experiments with the lab setup. Since natural gas is less reactive than hydrogen, it is simpler to run the tests with 100% natural gas. If control is achieved over the natural gas flame under these milder conditions, it could be extended to higher hydrogen content fuels in future tests. The flashback event is triggered by decreasing the average flow speed to critical conditions.

If the flashback event occurs, the supervisory system should detect it as fast as possible. Otherwise, the flame can travel past the counteraction system before a puff of air can be injected. In such case, the counteraction has failed and the burner has to be switched off.

The control parameters for this experiment are the injector valve opening time, ranging from 100 ms to 3000 ms, and the line pressure of the compressed air supply, ranging from 2 bar to 5 bar. It is tried to push the flame back from the confined to the desired unconfined location by varying these parameters.

5-5 Results and discussions

During the experiments, different results for counteracting after a flashback event were observed. These results are summarized in Table 5-1. It was difficult to oppose the flashback event as most experiments failed to push flame back on top of burner rim. For most experiments, either not enough air was injected or the injection timing was incorrect. Only one experiment resulted in a successful outcome.

Table 5-1: Summary of the different observations during the counteraction experiments.

Observation	Result
No injection	Flashback was not detected or failure in circuit
Too short injection	Flame failed to go back to top of the burner rim
Too little momentum	Upstream movement of flame movement was only temporally stopped
Too late injection	Injection did not stopped upstream movement
Successful	Flame was pushed back on top of the burner rim.

At the end of this chapter, Figure 5-3 shows the time sequence of images for the successful counteraction. Flashback occurred in the second image. After the detection, air was injected for $1.5s$ to push the flame back to the desired burning position on the rim in the third image. From image third to image nine, the flame was present in the premixing section. In image twelve, the flame was finally back on top, so the flashback event was successfully counteracted.

The poor performance could be the result of the direction the air is injected into the burner tube. The air is injected perpendicular to the core flow. This may have two disadvantages. Firstly, the perpendicular injection may not generate the required upward momentum to push the flame downstream. It either just temporally stopped the flow or temporally slowed the

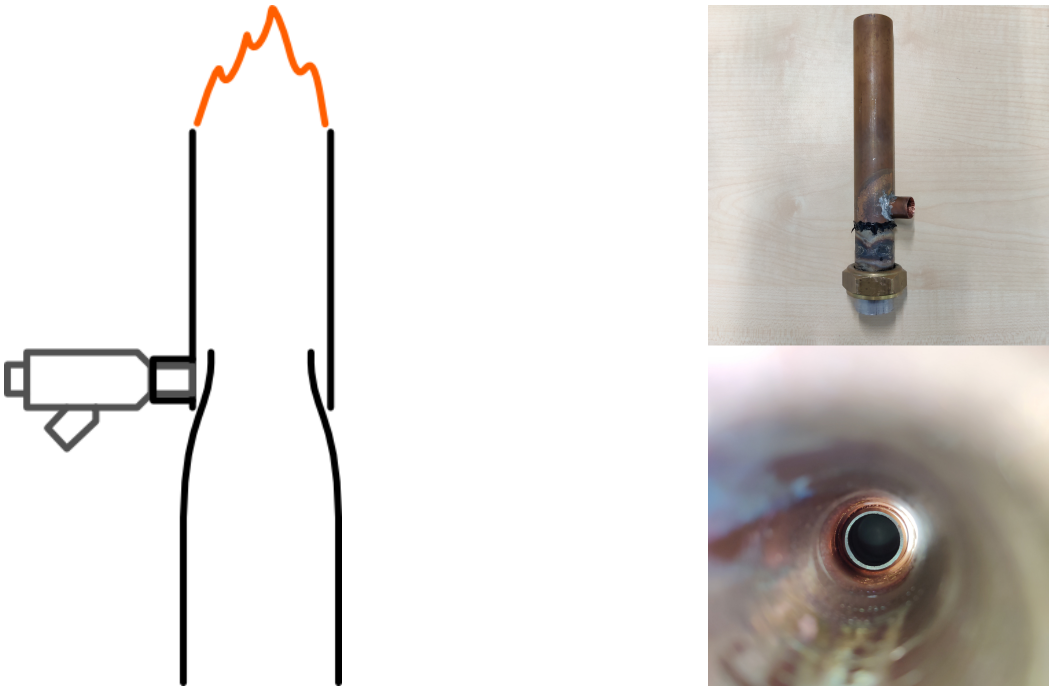

(a) Cross-section of the improved design. **(b)** Prototype of the improved design.

Figure 5-2: Improved counteraction system design

flame before traveling further upstream. Secondly, injecting air mainly in the bulk flow does not dilute the flow to reduce the flame speed enough. Since confined flames travel along the burner wall upstream, the perpendicular injection does not effect the boundary layer enough.

To generate enough upstream momentum along the burner wall, the injected air stream should be guided. In Figure 5-2a, the cross-section of an improved design is shown. An air ramp is applied by putting a narrowing tube inside the burner tube. If the air from the injector is pushed against this ramp, it will swirl upwards along the entire wall. The design has a disadvantage by disturbing the incoming flow. This affects the flashback resistance negatively. With this design the counteraction could be more reliable to oppose the flashback event, but further testing is required to validate the build. A prototype of the improved injector is shown in Figure 5-2b.

This chapter investigated the different options for counteracting the flashback event. The design of the injector system proved the concept of using active measures to counteract flashback. However, more design iterations and tests are required to get a properly working and reliable setup.This counteraction strategy can be implemented in the fault tolerant control framework to deal with flashback events in operation domains with high flashback propensities. This framework is discussed in the next chapter.

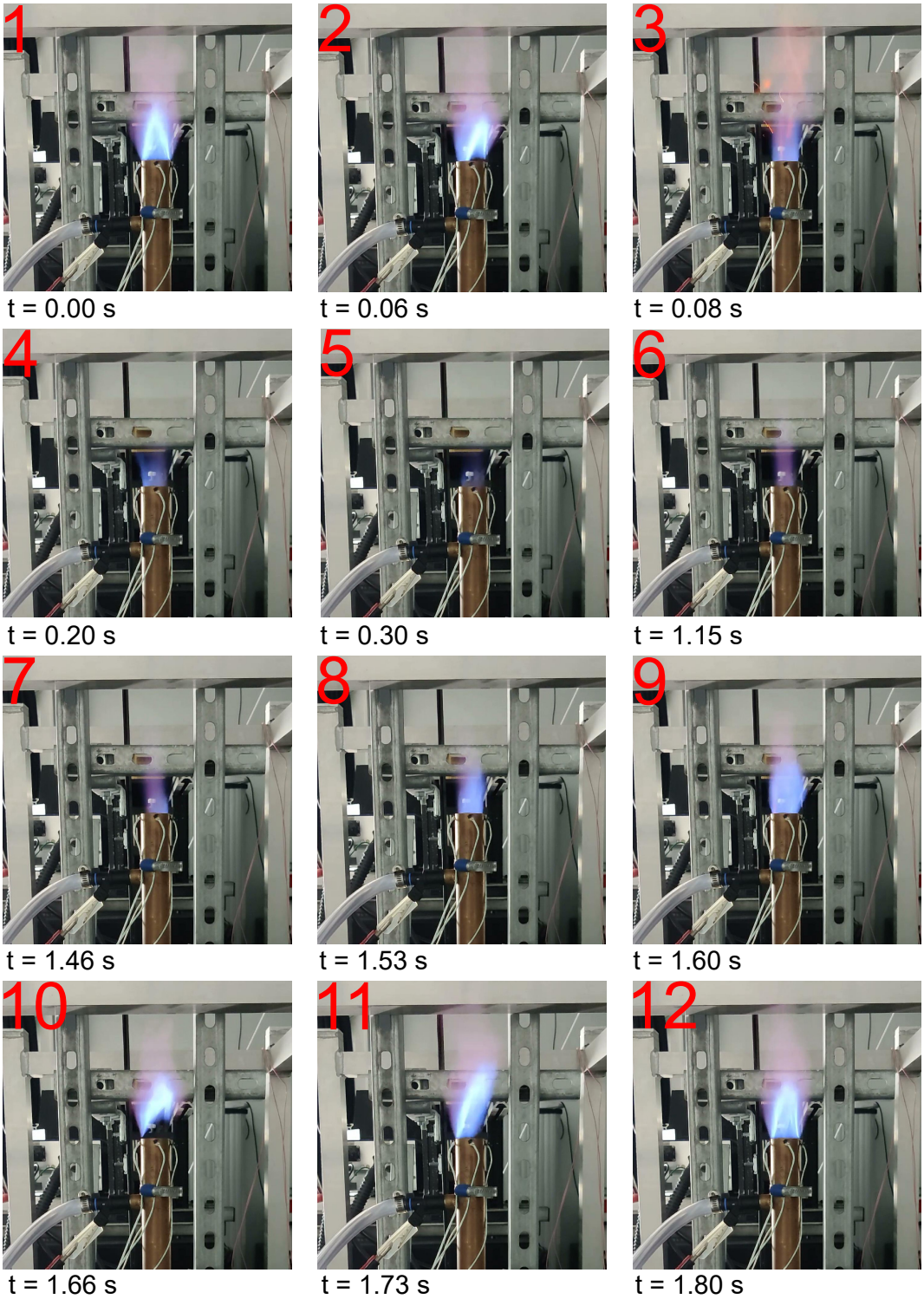

Figure 5-3: Time sequence of the cure of flashback by opposing the invent via injection of air at 60 mm from the burner tip. Injection opening time is 1500 ms at 2 bar pressure. The time interval between the images is variable. The flashback event occurred in image two. In the third image, air was injected. In image twelve, the counteraction was successfully completed.

Chapter 6

Fault-tolerant control framework

The flashback counteraction system, designed in Chapter 5, is a proof-of-concept for utilizing active actuators to oppose the effect of flashback to enable extended operation of the burner. Since prevention is better than cure, the to-be-designed controller should avoid the occurrence of flashbacks. As investigated in Chapter 4, the increasing temperature can indicate the flame movement towards conditions with a higher likelihood for flashback occurrence. This precursor could be used to steer away from flashback conditions. Both the prevention and counteractive measures are combined in the fault-tolerant control framework.

The design of the fault-tolerant control framework is presented in this chapter. In the first section, the burning system is decomposed in the different input, outputs and states. The second section explains the proposed fault-tolerant controller framework. This framework has three tasks between which is switched. In the third section, the first task, the prevention controller, is treated. The dynamics of the non-flashback model are identified. For a controller, different tuning methodologies are evaluated. The robustness of the proposed controller is verified through loop shaping interpretation. The section ends with simulation of the disturbance rejection and reference tracking behavior. In the fourth section, the flashback counteraction is treated. Flashback is identified and the flashback occurrence modelled. The same is done for the behavior of the counteracting system. The models are combined to simulate the flashback counteracting behavior. The fifth section explains the safety switch. This third task is explained and its behavior is modelled and simulated. In the last section, the supervisor mechanism is presented and the switching behavior of the controller and system are explained.

6-1 Description of the burner system

To get a better understanding of the burner system, as described in section 4-2, a block diagram is drawn in Figure 6-1. Two input streams, the fuel and air flow, enter the system.

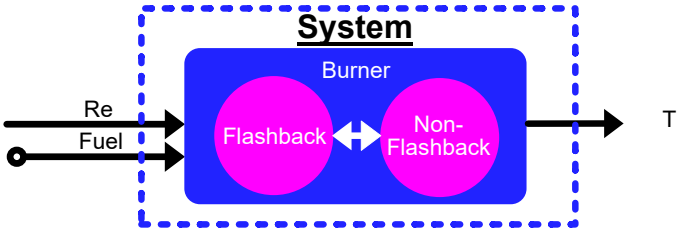

Figure 6-1: Block diagram of the system. The inputs are fuel and air, and the temperature is the output. The system has two states either flashback or non-flashback.

The air flow is expressed by the Reynolds number Re. This number has a linear relation with the air flow speed. However, the equivalence ratio ϕ and fuel content are considered constants. For simplicity, the framework is tested with pure natural gas as a starting point. Therefore, the Reynolds is assumed to be the only control variable. The Reynolds operating range is between 3200 and 6000 when operating at natural gas. Above Reynolds of 6000, the flame blows off and around a Reynolds of 3200, there is a large change in the occurrence of flashback. The flame blows off above approximately 6000 Reynolds and there is a large propensity for flashback around 3200 Reynolds.

The system has two states either flashback or non-flashback. The dynamics of both states are distinct. To switch between these system states, the additional variable δ_{fb} is defined. However, as explained before, the stochastic nature of the flashback onset is not fully understood. Thermocouples measure the system output as explained in Chapter 5. The output is expressed as a vector containing all temperature data $T = \begin{bmatrix} TC1 & TC2 & TC3 & TC4 \end{bmatrix}^{\mathsf{T}}$.

6-2 Proposed controller framework

To deal with the risk of flashback in the burner system , a complete fault-tolerant framework to control a flashback event is proposed. This framework increases the flashback resistance of the system and it counteracts possible flashback events. The block diagram of the controller is built around the burner system and is shown in Figure 6-2.

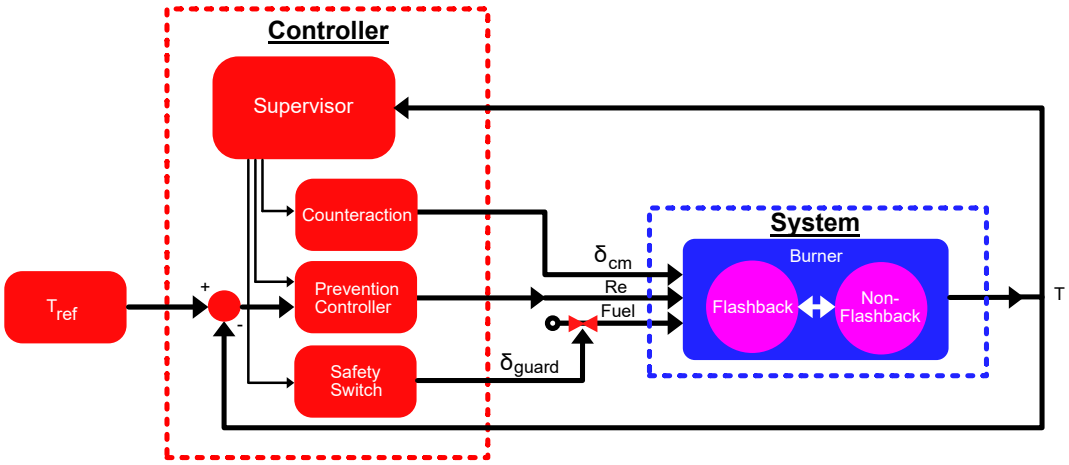

Figure 6-2: Block diagram of the fault-tolerant controller framework.

The burner system is an open-loop control system, where the output is not compared to the (reference) input of the system. Open-loop controlled systems have three main advantages compared to closed-loop systems [71]. Firstly, they are simple to construct. Secondly, they do not have a stability problem. Lastly, they are convenient when the system output is difficult to measure, as is the case in the flashback problem. However, external disturbances or varying parameters can cause errors in the output. For example, the fuel content or equivalence ratio

could change. This results in a drift of the temperature signal and leads to a premature flashback occurrence. Using a negative feedback loop avoids this problem. The measured output is fed-back and subtracted from a desired temperature reference signal. The resulting error term is the controller input. The closed-loop controller responds to this error term by adjusting the input signal. As a result, it is possible to use simpler models of the burner system to obtain an efficient controller.

The intelligence of the controller is in the supervisor block. This block decides which control actions should be activated, so the system has a fault-tolerant design. The fault-tolerant control strategy is threefold:

- Prevention controller: Temperature control in the non-flashback state. During this stable operation, the flame is steered away from high flashback propensity conditions to prevent the onset of flashback and follows the desired reference path.
- Counteraction: Detect flashback events and apply counteraction to oppose the fault.
- Safety switch: Shut fuel supply off when flame cannot be stabilized within a specific time frame as a last safety resort to fail safe.

The input of the controller framework is the temperature and the reference temperature. The different controller outputs are: $u = \begin{bmatrix} Re & \delta_{cm} & \delta_{safety} \end{bmatrix}^\intercal$. The flow speed of the approaching air is expressed by the Reynolds number Re, meaning changes in the Re are entirely from changes in the flow speed. $\delta_{cm} \in \{0, 1\}$ is a binary value indicating the activation of the counteraction. $\delta_{safety} \in \{0, 1\}$ is a binary value indicating the activation of the safety measure to safely stop the system operation.

6-3 Prevention controller

In this section, the design of an appropriate prevention controller is discussed. This controller is able to reject disturbances and follow a desired reference temperature T_{ref}. These actions steers the flame state away from flashback conditions above a critical temperature T_{fb} to prevent the occurrence of flashback. A control strategy is determined based on the following set of requirements:

- Disturbances that could steer the system towards flashback should be rejected.
- The distance to the reference temperature should be small.
- Overshoot of the temperature should be avoided as it can trigger flashback.
- $T < T_{fb}$, the temperature of the thermocouples should be outside the flashback domain.
- Large fluctuations in the controller output should be avoided as system instabilities result in flashback or blow-off.
- The actuation effort should be bounded as the flame can only exist in a specific Reynolds domain.

6-3-1 Non-flashback burner model identification

A model is a simplification of the real world. It should be as simple as necessary but not simpler than that. The system dynamics, captured by a model, are required for the controller design as it helps to shape the desired system response. Different methods are available

to obtain a model of the non-flashback burner system. In Section 3-2, different theoretical model proposals are listed to describe the boundary layer flashback phenomenon. Ljung [72] distinguishes three types of model structures:

- White box models: These models are constructed entirely from theoretical knowledge and physical inside.
- Grey box models: Engineering knowledge is used to suggest a model structure and order. The model parameters are estimated based on data.
- Black box models: The model is entirely estimated based on data as no physical insights are available.

For this flashback problem, grey box modeling method is employed as the physics of flames in the non-flashback situation are known. For system identification, the procedure of Verhaegen et al. [73] is used.

System identification experiment

First, a system identification experiment is designed. Input and output data is used for estimating the model parameters. The data is measured in open-loop to capture the dynamics of the system in the non-flashback case. If enough information is present in the data, input and output data measurements can reconstruct the model. If the input is persistently excited, the mapping to the output can identify the system [73]. For this property, the input should be different than zero. The data was collected using the burner setup, introduced in Section 4-3-2. The input sequence to the open-loop system is taken as a negative step in the flow velocity, expressed by the Reynolds number. Since the temperature dynamics of the system are slow, a large step is required to see a clear response in the output data. The Reynolds was stepped down from 4200 to 3500. The response for the four thermocouples, present in the setup, can be seen in Figure 6-3.

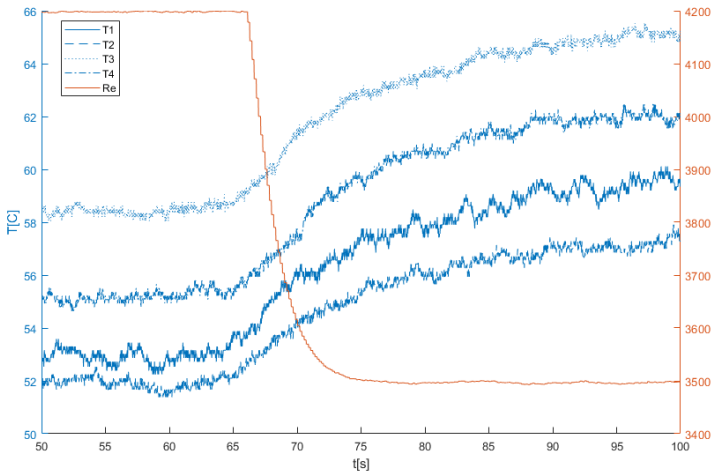

Figure 6-3: Result of the system identification experiment. It shows how the output temperature T responds to a negative step in the input Reynolds Re.

Data pre-processing

To improve the model estimate, pre-processing is applied to the data for better feature extraction. From all data signals, the offset is removed to start the step signal at zero. Unfortunately, the experiment was stopped before the system reached steady state. As a solution, the data stream was artificially extended by repeating the last 5 seconds of the experiment 20 times. This reduced the steady state error of the fit.

System identification

The step input provokes a system response, which is typical for a thermocouple. A first-order model describes this dynamics. The general structure of this first-order non-flashback system model is described by the transfer function G_{nom} in equation 6-1, where K_1 and K_2 are the parameters to determine. The Reynolds Re input is mapped to the temperature T. The temperature is both the state and output of the system are equal. The continues-time representation of this model is also shown in equation 6-2, where $T(s) = \mathcal{L}\{T(t)\}$ and $Re(s) = \mathcal{L}\{Re(t)\}$.

$$G_{nom}(s) = \frac{T(s)}{Re(s)} = \frac{K_1}{K_2 s + 1} \tag{6-1}$$

$$\dot{T}(t) = \frac{-1}{K_2} T(t) + \frac{K_1}{K_2} Re(t) \tag{6-2}$$

Then the parameters of the first-order model are determined for each thermocouple by using the Plant identification of the PID tuner from the Control Systems Toolbox in MATLAB version R2020a [74]. It combines both the input/output data and the model structure to determine the model parameters with non-linear least squares. This optimization method tries to minimize the sum of squared residuals between the determined output and the measured output.

Model validation

The estimated parameters and the fitness are shown in Table 6-1, where the Fit Percentage and MSE equations are given in equation 6-3 and 6-4 respectively. Here, n is the number of measurement points, T_i is the temperature value of the fit at time i, $\hat{T}_i$ is the measured temperature at time i and last but not least $\bar{T}$ is the average temperature. These fitness values are indicators for both the over-fitting performance and how well the model is a representation for the real underlying model. For simplification, the model is considered as a single-input and single-output (SISO) system. Only one of the obtained models is used as the behavior of the different sensors is approximately the same. Since model of thermocouple TC3 has the best scores, it is used to tune the controllers in the next sections. The first-order model fit is shown in Figure 6-4.

$$MSE = \frac{1}{n} \sum_{i=1}^{n} (T_i - \hat{T}_i)^2 \tag{6-3}$$

$$FitPercentage = (1 - \frac{\sum_{i=1}^{n}(T_i - \hat{T}_i)^2}{\sum_{i=1}^{n}(T_i - \bar{T})^2}) \times 100\% \tag{6-4}$$

Table 6-1: Results of the model fit for each thermocouple. The determined parameters are given in the second and third column. The goodness of the fit is expressed by the Fit percentage and the Mean Squared Error are presented in the fourth and fifth column.

	Parameter K_1	Parameter K_2	Fit percentage	MSE
TC1	-0.01213	18.04	84.8%	0.21
TC2	-0.009579	16.03	86.4%	0.10
TC3	-0.01229	17.4	87.5%	0.15
TC4	-0.01252	15.61	87.3%	0.15

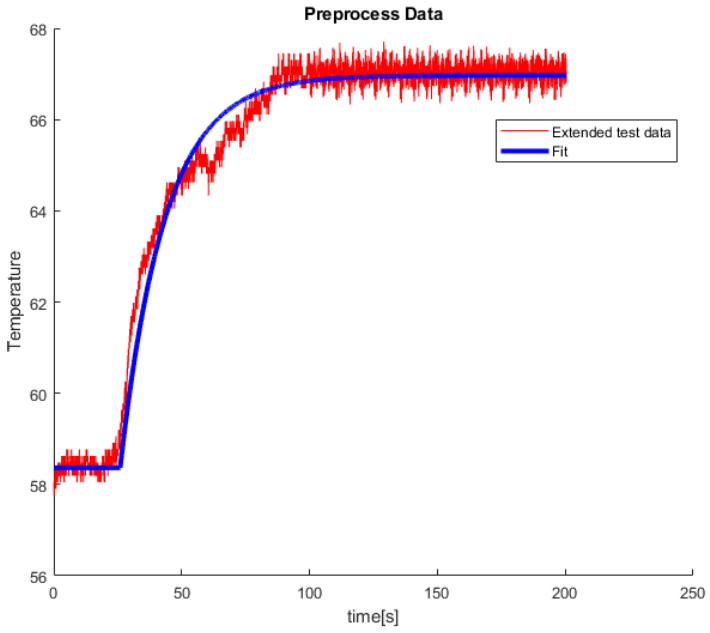

Figure 6-4: First-order model fit of thermocouple TC3 plotted on top of the extended training data.

6-3-2 Controller design

The model of the burner system is identified in the previous section as a simple first-order linear model. Three types of controllers are investigated for their control capabilities.

Simple control strategies available to control this model are in the class of linear closed-loop dynamics controllers. In process control, most control loops are a PID type of controller [75]. This type of controllers has the three abilities. Firstly, the system is controlled based on the proportionality of the error. Secondly, steady-state offsets are removed by integral action. Finally, the closed-loop stability is improved through derivative action. For many systems, PI gives good control performances.

Another type of control is Linear-Quadratic Regulator (LQR) control. According to a specified performance measure, the optimal controller action is determined, based on both the system states and controller output values. To eliminate the steady-state error, an integrator can also be added, which leads to the Linear-Quadratic Integrator (LQI) control.

The third investigated control type is Pole Polacement Regulator (PPR) control. The design is based on the characteristics of the desired closed-loop poles of the system. For small-order systems, as in this problem, this type of regulator is useful. A disadvantage is that the actuation effort is not taken into account, so it should be checked if they lay within the desired bounds. Otherwise, the gain should be reduced.

These three different controller can have the same control structure with both a proportional and integral action. This structure is shown in Figure 6-5. Here, K_P is the proportional gain and K_I is the integrator gain. In this section, the design methods for each controller are investigated. Eventually, the controller performances are compared to each other to decide on the method, used for the prevention controller.

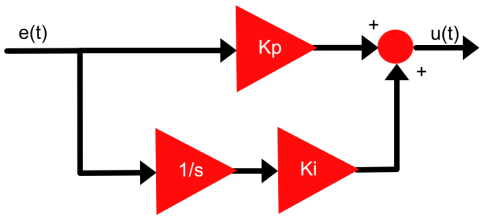

Figure 6-5: Schematic diagram of PI controller.

PI

Many types of PID controllers and there derivatives exist. In practical applications often PI is applied for two reasons. Firstly, since noise is present in the thermocouple measurements, using derivative controller action results in high fluctuations in the controller output. This causes wearing in the valves. Secondly, the derivative action increases the control complexity. For these reasons, the derivative is not used and undesirable for many industrial applications.

The PI controller removes the steady state offset and gives a good transient response to the set point. The proportional action provides a control action proportional to the control error of the system $e = T_{ref} - T$, which can be tuned by the term K_P. A larger control gain implies a larger control action in case of a large error. The integral action provides a control action proportional to the accumulative control error, $e_I = \int e(t)dt$. It removes the offset when the system is in the steady-state and is tuned by the term K_I. Using the Laplace transform the transfer function of the controller is written in equation 6-5.

$$K(s) = K_P + \frac{K_I}{s} \tag{6-5}$$

The controller is tuned by using the PID tuner from the Control Systems Toolbox in MAT-

LAB. The gains are tweaked, such that the overshoot is minimized and settling time appropriate.

LQI

In a Linear-Quadratic (LQ) problem, linear sets of differential equations describe the system dynamics. A quadratic function describes the related costs. This problem can be solved by the LQR feedback controller. The LQR has the property to minimize the steady-state error instead of converting to zero steady-state error. Applying high gains is a dissatisfactory solution. Young and Willems [76] proposed a different solution. They removed the steady-state error by using both the nominal state and the integral error x_i in the control law. This integral error is the difference between the reference signal and the system output. This control law is known as the Linear Quadratic Integrator (LQI) controller. It results in the same control structure as shown in Figure 6-5.

If the initial state is not considered then the infinite-horizon discrete-time LQI cost function is described by equation 6-6, where $z = \begin{bmatrix} x & x_i \end{bmatrix}^\intercal$ are the nominal state x and integrated error x_i and the system state is u. The weighting matrices Q, R and N are describing the cost. The optimal control law is given in equation 6-7. The controller gain matrix K is determined by using equation 6-8, where P is a positive definite matrix and the solution of the Discrete Algebraic Riccati equation found in equation 6-9. To be able to solve the Riccati equation, the state matrix A and input matrix B should be controllable, $R \succ 0$ and $Q, P \succeq 0$. For simplification, the cross term weighting matrix is omitted, so $N = 0$. Tuning is done by tweaking the cost matrices Q and R.

$$J = \sum_{k=0}^{\infty} (z_k^\intercal Q z_k + u_k^\intercal R u_k + 2 z_k^\intercal N u_k) \tag{6-6}$$

$$u_k = -K z_k \tag{6-7}$$

$$K = R^{-1}(B^\intercal P + N^\intercal) \tag{6-8}$$

$$A^\intercal P + PA - (PB + N)R^{-1}(B^\intercal P + N) + Q = 0 \tag{6-9}$$

Pole placement

To tune the pole placement regulator, the characteristic of the poles of the closed loop are required. The closed-loop transfer function is derived in equation 6-11, using the open-loop transfer function in equation 6-10.

$$L(s) = K(s)G(s) = \frac{K_P s + K_I}{s} \frac{A}{Bs + 1} = \frac{AK_P s + AK_I}{Bs^2 + s} \tag{6-10}$$

$$J(s) = \frac{L(s)}{1 + L(s)} = \frac{AK_P s + AK_I}{Bs^2 + s + AK_P s + AK_I} = \frac{(AK_P/B)s + AK_I/B}{s^2 + (1 + AK_P)/Bs + AK_I/B} \tag{6-11}$$

The denominator of the closed-loop transfer function identifies as the characteristic equation. The definition of the characteristic equation is presented in equation 6-12, where ζ is the damping ratio and ω_n is the undamped natural frequency. It is the standard form of a second-order system [71]. The closed-loop response is described by the variables ζ and ω_n.

$$s^2 + 2\zeta w_n s + w_n^2 \tag{6-12}$$

The overshoot M_p can be expressed by these variables as in equation 6-13. The same applies to the settling time t_{set}, where the response converges within a 2% margin range, as given in equation 6-14.

$$M_p = e^{-(\zeta/\sqrt{1-\zeta^2})\pi} \tag{6-13}$$

$$t_{set} = \frac{4}{\zeta\omega_n} \tag{6-14}$$

The damping ratio ζ is determined from the overshoot M_p in equation 6-13. Using this ζ and the desired settling time in equation 6-14, the required natural frequency ω_n is determined.

The controller gain values K_P and K_I are determined by equalizing the desired second-order behavior of the characteristic equation 6-12 with the denominator of equation 6-11. Afterwards, the controller output response must be checked because the additional zero in the closed-loop transfer function in equation 6-11 can influence the performance.

Comparison

The performance of the different tuned controllers are evaluated in this section. Based on the requirements in the beginning of section 6-3, the most appropriate tuning method is selected. The controllers are tuned to get the performance to an unit step input, shown in Figure 6-6. The tuning of the PI controller resulted in:

$$K_P = -40 \ , \ K_I = -3.7$$

The weighting matrices for the LQI controller are tuned to:

$$Q = \begin{bmatrix} 5 & 0 \\ 0 & 1000 \end{bmatrix}, R = \begin{bmatrix} 100 \end{bmatrix}$$

The damping ratio and undamped natural frequency of the PPR controller are tuned to:

$$\zeta = 0.8261 \ , \ \omega_n = 0.0807$$

The characteristic information about the gains, overshoot, settling time, and maximum controller gain of Figure 6-6 is shown in Table 6-2. The PI has a slightly longer settling time than the pole-placement controller, but the overshoot is lower. the PPR controller fits these requirements the best as it has the fastest settling time and a descend overshoot. Therefore,

the controller gains of the PPR will be implemented for the prevention controller to follow the temperature reference. Although, the controllers in the class of linear closed-loop dynamics are robust against disturbances, determined in the next subsection, these type of controllers are less suitable to deal with parameter-varying. It requires an extended identification procedure in different operating conditions. The gains of the model will vary in accordance with the varying of the system parameters.

Table 6-2: Controller gains of the different controller options

	K_P	K_I	$M_p[\%]$	$t_{set}[s]$	$\|\|u_{max}\|\|$
PI	-40	-3.7	1.08	63.2	85
LQI	-2.0	-3.2	8.2	125.9	90
PPR	-107.4	-9.2	3.2	58.3	110

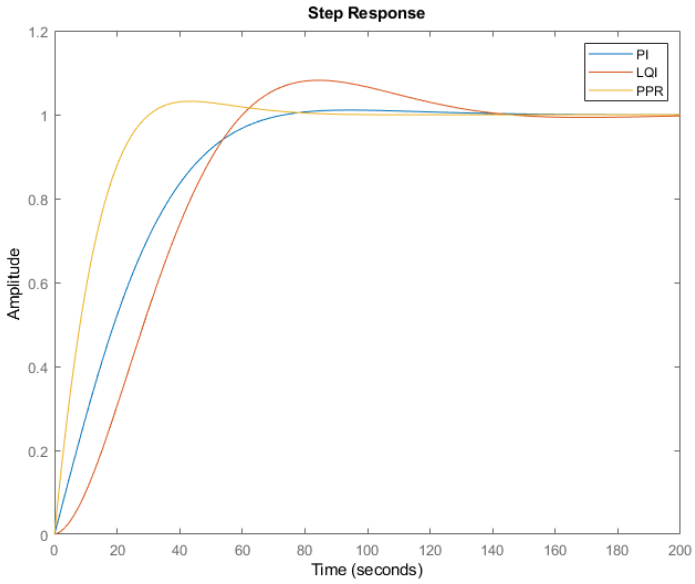

Figure 6-6: Closed-loop performance of PI, LQI and PPR controller to an unit step response.

6-3-3 Robustness

To determine the robustness of the prevention controller, the effect of disturbances at different locations in the closed-loop are evaluated through the loop shaping interpretation [77]. The general closed-loop feedback configuration is shown in Figure 6-7. The controller output of this system is expressed in equation 6-15 and the plant output is written in equation 6-16. Here, r is the reference signal, n is sensor noise, d_i is disturbance on the controller output and d is the disturbance on the system output with dynamics G_d, T' is the output of the plant and T is the temperature with the disturbance on the system output. The controller is defined by the block K and the non-flashback burner model is defined by the block G_{nom}. Possible sources of the disturbances are partly covered in section 6-2. They can lead to the occurrence of premature flashback.

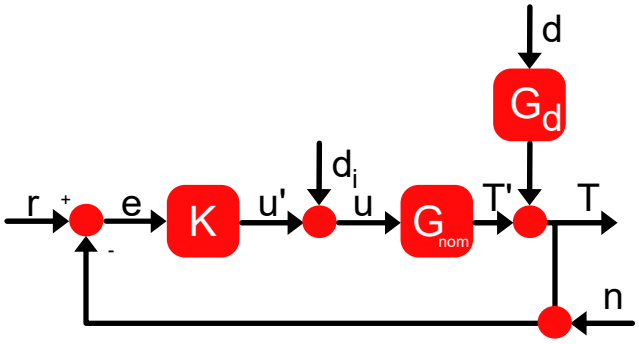

Figure 6-7: The general closed-loop feedback configuration. Based on Zhou [16]

$$u(s) = K(s)(r(s) - n(s) - T(s)) + d_i(s) \tag{6-15}$$

$$T(s) = G_{nom}(s)u(s) + G_d(s)d(s) \tag{6-16}$$

The open-loop transfer function is given in equation 6-17. This equation can be used to simplify, both the sensitivity transfer function and complementary sensitivity transfer function. These transfer functions for SISO systems are defined in equation 6-18 and 6-19 respectively . Together, they sum to the identity matrix $S(s) + Z(s) = I$. The sensitivity transfer function maps the output disturbance to the temperature and the complementary sensitivity transfer function maps either the reference or the negative of the sensor noise towards the temperature. Using equations 6-15 up to 6-19, the closed-loop transfer function of the control system can be written as in equation 6-20. These definitions are used to describe the robustness of the controlled system in the remainder of this subsection.

$$L(s) = G_{nom}(s)K(s) \tag{6-17}$$

$$S(s) = \frac{1}{1 + G_{nom}(s)K(s)} = \frac{1}{1 + L(s)} \tag{6-18}$$

$$Z(s) = \frac{G_{nom}(s)K(s)}{1 + G_{nom}(s)K(s)} = \frac{L(s)}{1 + L(s)} \tag{6-19}$$

$$T(s) = Z(s)(r(s) - n(s)) + S(s)G_{nom}(s)d_i(s) + S(s)G_d(s)d(s) \tag{6-20}$$

Reference tracking performance

The reference tracking performance indicates for the accuracy the system can follow reference signals. The reference tracking performance are determined, using the transfer function in equation 6-21. Here, the error is mapped to the temperature, which is the open-loop transfer function. The bode plot of the transfer function is shown in Figure 6-8. The system has good tracking performance for frequencies below f_{track}, which is the frequency in the bode plot where the open-loop transfer function crosses the +20dB line. All frequencies below that frequency f_{track} amplify the error signal by at least 99%.

$$\frac{T(s)}{e(s)} = L(s) \tag{6-21}$$

Disturbance rejection performance

The system has good rejection performance for the high frequencies in the error signal above the frequency f_{dist}, which is the frequency in the bode plot where the open-loop transfer function $L(s)$ crosses the -20dB line. All frequencies above the frequency f_{dist} attenuate the signal by at least 90.9%, so higher frequencies signals are rejected.

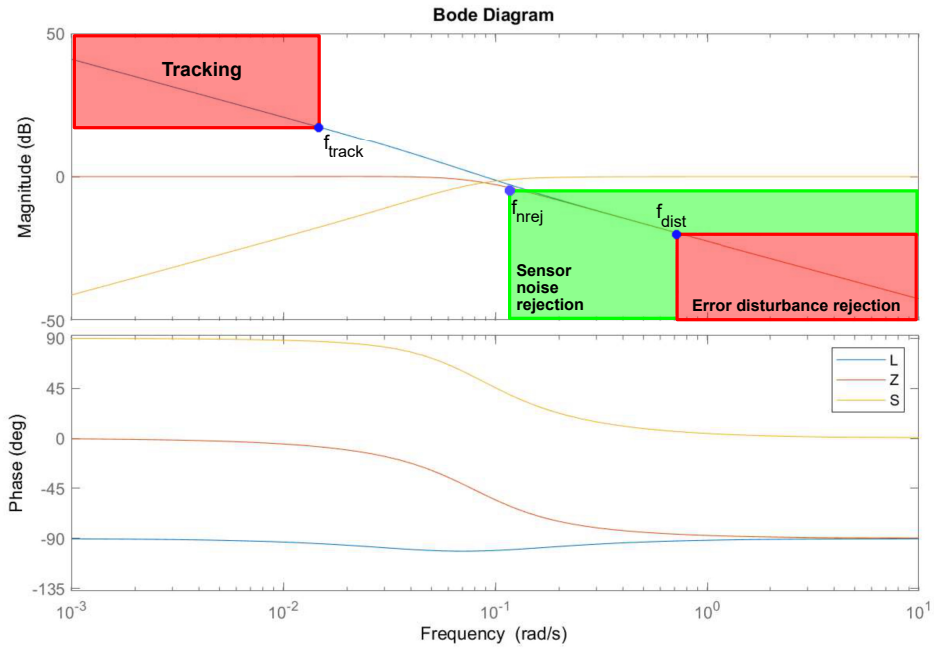

Figure 6-8: Bode plot of the open-loop, sensitivity and complementary sensitivity transfer function.

Sensor noise attenuation performance

Noise in the environment has a negative effect on the sensor measurements. The effect of the sensor noise on the output is therefore evaluated. The transfer function of this relation is given in equation 6-22. The bode plot of $Z(s)$ is given in Figure 6-8. The sensor noise attenuation performance is defined by the crossing of -3dB line. Here, the controller cuts off at least half of the power for frequencies higher than the cross-frequency f_{nrej}. All frequencies above the cross-frequency f_{nrej} are considered as rejected.

$$\frac{T(s)}{n(s)} = -Z(s) \tag{6-22}$$

Output disturbance attenuation performance

Unmodeled dynamics or disturbances have an effect on the system model output. The transfer function of the relation between these disturbances and the output is given in equation 6-23,

where the dynamics of the unknown disturbance are also present. Since the dynamics of the disturbance are not known, they will be considered unity. The system has good rejection performance for the disturbance frequencies in the error signal above the frequency $f_{odistrej}$, which is the frequency where the transfer function crosses the -3dB line. The controller attenuates at least half of the power for frequencies higher than this cross-frequency. All frequencies above $f_{odistrej}$ do not influence the system performance.

$$\frac{T(s)}{d(s)} = S(s)G_d(s) \tag{6-23}$$

Input disturbance attenuation performance

Also, disturbances on the input could have an effect on the output of the model. The transfer function relating these disturbances and the output is given in equation 6-24. The bode plot is shown in Figure 6-9. As can be seen in the bode plot in Figure 6-9, all frequencies have magnitudes below -3dB. Therefore, all signals are sufficiently attenuated. This disturbance does not significantly influence the system performance.

$$\frac{T(s)}{d_i(s)} = S(s)G_{nom}(s) \tag{6-24}$$

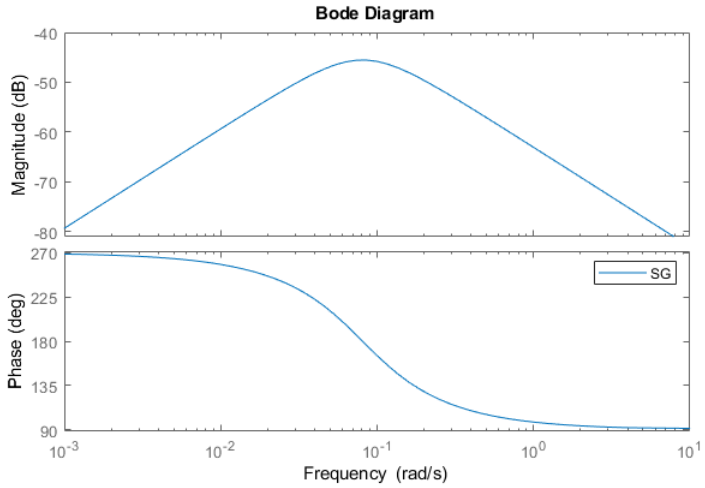

Figure 6-9: Bode plot of the input disturbance transfer function.

All the above described performance and robustness measures are summarized in Table 6-3.

6-3-4 Simulation tracking and disturbance rejection

The virtual performance of the controller are tested to demonstrate its use. The simulations are done in Simulink [74]. For more information about the designed simulation model, see Appendix B. For these simulations, a scenario is written where the reference temperature follows a predefined path. The reference signal is set to the arbitrary constant value 55^oC,

which is below flashback conditions. The system is initiated at 50^oC and the controller pushes the temperature to the reference value. After 100 seconds, an artificial bounded disturbance is added to the system. This disturbance could represent for example an undesired increase in the equivalence ratio. The disturbance is modeled as a ramp function, representing a slow drift towards flashback conditions in the measured temperature. The temperature path of the disturbance is shown in Figure 6-10a. Since the Reynolds is assumed to be the only controllable parameter, the system will correct itself by increasing the Reynolds number of the incoming flow to a new equilibrium value, shown in the output controller signal in Figure 6-10b. The temperature response of the system is shown in Figure 6-10a. The controller tracks the reference temperature and disturbances are rejected.

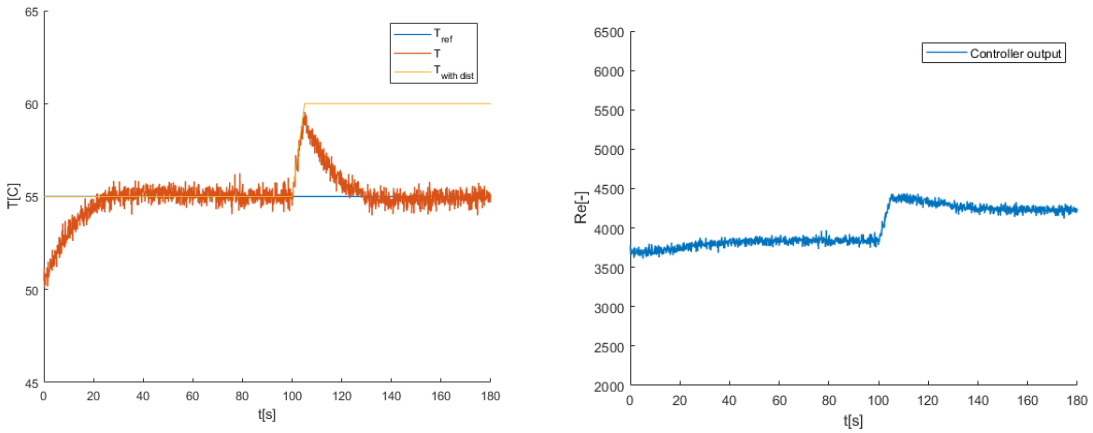

(a) Simulation of the prevention controller, which tracks a predefined reference path and rejects a disturbance.

(b) Output control signal of the prevention controller.

Figure 6-10: Prevention controller simulation

6-4 Flashback counteraction

The previous section discussed the prevention controller. However, flashback cannot always be prevented. For example, when the burner is operating in an unstable regime. Although prevention is better than cure, the abrupt occurrence of flashback cannot be predicted accurately. To limit the negative effects of a flashback event, the flashback counteraction from Chapter 5 is implemented in the framework.

Table 6-3: Robustness performance of the prevention controller. Expressed by the frequency in Hertz.

Cutoff frequency	definition	performance
f_{track}	amplify the error signal in open-loop up to 99%	< 0.0019 Hz
f_{dist}	attenuate the error signal in open-loop up to 90.9%	> 0.1239 Hz
f_{nrej}	attenuate the sensor noise in close-loop up to 70.79%	> 0.0159 Hz
$f_{odistrej}$	attenuate the output disturbance in close-loop up to 70.79%	> 0.0111 Hz

In Figure 6-11, a sequence of illustrations shows the position of the flame front at the different stages during the counteraction of flashback. In the first illustration, the system operates at a high Reynolds number, so the flame profile is elongated. In the second illustration, the Reynolds is reduced, so the flame tip approaches the burner rim. Flashback occurred in the third illustration, thus the flame travels upstream. In the fourth illustration, flashback is detected and the counteraction is activated by setting $\delta_{cm} = 1$. A puff of air is injected to push the flame back downstream in illustration five. In illustration six, the flame is back at the desired location and the counteraction is stopped.

This nature is discussed in this section, so the behavior of the counteraction can be simulated. First, this section discusses the trigger of flashback. The second subsection covers the modeling of the flashback behavior. The third subsection explains the flashback detection and counteraction activation. Fourth, the model of the counteraction behavior itself is discussed. Finally, the simulation results are shown.

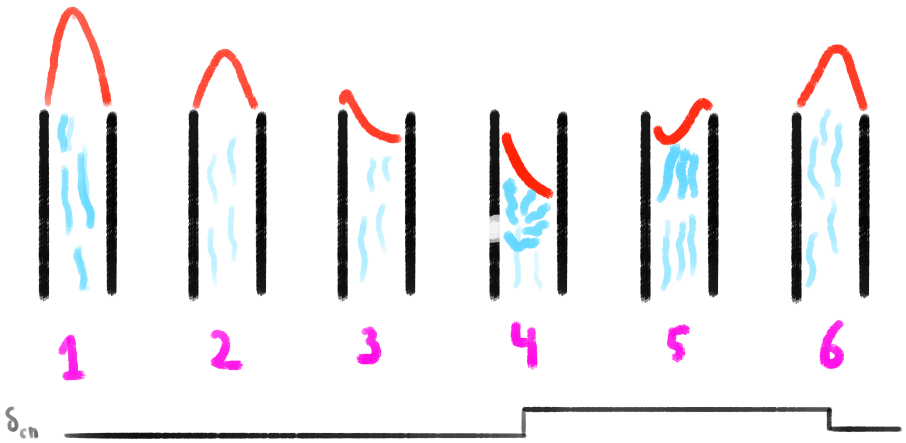

Figure 6-11: Sequence of illustrations showing the flame front position at different stages during the counteraction of flashback.

6-4-1 Probability of the flashback occurrence

Since the onset of flashback is not fully understood it is also challenging to implement a model which describes the occurrence of the phenomenon. Therefore, a trigger is designed to determine when flashback occurs. At this time instant, the disturbance variable δ_{fb} changes to indicate the presence of flashback. From previous experiments, flames observed to have a higher tendency to flashback at higher temperatures. At these elevated temperatures, the flow speed is reduced and the flame moved closer to the rim. The temperatures were in the same order of magnitude at the time step before the high flashback peak occurred. In Table 6-4, both the average and limits of the flashback temperature can be seen for the different thermocouple, obtained from six experiments. This observation resulted in the following hypothesis: flashback occurs as a certain temperature limit is exceeded. This trigger can be modeled as a hard line, representing the flashback temperature limit T_{fb}. Flashback is activated when this limit is crossed.

Table 6-4: Average, minimum and maximum temperatures of the flashback limit T_{fb} just before flashback, determined from six experiments.

Thermocouple	TC1	TC2	TC3	TC4
Average	71	67	75	74
Minimum	67	62	71	69
Maximum	77	71	80	80

However, the flashback temperatures are not equal in each experiment. Some variance is present in the data. To take this probabilistic nature of the phenomenon into account, the flashback limit model is considered as stochastic. Since only a limited amount of experiments is conducted, it is impossible to accurately state the likelihood of flashback onset at a certain temperature. The minimum and maximum temperatures can give limits on the domain of an arbitrary outcome. This can be described by assuming a uniform distribution, defined in equation 6-25 with lower boundary T_{llim} and upper boundary T_{ulim} [78]. This probability function determines at each time step the critical flashback temperature. If the current temperature exceeds this limit, the model will trigger flashback.

$$f(T_{fb}) = \begin{cases} \frac{1}{T_{ulim} - T_{llim}} & \text{, for } T_{llim} \leq T_{fb} \leq T_{ulim} \\ 0 & \text{, for } T_{fb} < T_{llim} \text{ or } T_{fb} > T_{ulim} \end{cases} \tag{6-25}$$

6-4-2 Flashback model identification

The response of the system during non-flashback and flashback conditions is distinct from each other, as observed in the temperature measurements in Chapter 4-3. Flashback is considered as a external disturbance in the system. Another model is then added to the non-flashback model to output the flashback behavior. For the identification of the flashback model, the temperature data from a flashback experiment is used. The temperature response is shown in Figure 6-12. The observed temperature peak during flashback is due to the flame passing by the thermocouple. This results in contact between the hot flame and sensor as the flame travels upstream. The identification is different from the non-flashback model because instead of using the Reynolds as the input signal, the variable δ_{fb} is used. This variable indicates in simulations when the flashback dynamics should be present in the model. If flashback occurs, the variable will change with a positive unit step. To get a better fit, the temperature data is pre-processed by removing the off-set. The temperature response can be fit with a second-order model. Again the Plant identification of the PID tuner from the Control Systems Toolbox in MATLAB is used for fitting. The transfer function is given in equation 6-26. This result is also plotted in Figure 6-12 on top of the experimental data.

$$G_{fb}(s) = \frac{K_3 s + K_4}{s^2 + K_5 s + K_6} = \frac{16.5s - 16.5}{s^2 - 1.933s + 0.9328} \tag{6-26}$$

6-4-3 Flashback detection for counteraction activation

After the detection of flashback, the counteraction system is activated. In this subsection, the flashback detection method is selected. The thermocouples, discussed in Chapter 4, revealed

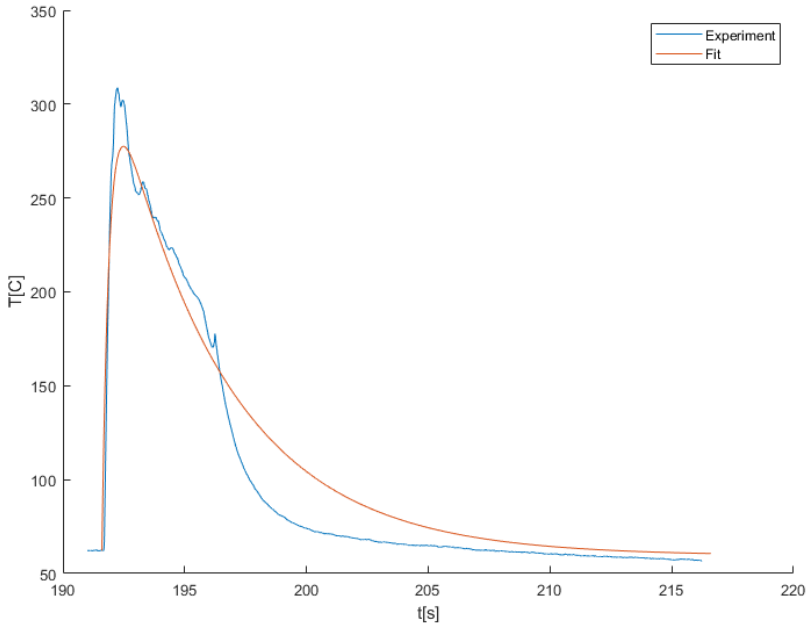

Figure 6-12: Second-order model fit based on experimental data from a flashback event.

high peaks in the temperature data during flashback events. Flashback is a fault with a very abrupt step behavior. The goal of the fault detection is threefold [79]. Firstly, the missed detection rate should be minimized. Secondly the false alarm rate should be minimized and thirdly, the time between the faulty event and the detection should be minimal. The speed of detection and accuracy are therefore important to take counteractive measurements in time. Different methods are available for flashback detection. Three main groups of fault detection methods are identified: Signal-based, model-based and knowledge-based methods [80]. The most simple and frequently used method to detect a fault is the deterministic limit checking test [29]. In its most simple form it checks if the measured value exceeds a specific threshold, either an upper or lower limit. The normal operation domain is defined by equation 6-27. Here, $T(t)$ is the current temperature, T_{llim} is the lower fault detection limit and T_{ulim} is the upper fault detection limit. These limits may not be set strict because normal fluctuations can trigger false alarms. However, a too high threshold should also be prevented to minimize the detection time. Another method is to use trend checking. Here, the first derivative is compared to limits. The relative change of variables between two timesteps should be within a specific domain as defined in equation 6-28.

$$T_{llim} < T(t) < T_{ulim} \tag{6-27}$$

$$\dot{T}_{llim} < \dot{T}(t) < \dot{T}_{ulim} \tag{6-28}$$

In Figure 6-13, the trend checking method is tested on experimental data from a flashback experiment. The limit $\dot{T}_{ulim}$, is placed as close to the data as possible to prevent false alarms, but not so close that normal temperature fluctuations could trigger flashback. The algorithm has good performance for detecting flashback, so it is implement in the fault-tolerant controller framework.

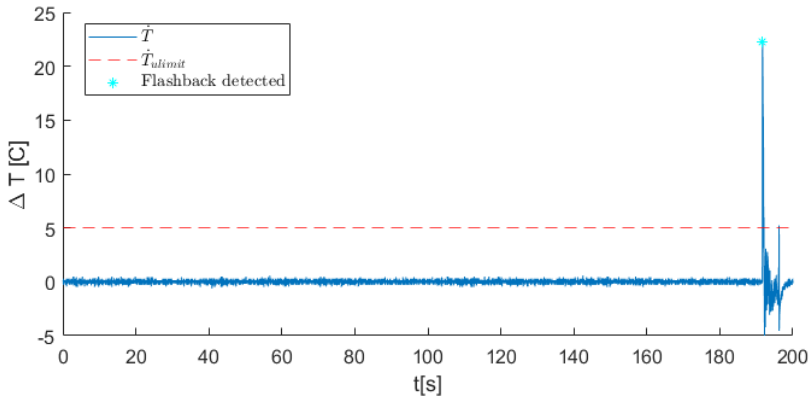

Figure 6-13: Experimental data of flashback event. Flashback detection is demonstrated by using limit checking with in this case the limit $\dot{T}_{ulim} = 5$.

For the flashback detection problem, a hypothesis is defined in equation 6-29. The trend checking algorithm should accepts or rejects the hypothesis. The first temperature derivative is determined by recording the relative change between each time step. If the signal is below the defined temperature upper limit, flashback is not present or not detected. If this is not true, flashback is detected and the flashback detection variable is $\delta_{cm} = 1$. The limit is iteratively determined to $\dot{T}_{ulim} = 3.8$, so both the amount of false positive detection and the detection time are minimized.

$$\begin{cases} \delta_{cm} = 0 & \text{, for } \dot{T}(t) < \dot{T}_{ulim} \\ \delta_{cm} = 1 & \text{, for } \dot{T}(t) \geq \dot{T}_{ulim} \end{cases} \tag{6-29}$$

6-4-4 Counteraction model identification

In the previous section, the flashback detection is discussed. After the detection, the counteraction system is activated to stop the upstream propagation of the flame and push the flame back on top of the burner rim. In Figure 6-11, the flame behavior during counteraction was explained. The corresponding temperature profile has been observed in an experiment, shown in Figure 6-14a. During this experiment, the flame managed to escape from flashback by itself and jumped outside the premixing section. Shortly thereafter, the safety valve closed. Due to a slightly different thermocouple configuration in this experiment, the flame temperatures are higher than observed in Figure 6-12. The hot flamelets touching the thermocouples cause high peaks in the temperature response. The first flashback peak is previously modeled by the transfer function of the flashback event in equation 6-26. However, a model for the second peak has to be identified. This second peak results from the flame passing the thermocouple again to go back on top of the burner. The model G_{cm} describes the flame behavior after a successful counteraction. The dynamics look similar but the second peak is lower than the first peak because there was not enough time for full cool down. The temperature increase is 71% lower. The model of the flashback peak is therefore used with a reduction factor K_{red}

to reduce the temperature increase, shown in equation 6-30.

$$G_{cm}(s) = K_{red}\frac{K_3 s + K_4}{s^2 + K_5 s + K_6} = \frac{2}{7}\frac{16.5s - 16.5}{s^2 - 1.933s + 0.9328} \tag{6-30}$$

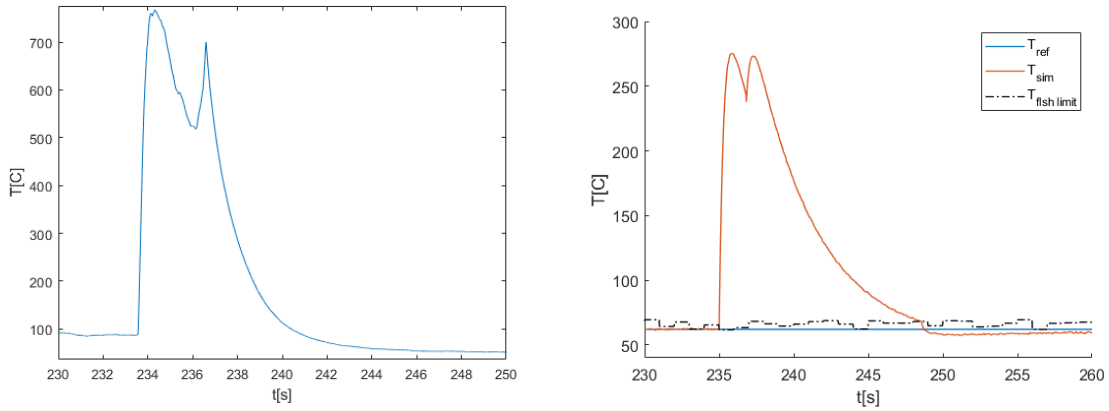

(a) Experiment showing the thermocouple behavior for a flame experiencing incomplete flashback as the flow pushed the flame out of the burner by itself.

(b) Simulation of the trigger of flashback and the successful counteraction of flashback.

Figure 6-14: Experimental and simulated temperature signal for flashback counteraction.

The time between the two peaks Δt_{peak}, is the accommodation time of the flame in the burner tube before the counteraction is successful. From Figure 6-14a, the peak to peak time Δt_{peak}, has been determined at approximately $1.8s$. This value is added as a delay in the model to accommodate the residence time of the flame in the tube.

At some time the model should switch off the counteraction and operate again with the prevention controller as flashback is over. The proposed criteria is given in equation 6-31. If the temperature is again within a set bandwidth of the reference temperature, the supervisor switches the control action. The bound η_{switch} is set within 5%.

$$\frac{T(t) - T_{ref}(t)}{T_{ref}(t)} \leq \eta_{switch} \tag{6-31}$$

6-4-5 Simulation

The virtual behavior of the counteraction controller are tested to demonstrate its use. The simulations are done in Simulink [74]. For more information about the designed simulation model, see Appendix B. The simulation result is shown in Figure 6-14b. The reference track is set to 62^oC, which is equal to the lower bound of the flashback limit T_{fb}. This way, the onset of flashback is forced. At $t = 235s$, the flashback limit is exceeded and the flashback model becomes active as $\delta_{fb} = 1$, shown in Figure 6-16. The peak is clearly detected in Figure 6-15, so the counteraction model could be quickly activated. The peak from the counteraction model is also detected by the trend checking algorithm.

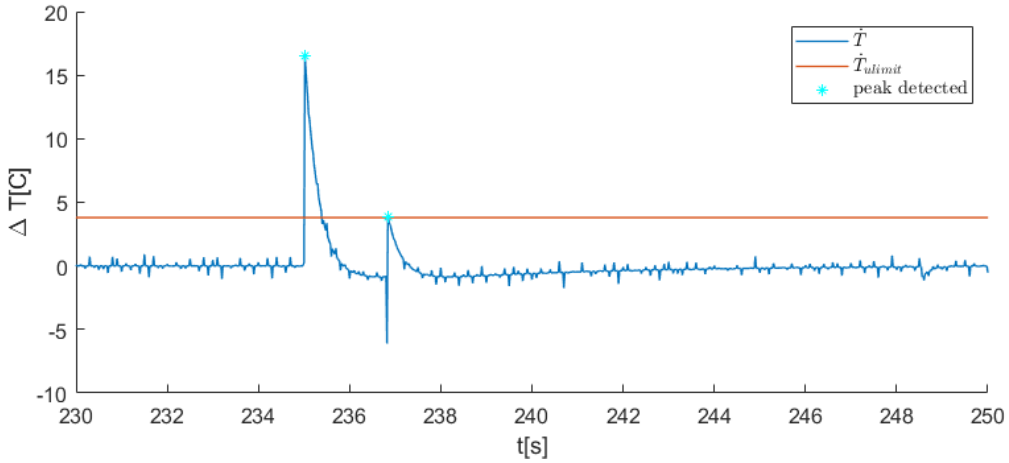

Figure 6-15: Simulation of flashback detection. Peak detection is used for counteraction activation. A peak is detected if ΔT exceeds the limit $\dot{T}_{ulim} \leq 3.8$.

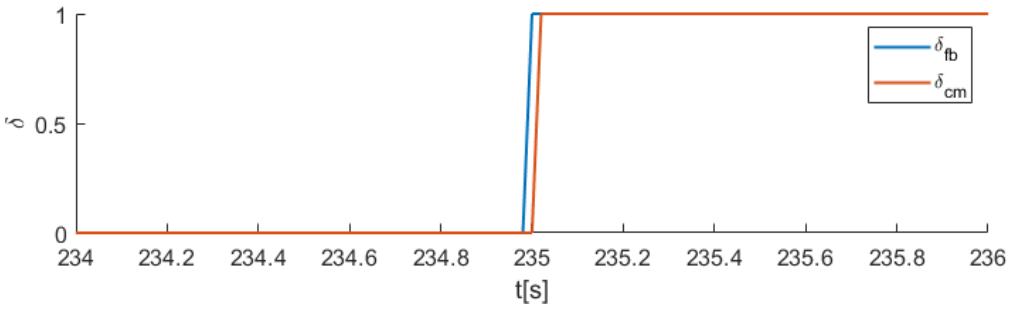

Figure 6-16: The change of δ_{fb} and δ_{cm} during the simulation of counteracting flashback.

6-5 Safety switch

The counteraction system, discussed in Chapter 5, is not perfect. In the case counteracting flashback has failed, additional safety measures are required. This safety switch shuts off the fuel supply to safely stop the upstream movement of the flame. In Figure 6-17, a sequence of illustrations shows the position of the flame front at the different stages of the safety switch. The first three illustrations depict the build-up towards flashback, as previously explained in section 6-4-4. In the fourth illustration flashback is detected and the air injector is activated. However, the action was not able to push the flame back, so the fifth illustration shows the continued upstream movement of the flame. The safety switch is activated if a flame peak is not detected again within a reasonable time frame. It both switches off the fuel supply and stop the counter action, so the flame is extinguished.

6-5-1 Safety switch model identification

When the safety switch is activated, the variable $\delta_{safety} = 1$. The temperature response after the activation of the safety switch could already be seen in the experiment of Figure 6-18. It is observed as a nod in the cooling down rate at 196 seconds. During the experiment, the safety

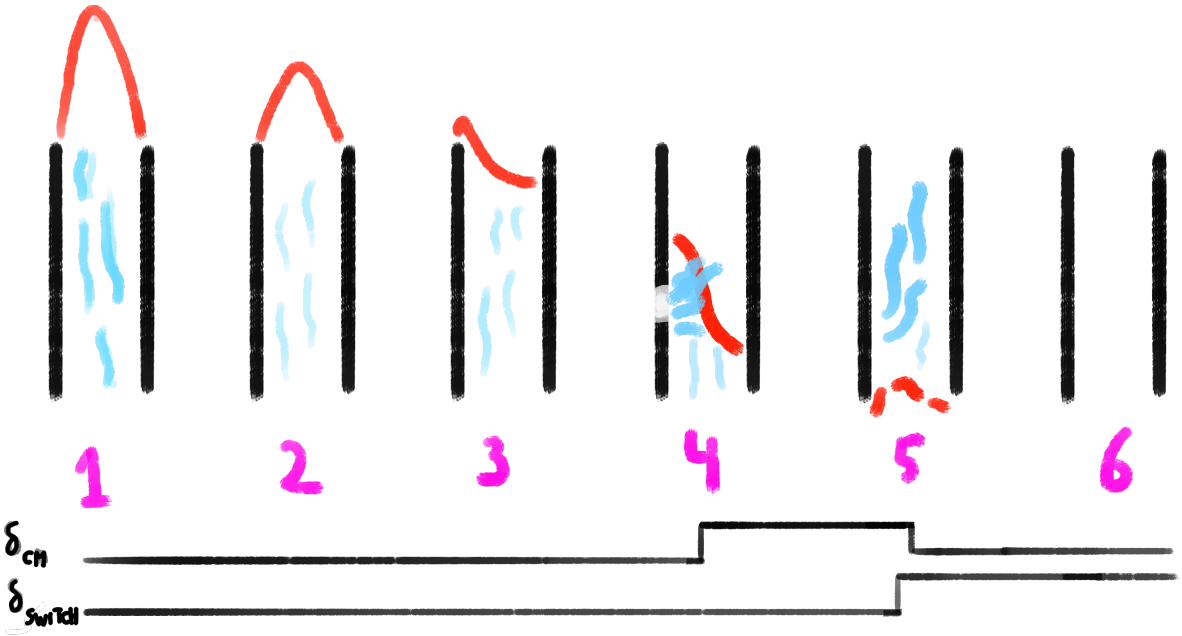

Figure 6-17: Illustration of the working of the the behavior of the safety switch.

system switched off the fuel supply because the Ultraviolet (UV) sensor in the lab detected no longer a flame at the desired location. The natural cooling down rate of the system is determined with this response. A first-order model describes this behavior with an unit step input. The transfer function is given in equation 6-32. Again the model is fitted with the Plant identification of the PID tuner from the Control Systems Toolbox in MATLAB.

$$G_{safety} = \frac{K_6}{s + K_7} = \frac{-1.536}{s - 0.9855} \tag{6-32}$$

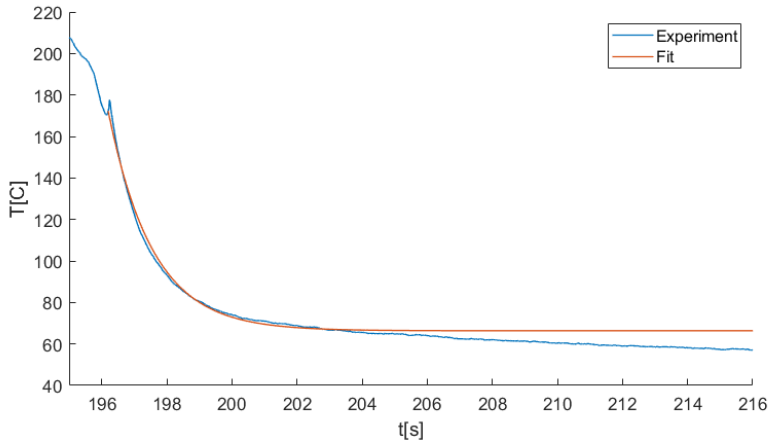

Figure 6-18: Safety switch modeled by first order model based on experimental data of extinguished flame. In this experiment, the fuel supply was shut off after 196 seconds. Zoomed in version of Figure 6-12.

6-5-2 Simulation

To test the virtual performance of the safety switch, the change is added to the simulation that the counteraction do not succeed $\delta_{succes} = 0$. The exact success-rate of the designed system is not known. Therefore, the assumption is made that one out of three counteractions fails. Based on the experiment in Figure 6-14a, the residence time of the flame in the tube is in the order of one to three seconds. Therefore, the allowable time between the peaks is set to $\Delta t_{peak} < \Delta t_{lim} = 3s$.

In Figure 6-20, the simulation result is shown. The first two flashback events are counteracted successfully, but the third counteraction failed. According to Figure 6-20, the event was detected. However, the flame was not pushed back on top of the rim within the time Δt_{peak}. Therefore, the supervisory system enabled the safety switch to blow the flame off, as a result the systems cools down to ambient temperatures. The gain is compensated by a factor 0.25 to converge to this temperature. At the point the flame blew off, a nod is slightly visible in the data. A restart of the burner is required to continue operating. Nevertheless, two flashback events has been counteracted, so the simulation showed the enlarged operation time of the burner.

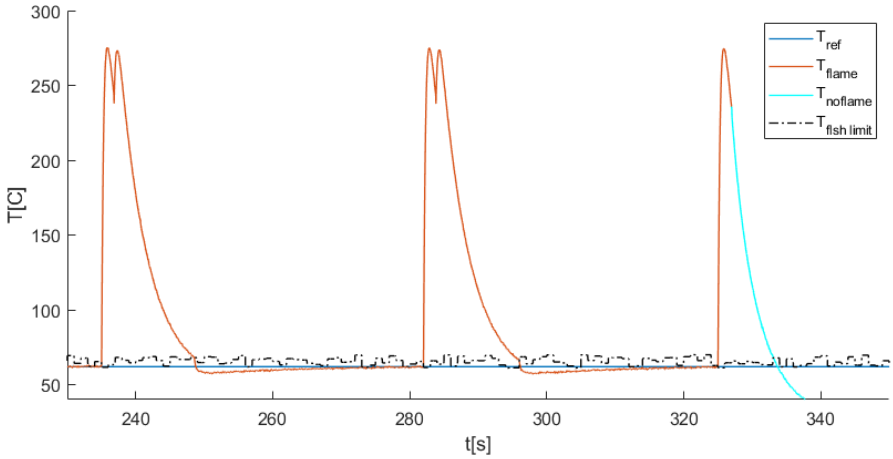

Figure 6-19: Simulation of the burner operating. Two flashbacks are successfully counteracted, but the third is not, so the safety switch is activated and turned of the flame.

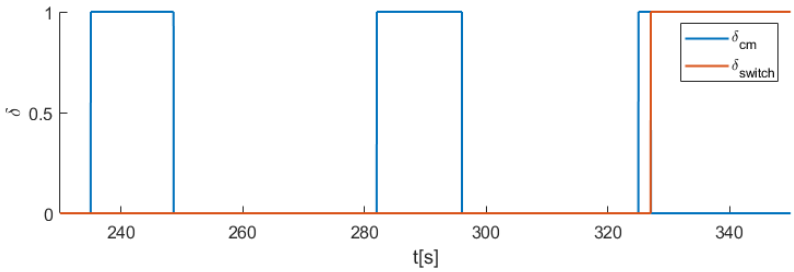

Figure 6-20: Simulation output of the controller variables. Two flashbacks are successfully counteracted. The counteraction δ_{cm} is deactivated after convergence. However, the third event is not successfully counteracted, so the safety switch δ_{safety} is activated to blow out the flame.

6-6 Supervisor

The behavior of all the subsystems of the proposed controller framework are explained and defined in the previous sections. The supervisor does the detection and decisions for which controller task should be applied based on the measured temperature output. Both the dynamics of the burner and the controller framework are switching. The burner switches between flashback, non-flashback conditions and cooling down dynamics. The controller switches between the three controller tasks. A hybrid automaton provides a general framework for the specification and algorithmic analysis of switching systems [81]. It is a finite-state machine with continues variables, evolving according to their dynamical laws. The discrete and continues nature of the system dynamics are combined. This model is used to describe the behavior of the designed fault-tolerant control framework.

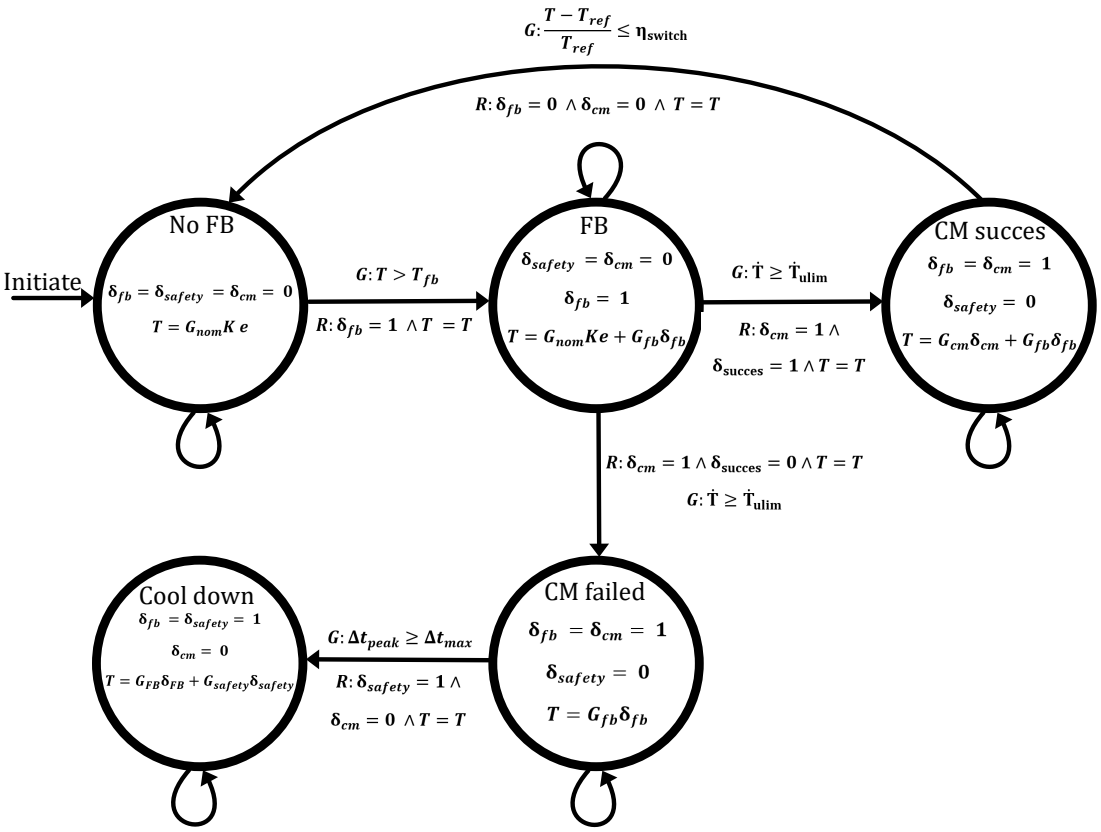

Figure 6-21: Hybrid automaton of the switching system.

The switching system

Using the hybrid automaton in Figure 6-21, the switching behavior of the system is explained. The system is initiated in the non-flashback state. The prevention controller keeps the temperature at the desired T_{ref}. The gatekeeper decides when a system may switch to another

state is denoted by G, accompanied by a state reset, denoted by R. If the output temperature T exceeds the critical flashback limit T_{fb}, the system will switch to the flashback state. Here, the dynamics of flashback are added as a disturbance to the temperature output. During the switch, the flashback variable is set to $\delta_{fb} = 1$, and the temperature state is reset to the last value of the non-flashback temperature state to remove discontinues. The supervisor detects flashback if the trend checking exceeds the limit $\dot{T}_{ulim}$. The counteraction system is activated $\delta_{cm} = 1$. The random variable δ_{succes} determines the success rate of the counteraction. If this is the case $\delta_{succes=1}$, the counteraction dynamics pushes the flame back to the unconfined configuration. When the temperature is within a specific bound of the reference, the supervisor decides to switch back to the prevention controller to follow the reference temperature. The states of the controllers are reset. However, if the counteraction has failed $\delta_{succes} = 0$, the supervisor will activate the safety switch $\delta_{safety} = 1$ to switch off the system, so the temperature cools down to ambient conditions. The safety switch is activated if no flame passes the thermocouple within Δt_{max} time after the flashback occurred.

Chapter 7

Conclusion

Hydrogen is a promising fuel for both reducing greenhouse gas emissions and being used as an energy carrier for renewable energy sources. The adaption of hydrogen instead of natural gas as a fuel in gas turbine combustors introduces additional challenges regarding flame stability. One instabilities is boundary layer flashback. This phenomenon occurs if the flame speed exceeds the local flow velocity. Then the flame can propagate upstream, which can result in equipment failure. Lean premixed hydrogen mixtures are more prone to boundary layer flashback because hydrogen flames have both a smaller quenching distance and higher flame speed compared to natural gas. Therefore, operating at 100% hydrogen fuel content is an enormous challenge. Therefore, a fault-tolerant control framework has been proposed to actively control the prevention of boundary layer flashback in unconfined Bunsen burners.

Flashback is a stochastic process, where the unconfined flame abruptly enters the burner tube. The change of flashback increases as the Reynolds number of the flow is reduced. This might have two causes related to the increase in Reynolds stresses. Firstly, at lower flow velocities, the flame front becomes unstable as the thermal-diffusive instabilities have more time to develop. Less high velocity streaks are present to push the flame back and the flame has more time to burn its way towards the tube. Secondly, the flame angle increases. This results in higher accelerations across the flame front and hence increase in Reynolds stresses. Both the increase in flame fluctuations and reduction in flame angle are reasonable as indicators for a flame moving towards flashback.

However, the complex nature of a flame makes it challenging to measure these effect in a flame. Four types of sensors are investigated in their ability to detect flashback and find precursors in the data, indicating the onset of flashback. Each investigated sensor type uses a different physical mechanisms of the flame.

- The ion sensor uses the presence of free ions in the combustion reaction to measure the flame front. The flame's upstream movement along the sensor was detected, but since no intermittent flashback event were present, no precursor indicating the onset has been found.
- The microphone measures the pressure fluctuations produced by the flow and the flame. The noise produced during a flashback event is visible in the data. The sound of the flame is difficult to distinguish from the flow. Towards flashback, the power of the signal reduces as the lowered velocity of the flow produces less noise. No precursors are found, announcing the onset of flashback.
- The photo-detector detects the light spectrum emitted by the flame. Using a single binary IR sensor, only detects the presence of a flame. This is not useful for finding precursors, but it is appropriate for a secondary sensor to verify the existence of a flame at the burner rim.

- The thermocouples measure the flame temperature. The flashback and non-flashback case are simple to distinguish as a peak is present in the data. The temperature is a precursor for the onset of flashback since the temperature increases with increasing flame angle. Also, by placing multiple thermocouples in 360^oC configuration on the burner rim, it is possible to estimate the position, where the flame entered the burner.

Of the investigated sensors, the thermocouple is the most promising sensor for both flashback detection and use the temperature signal as a control variable. It is used to detect flashback and activate the counteraction system.

A proof-of-concept has been designed for a method to counteract flashback. The stochastic nature of flashback always introduces the potential risk of flashback. Although prevention is better than cure, a counteraction method is required to extend the operational time after the occurrence of flashback. In conventional burners, the fuel supply is shut off in the case of flashback detection. This blows off the flame and requires restart. For the detection of flashback, the temperature data is combined with a trend checking algorithm. Different options are possible to interact with the flame and flow either by decreasing flame speed, increasing flow speed and local flame blow-off. A proof-of-concept build for the injection of air close to the burner rim to both dilute the boundary layer and increase the flow speed. Despite the difficulty to oppose a flashback event, the design of the injector system proved the concept of using active measures to counteract flashback as it was possible to push flame back on top of burner rim. More design iterations and tests are required to get a properly working and reliable setup. This counteraction strategy can be implemented in the fault tolerant control framework to deal with flashback events in operation domains with high flashback propensities

The actuator and sensors are integrated in the fault tolerant control framework. This framework increases the flashback resistance of the system and it counteracts possible flashback events, which is considered as a fault in the system. A supervisor block has two functions. Firstly, the supervisor uses a fault detection method, known as trend checking, to detect flashback. Secondly, it decides which strategy should be applied, based on the temperature measurements. The fault-tolerant control strategy is threefold:

- Prevention controller: A non-flashback burner model has been identified for temperature control. By closing the loop, the prevention controller is able to track a desired temperature reference and reject disturbances, which normally steers the temperature towards flashback conditions. Thereby, this controller keeps the system in a stable domain. Different tuning methodologies based on the traditional PI, LQI, and PPR are explored for this purpose. The robustness of the proposed controller was verified through loop shaping interpretation. The PPR tuning resulted in the most appropriate controller dynamics, so these gains are used in the controller.
- Counteraction: After the detection of flashback by the supervisor, the counteraction system should be activated to counter act the upstream flame propagation. To continue the burner operation, the flame is pushed back in the unconfined configuration. The counteraction model has been identified together with a measure for the probability of flashback occurrence.
- Safety switch: Since not all counteractions are successful, the safety switch operates as a last resort. If the flame is not stabilized within a specific time frame, the fuel supply is switched off to fail safe.

The proposed fault tolerant control framework is intended to increases the flashback resistance of the system by being more robust towards disturbances and flashback events that would normally require a restart of the system. Its potential to do so has been confirmed by simulations. However, further research is still required to run burners on 100% hydrogen without flashback.

Recommendations and future developments

1. **Implementing** the framework in practise. The next step is to build the controller and implement it in the setup to test its performance and capabilities in a real world environment. The performance can be evaluated for different fuel (not just natural gas), equivalence ratio and Reynolds compositions.

2. **Improving** the design of the injector system to boost the success rate of the active counteraction system. A proposal has already been made to guide the injected air flow upwards by placing a ramp in the burner.

3. **Extending** the identification for different fuel, equivalence ratio and Reynolds compositions. The prevention controller may experience performance degradation as parameters vary. Therefore, gain scheduling can be a solution.

4. **Investigating** flashback indicators for there capability to predict flashback in more depth. More information about the flame angle and flame front fluctuations might be found in video images of the flame front captured with a high resolution camera. This requires offline and more advanced analyzing tools.

5. **Controlling** the confined flame configuration. For unconfined flames the onset of flashback is difficult to predict as there is no direct relation between flow and flame. A better control problem would be controlling the flame height in a confined flame configuration. In the tube, there is a stronger coupling between flame and flow, and the flame location in the tube is a clearer system state.

Appendix A

The experimental setup

In this chapter the experimental setup is explained, located in the combustion lab at the TU Delft. It is used to test the multiple sensors and actuators. The setup consists of the main burner tube with an interchangeable piece of copper tube in the last section, such that different sensor and/or actuator configurations could be easily tested.

Main setup of the experiment

A schematic overview of the setup is shown in Figure A-1. The dimensions are given in Table A-2. The main setup was used before in other master thesis projects of Faldella [7], Lambers [37] and Willems [13]. The fuels (natural gas and hydrogen) and oxidizer (air) were line supplied. The specifications of the supply line can be seen in Table A-1. The flow of the gasses was controlled by three mass flow controllers. A Labview control panel was used to interact with mass flow controllers. The fuel mixture and oxidizer were mixed upstream, which flowed through the burner and was ignited at the burner exit. The exit of the main burner was a simple copper tube with an outer diameter $d_o = 28mm$. Since different sensor and actuator configurations were tested, a removable copper tube connected via a compression fitting was installed on top of the main setup. In the next section the interchangeable setups are explained.

Gas	Max throughput $[L(min)^{-1}]$	Line pressure $[bar]$
Air	1000	6
Natural gas	100	2
Hydrogen	250	5

Table A-1: Specifications of fuel and oxidizer supply

	Corner	Horizontal tube	Vertical tube	End tube
Internal tube diameter d_i (mm)		25.0	25.67	25.67
Wall thickness tube t_h (mm)		2.0	1.1	1.1
Length l (mm)		2300	1000	20 to 30
Radius of curvature r_c (mm)	85			
Material	PVC	Copper	Copper	Copper

Table A-2: Specification of the setup

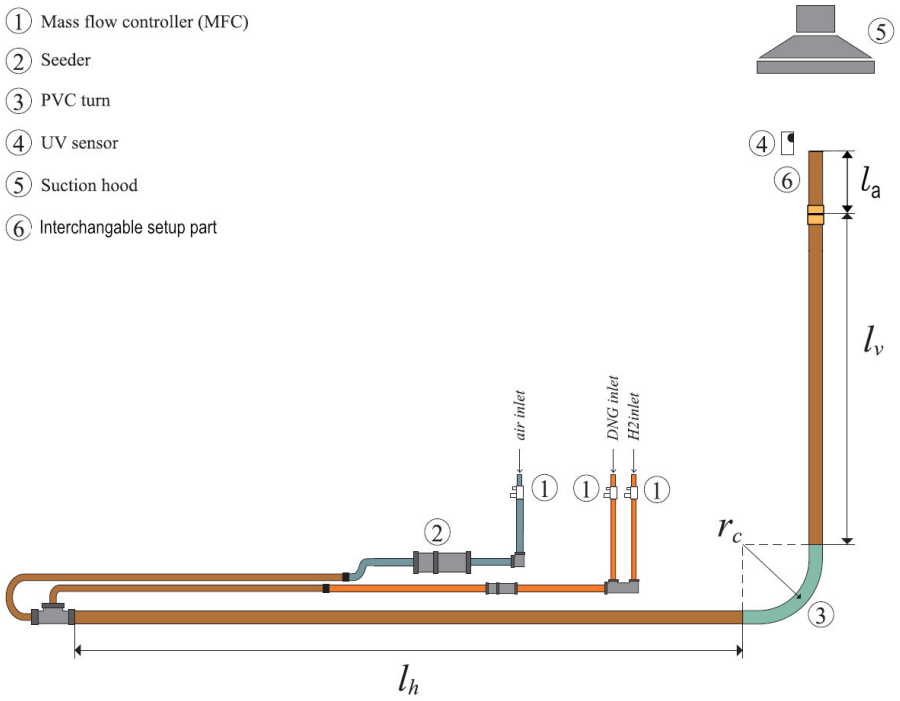

Figure A-1: Schematic view of the burner setup in the experimental facility. Modified image of Faldella [7]

Interchangeable setups

The main setup explained in the previous section was expanded with different additional tubes to conduct experiments with different sensors and actuator configurations. During the entire duration of this master thesis, five different setups were manufactured. These tubes were connected to the main setup via a compression fitting. All the setups were made of copper tubes with an outer diameter of 28 mm. In this section, the sensors and their mounting location are explained in more detail.

Setup S1

The first generation setup was built to accommodate the ion sensor on top of the copper tube. The ion sensor was build from a drilled out compression fitting and was clamped on top of a piece of copper tube, which could be connected to the main setup. The cathode was attached to a body ring and the anode was attached to the copper tube. To electrical insulate the two metals from each other a single sheet of the mineral Mica.

At 45 mm distance from the top of the copper tube a small 15 mm diameter tube was hard soldered at right angle to the copper tube. It was used to mount different pressure sensors. One of the pressure sensors was a Validyne pressure transducer model DP103-12, which has a pressure range of 140 Pa. It was connected via a flexible tube to the setup. The other pressure sensor was a microphone, the Sonion microphone 8040, which was put into use together with a infinity tube. This setup is shown in Figure A-2a. The infinity tube is connected to the

small copper tube of the setup with flexible tubes and the microphone was aligned in front of hole of the infinity tube. The infinity tube had a length of more than one meter.

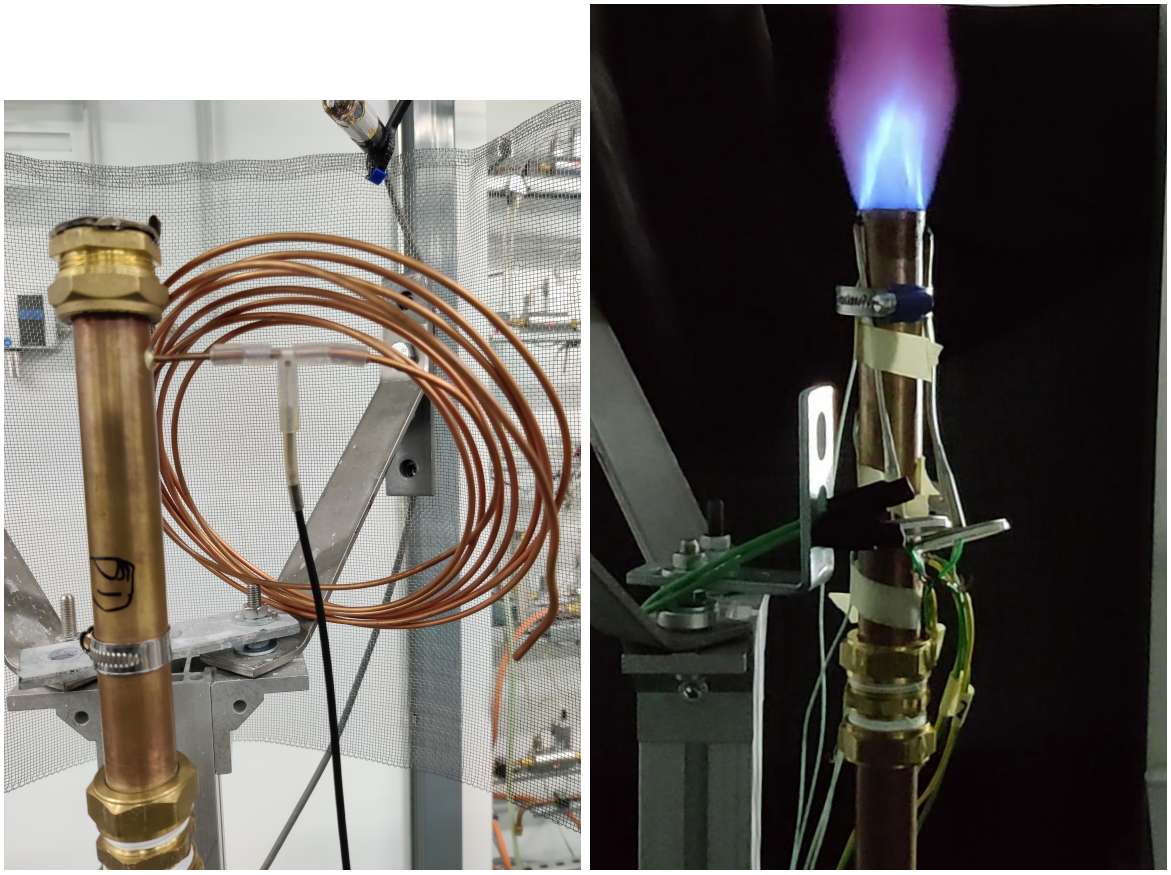

(a) Setup S1 with microphone connected together with an infinity coil to the setup and ion sensor mounted on top of the burner.

(b) Setup S2 with four thermocouples in 360^o degree configuration.

Figure A-2: The first iteration and the second iteration of the setup.

Setup S2

The second iteration of the setup was build to test different thermocouple configurations. There are multiple types of thermocouples, which differ in material composition, sensitivity and temperature range. For this experiment, the K-type is used, which is a combination of Chromel and Alumel and has a wide temperature range (-270^oC to 1260^oC) and is reliable and accurate [56]. By using multiple thermocouples a better estimate of the flame's (flashback) location can be made. The thermocouples can be aligned in different configurations:

- By placing the thermocouples as a liner into the tube the position of the upstream propagating flame can be determined. By interpolating the data the current location of the flame can be estimated.
- By placing thermocouples in a 360^oC configuration around the burner rim, the effect of the wiggling flame can be detected. If the flame tip moves from one side to another,

one sensor will cool down as the other will heat up. Furthermore, the flashback location can be detected since at this location the sensor heats up first

In this design both configurations are applied. There are four thermocouples placed at 90^o degrees from each other at 5 mm from the top of the rim. Furthermore, thermocouples are placed in the liner for estimating the position of the confined flame after flashback. There are four thermocouples placed at 10, 30,90 and 150 mm from the rim respectively. The setup S2 is shown in Figure A-2b.

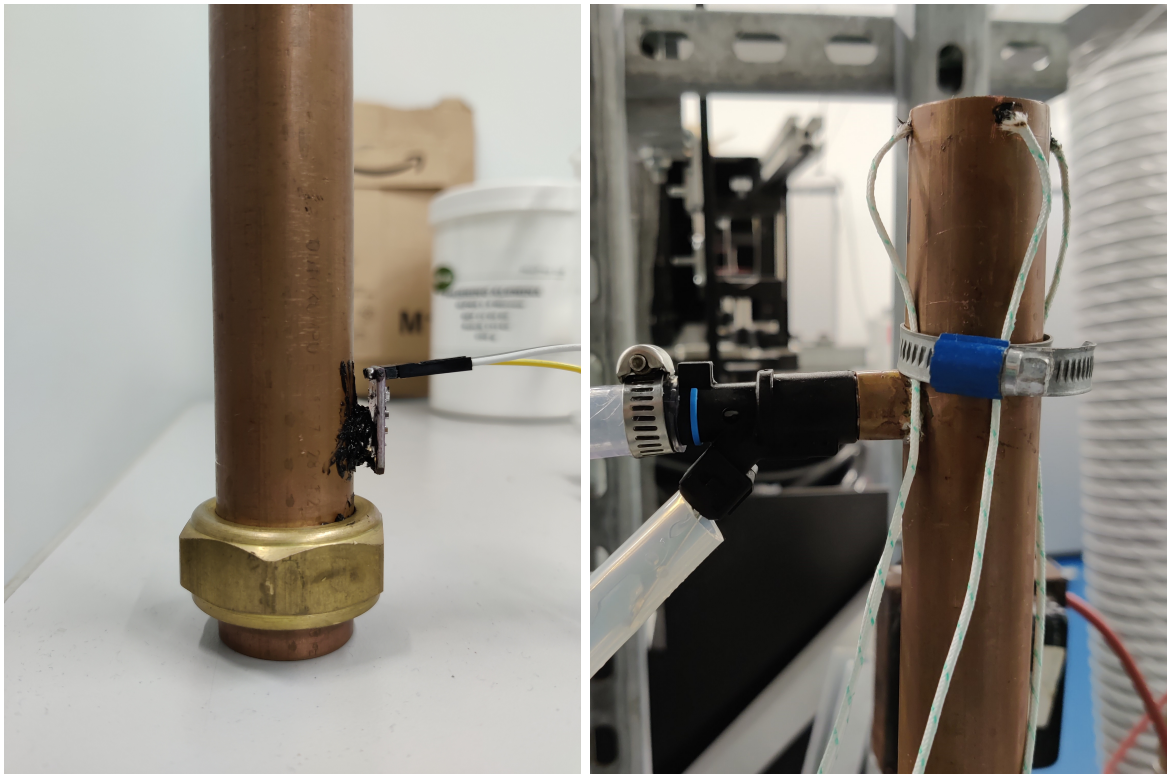

(a) Setup S3 with connections for an electret microphone and four thermocouples in 360^oC configuration.

(b) Setup S4 with connections four the injector and four thermocouples in 360^oC configuration.

Figure A-3: The third iteration and fourth iteration of the setup.

Setup S3

In the third iteration of the setup the findings from the previous setups are applied to improve the design. The thermocouples in the 360^o configuration were moved closer to the rim. They are placed at 2 mm measured from the top of the rim to sense the flame better. Also, the holes of the thermocouples should be as small as possible and sealed to prevent air leakage. The additional air makes the fuel mixture locally leaner. The tip of the thermocouples should stick out as little as possible because both the flow can be disturbed, and the flame can hatch to the thermocouple instead of the rim. The liner configuration was not investigated further because the main interest in this research is to keep the flame on top of the rim. Next to the improved thermocouple configuration, an electric condenser microphone was tested. This microphone has a fixed plate and a vibrating plate. This moving plate vibrates due to the

sound waves, generating the sensor output. The microphone was integrated in an MAX4466 Arduino board. The microphone is mounted in a 9 mm hard soldered tube connected at right angle of the burner tube at 170 mm from the top. The setup S3 is shown in Figure A-3a.

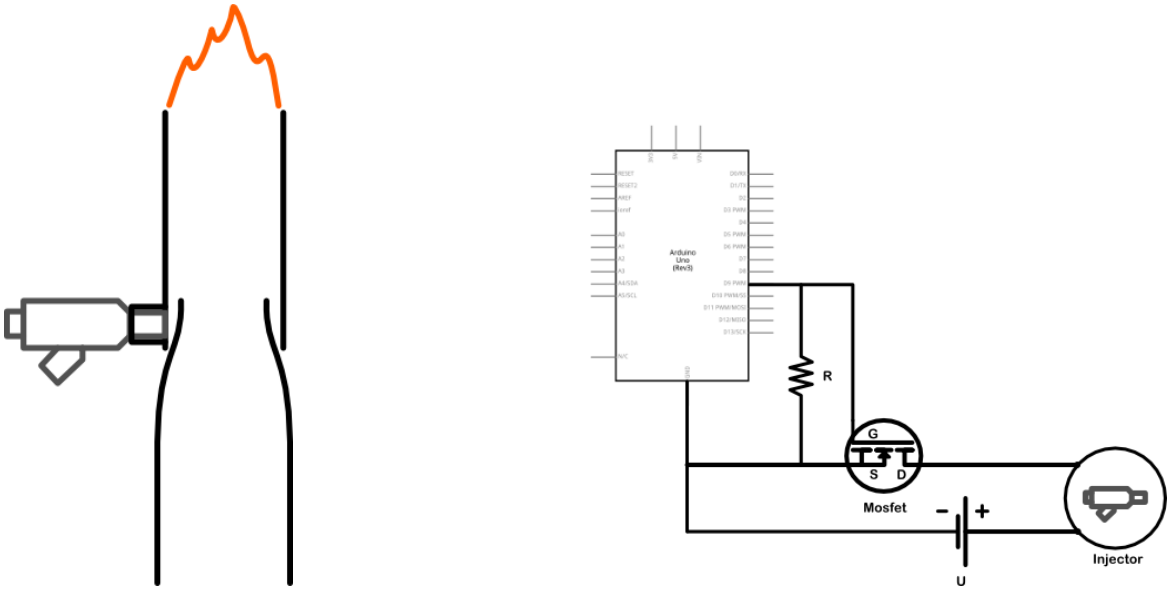

(a) Cross-section of the improved injector system.

(b) Electric circuit for operating the injector, where R is a resistance and U is the power supply

Figure A-4: Injector system configuration

Setup S4

In the fourth iteration, the goal was to close the loop and build a system to test the-proof-of-concept by counteracting a flashback event. The same 360^o thermocouple configuration was used as in the previous setup. Injection of pressurized air was tested for the capability to counteract the effect of flashback. For injection, the fuel injector 1984EO for a Peugot 206, was used. Normally, this injector is used in a combustion engine to inject fuel in the air manifold before the intake valve. The injector can handle pressures up to 5 bar. The injector was mounted via a hard soldered mount at right angle of the main burner tube. The pressurized air was supplied via polymer tube and the solenoid valve in the injector was activated via a 12 V signal. The setup S4 is shown in Figure A-3b.

The valve of the actuator is controlled by a solenoid. When it is energized, the nozzle will open and let air through [82]. The solenoid in the actuator is controlled by a Arduino board. The electric circuit for controlling the injector is shown in Figure A-4b. The Arduino board communicates via a serial connection with the main computer. The supervisor runs at the main computer and decides on the activation of the counteraction system, explained in more detail in Chapter 6. When the counteraction is activated, the Arduino board is requested to output a 5 volt signal. This signal controls the guard terminal of the field-effect transistor. The guard terminal decides on the conductivity between the drain and source terminal to close the gate of the 12 volt circuit. This higher voltage circuit is connected with the solenoid. When a current flows through the solenoid, the magnetic force moves the needle in the core

of the injector and the nozzle is opened to blow air in the burner tube. The amount of air injected depends on the time it is energized and on the pressure of the supply line, so these are the control variables of the injector.

Setup S5

For the fifth generation, the injector system was optimized. In Figure A-4a an illustration of the new injector setup cross-section is shown. The injector is mounted perpendicular to the burner tube as it is the easiest to solder it against the tube. To generate a flow that can push a flame back to the rim the air flow from the injector should be guided upwards along the entire wall. Therefore, an additional ramp is installed by putting a narrowing tube inside the burner. If the air from the injector is pushed against this form, it will be guided upwards along the wall. The disadvantage is that the incoming flow is disturbed, so this can have a negative effect on the flashback resistance of the burner.

Data acquisition

DATAQ

For the data acquisition, the DATAQ instruments DI-2008 was used, which can acquire thermocouple and voltage data. It has a sampling rate of 2000 Hz for single channel and up to 200 Hz combined sampling rate for multiple channel measurements [83].

Arduino

The measurements of the electric condenser microphone were sampled with an Arduino Uno board. Furthermore, it was used to control the injector system by generating a control signal if flashback was detected.

Labview

The mass flow controllers communicated with Labview, which controlled the amount of fuel and air flowing through the system. In the control panel the operator could set the desired equivalence ratio, hydrogen content and Reynolds of the flow. The control panel determined the right parameters for the mass flow controllers based on the set ambient conditions in the lab. Furthermore, the flow data of an experiment could be saved with 6 Hz sampling rate.

Appendix B

Simulink model

To simulate the behavior of the designed flashback resistant system, the fault-tolerant control framework shown in Figure 6-2 is implemented in Simulink [74]. The overview of the model is shown in Figure B-1. The red blocks indicate the subsystems related to the controllers which includes the supervisor, prevention controller, counteraction activation, and safety switch. The blue blocks indicate the subsystems related to the burner which include the burner system and flashback activation.

The Simulink code and supporting Matlab files developed in this work can be found under https://github.com/Fedor1997/MscThesis-Boundary-layer-flashback-by-active-control with the description *Masters' thesis Simulink model of a fault-tolerant control framework to counteract flashback*

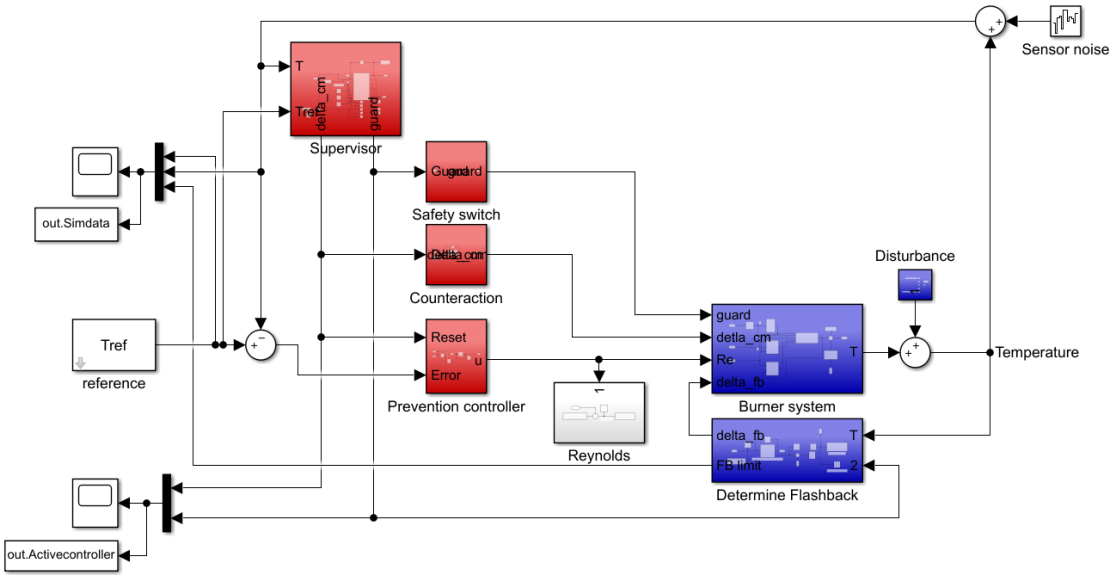

Figure B-1: Overview of the Simulink model

Bibliography

[1] L. Capuano, "International energy outlook 2020," october 2020. https://www.eia.gov/outlooks/ieo/pdf/ieo2020.pdf; accesed at 31-1-2021.

[2] P. Fairley, "The h2 solution," *Scientific American*, vol. 322, no. 2, pp. 36–43, 2020.

[3] D. Dunn-Rankin, *Lean Combustion*. Elsevier, 2008. https://linkinghub.elsevier.com/retrieve/pii/B9780123706195X50018.

[4] M. Blanke, M. Kinnaert, J. Lunze, M. Staroswiecki, and J. Schröder, *Diagnosis and Fault-Tolerant Control*. Springer-Verlag, 2006.

[5] N. Peters, "Turbulent combustion," 2000.

[6] K. E. Son, "Reduction of the complete system of chemical kinetics equations for multicomponent high temperature gas flows based on the partial local equilibrium method," *High Temperature*, vol. 58, pp. 83–91, Jan. 2020. https://doi.org/10.1134/s0018151x20010198.

[7] F. Faldella, *Experimental investigation of boundary layer flashback in high H2 concentration turbulent premixed jet flames*. Thesis, TU Delft, 2020.

[8] A. Kalantari and V. McDonell, "Boundary layer flashback of non-swirling premixed flames: Mechanisms, fundamental research, and recent advances," *Progress in Energy and Combustion Science*, vol. 61, pp. 249–292, 2017. http://www.sciencedirect.com/science/article/pii/S0360128516301253.

[9] C. Eichler and T. Sattelmayer, "Premixed flame flashback in wall boundary layers studied by long-distance micro-piv," *Experiments in Fluids*, vol. 52, no. 2, pp. 347–360, 2012. http://link.springer.com/10.1007/s00348-011-1226-8.

[10] C. Eichler, *Flame flashback in wall boundary layer of premixed combustion systems*. Phd, TU München, 2011.

[11] V. Hoferichter, C. Hirsch, and T. Sattelmayer, "Analytic prediction of unconfined boundary layer flashback limits in premixed hydrogen–air flames," *Combustion Theory and Modelling*, vol. 21, no. 3, pp. 382–418, 2017. https://doi.org/10.1080/13647830.2016.1240832.

[12] C. E. Schneider and A. M. Steinberg, "Statistics and dynamics of intermittent boundary layer flashback in swirl flames," *Journal of Propulsion and Power*, vol. 36, no. 6, pp. 940–949, 2020. https://www.scopus.com/inward/record.uri?eid=2-s2.0-85095123433&doi=10.2514%2f1.B37815&partnerID=40&md5=35032be31f284a848392ee60fde58c94.

[13] G. Willems, *Visualizing boundary layer flashback of turbulent premixed hydrogen/natural gas/air flames through quartz glass Bunsen burner using PIV*. Thesis, TU Delft, 2022.

[14] M.christman, *Taking the pulse of combustion*. IMI Sensors, New York, 2021.

[15] R. Schefer, W. Kulatilaka, B. Patterson, and T. Settersten, "Visible emission of hydrogen flames," *Combustion and Flame*, vol. 156, pp. 1234–1241, June 2009.

[16] K. Zhou and J. C. Doyle, *Essentials of robust control*. Upper Saddle River, NJ: Pearson, Sept. 1997.

[17] V. Masson-Delmotte, P. Zhai, A. Pirani, S. Connors, C. Péan, S. Berger, N. Caud, Y. Chen, L. Goldfarb, M. Gomis, M. Huang, K. Leitzell, E. Lonnoy, J. Matthews, T. Maycock, T. Waterfield, O. Yelekçi, R. Yu, , and B. Z. (eds.), *Climate Change 2021: The Physical Science Basis. Contribution of Working Group I to the Sixth Assessment Report of the Intergovernmental Panel on Climate Change*. Cambridge University Press, 2021.

[18] WMO, *2020 was one of three warmest years on record*. World Meteorological Organization, Jan 2021. https://public.wmo.int/en/media/press-release/2020-was-one-of-three-warmest-years-record;accessedat31-1-2021.

[19] United Nations, *Paris Agreement*. United Nations, 2016. https://treaties.un.org/doc/Treaties/2016/02/20160215%2006-03%20PM/Ch_XXVII-7-d.pdf.

[20] The European Commission, *A Clean Planet for all A European strategic long-term vision for a prosperous, modern, competitive and climate neutral economy*. The European Commission, 2018. https://eur-lex.europa.eu/legal-content/EN/TXT/PDF/?uri=CELEX:52018DC0773&from=NL.

[21] EUTurbines, *The gas turbine industry's commitments to drive the transition to renewable-gas power generation*. www.powertheeu.eu, 2019.

[22] IEA, "Technology perspectives 2017," in *Technology Perspectives 2017*, 2017.

[23] G. F. M. De Souza, ed., *Thermal Power Plant Performance Analysis*. Springer series in reliability engineering, London, England: Springer, 2012 ed., Jan. 2012.

[24] A. C. Benim and K. J. Syed, *Flashback Mechanisms in Lean Premixed Gas Turbine Combustion*. Elsevier, 2015. https://linkinghub.elsevier.com/retrieve/pii/C20130188472.

[25] J. Goldmeer, "Power to gas: Hydrogen for power generation," in *Power to gas: Hydrogen for power generation*, General Electric Company, 2019.

[26] V. Hoferichter, *Boundary layer flashback in premixed combustion systems*. Thesis, TU München, 2017.

[27] ETN, *The path towards a zero-carbon gas turbine*. ETN Global, 2020.

[28] R. Dennis, *The Gas Turbine Handbook*. U.S. Department of Energy, 2006. https://netl.doe.gov/carbon-management/turbines/handbook; accesed at 27-7-2022.

[29] R. Isermann, "Supervision and fault management of processes — tasks and terminology," in *Fault-Diagnosis Systems*, pp. 13–30, Springer Berlin Heidelberg, 2006. https://doi.org/10.1007/3-540-30368-5_2.

[30] M. Kalantari, "Flashback propensity of turbulent hydrogen-air jet flames at gas trubine conditions," *Journal of Engineering for Gas Turbines and Power*, 2016.

[31] C. K. Law, *Combustion Physics*. Cambridge University Press, 2006.

[32] P. Kundu, I. Cohen, and D. Dowling, *Fluid Mechanics*. Elsevier, 2016. https://doi.org/10.1016/c2012-0-00611-4.

[33] S. B. Pope, "Turbulent premixed flames," *Annual Review of Fluid Mechanics*, vol. 19, pp. 237–270, Jan. 1987.

[34] I. Glassman, R. A. Yetter, and N. G. Glumac, *Combustion*. Academic press, 2014.

[35] C. Eichler, G. Baumgartner, and T. Sattelmayer, "Experimental investigation of turbulent boundary layer flashback limits for premixed hydrogen-air flames confined in ducts," *Journal of Engineering for Gas Turbines and Power*, vol. 134, no. 1, 2011. https://doi.org/10.1115/1.4004149.

[36] G. Baumgartner, L. R. Boeck, and T. Sattelmayer, "Experimental investigation of the transition mechanism from stable flame to flashback in a generic premixed combustion system with high-speed micro-particle image velocimetry and micro-plif combined with chemiluminescence imaging," *Journal of Engineering for Gas Turbines and Power*, vol. 138, no. 2, 2016. https://doi.org/10.1115/1.4031227.

[37] T. Lambers, *Boundary layer flashback of turbulent premixed hydrogen/DNG/air flames produced by a Bunsen burner*. Thesis, TU Delft, 2021.

[38] B. Lewis and G. von Elbe, "Stability and structure of burner flames," *The Journal of Chemical Physics*, vol. 11, no. 2, pp. 75–97, 1943.

[39] G. L. Dugger, "Flame stability of preheated propane-air mixtures," *Industrial and Engineering Chemistry*, vol. 47, no. 1, pp. 109–114, 1955. https://doi.org/10.1021/ie50541a038.

[40] T. C. Lieuwen, *Unsteady Combustor Physics*. Cambridge University Press, 2012. https://doi.org/10.1017/cbo9781139059961.

[41] A. Gruber, J. H. Chen, D. Valiev, and C. K. Law, "Direct numerical simulation of premixed flame boundary layer flashback in turbulent channel flow," *Journal of Fluid Mechanics*, vol. 709, pp. 516–542, 2012.

[42] V. Hoferichter, C. Hirsch, and T. Sattelmayer, "Prediction of confined flame flashback limits using boundary layer separation theory," in *ASME Turbo Expo 2016: Turbomachinery Technical Conference and Exposition*, vol. Volume 4A: Combustion, Fuels and Emissions, (V04AT04A006), 2016. https://doi.org/10.1115/GT2016-56155.

[43] B. S. Stratford, "The prediction of separation of the turbulent boundary layer," *Journal of Fluid Mechanics*, vol. 5, no. 1, p. 1–16, 1959.

[44] Helmenstine, A.M., "Is fire a gas, liquid or solid?," 2020. https://www.thoughtco.com/what-state-of-matter-is-fire-604300,Accessed: 2021-12-06.

[45] T. Addabbo, A. Fort, M. Mugnaini, L. Parri, V. Vignoli, M. Allegorico, M. Ruggiero, and S. Cioncolini, "Ion sensor-based measurement systems: Application to combustion monitoring in gas turbines," *IEEE Transactions on Instrumentation and Measurement*, vol. 69, no. 4, pp. 1474–1483, 2020.

[46] N. Docquier and S. Candel, "Combustion control and sensors: a review," *Progress in Energy and Combustion Science*, vol. 28, no. 2, pp. 107–150, 2002. https://www.sciencedirect.com/science/article/pii/S0360128501000090.

[47] H. Calcote, "Mechanism for the formation of ion in flames," *Combustion and Flame*, vol. 1, pp. 385–403, 1957.

[48] "Flame sensing - the basics." https://www.hvacrschool.com/flame-sensing-the-basics/. accessed at 1-3-2021.

[49] J.D. Thornton and D.L. Straub, "A combustion control and diagnostics sensor for gas turbines," in *Proceedings of ASME Turbo Expo 2004*, 2004.

[50] J. D. Thornton, G. A. Richards, D. L. Straub, E. A. Liese, J. L. Trader Jr, and G. E. Fasching, "Flashback detection sensor for lean premix fuel nozzles," 2002. US Patent 6,429,020.

[51] K. Benson, J. D. Thornton, D. L. Straub, E. D. Huckaby, and G. A. Richards, "Flame ionization sensor integrated into a gas turbine fuel nozzle," *Journal of Engineering for Gas Turbines and Power*, vol. 127, pp. 42–48, Jan. 2005. https://doi.org/10.1115/1.1788686.

[52] W. K. Cheng, T. Summers, and N. Collings, "The fast-response flame ionization detector," *Progress in Energy and Combustion Science*, vol. 24, no. 2, pp. 89–124, 1998. https://www.sciencedirect.com/science/article/pii/S0360128597000257.

[53] L.L. Ongkiehong, "The hydrogen flame ionization detector," 1960. https://research.tue.nl/en/publications/the-hydrogen-flame-ionization-detector(816da299-8671-4e63-b656-bb8b128966a9).html.

[54] T. Holm, "Aspects of the mechanism of the flame ionization detector," *Journal of Chromatography A*, vol. 842, no. 1, pp. 221–227, 1999. https://www.sciencedirect.com/science/article/pii/S0021967398007067.

[55] "Novamica thermex." https://eriks.nl/dam/nl/downloads-eriks-nl/productdatasheets/flensafdichtingen/grafiet-flensafdichtingen/Novamica-THERMEX.pdf, 2016. Accessed: 2021-06-01.

[56] R. S. Figliola and D. E. Beasley, "Theory and design for mechanical measurements," *Measurement Science and Technology*, vol. 7, no. 7, 1996. http://dx.doi.org/10.1088/0957-0233/7/7/016.

[57] R. Park, R. Carroll, G. Burns, R. Desmaris, F. Hall, M. Herzkovitz, D. MacKenzie, E. McGuire, R. Reed, L. Sparks, and T. Wang, *Manual on the Use of Thermocouples in Temperature Measurement, Fourth Edition, Sponsored by ASTM Committee E20 on Temperature Measurement.* ASTM International, Jan. 1993.

[58] Omega, "Temperature measurement volume 2." Brochure, 2017. https://www.omega.co.uk/techref/pdf/OMEGA_Thermocouple_Brochure_2017.pdf; accessed at 13-4-2021.

[59] Omega, "Thermocouple response time." https://www.omegaeng.cz/temperature/z/thermocoupleresponsetime.html;accessedat13-4-2021.

[60] AVNET ABACUS, "Types of pressure sensors: A comprehensive overview." https://www.avnet.com/wps/portal/abacus/solutions/technologies/sensors/pressure-sensors/types. accessed at 25-2-2021.

[61] W. C. Strahle, "Combustion noise," *Progress in Energy and Combustion Science*, vol. 4, no. 3, pp. 157–176, 1978.

[62] P. Clavin and E.D. Siggia, "Turbulent premixed flames and sound generation," *Combustion Science and Technology*, vol. 78, no. 1-3, pp. 147–155, 1991. https://doi.org/10.1080/00102209108951745.

[63] R. Rajaram and T. Lieuwen, "Acoustic radiation from turbulent premixed flames," *Journal of Fluid Mechanics*, vol. 637, pp. 357 – 385, 10 2009.

[64] S. Daniele, P. Jansohn, and K. Boulouchos, "Flashback propensity of syngas flames at high pressure: Diagnostic and control," in *ASME Turbo Expo 2010: Power for Land, Sea, and Air*, vol. Volume 2: Combustion, Fuels and Emissions, Parts A and B, pp. 1169–1175, 2010.

[65] MSAsafety, "How to select a flame detector," *MSA Safety*, 2018. http://www.MSAsafety.com/detection.

[66] V. Hoferichter, P. M. Keleshtery, C. Hirsch, T. Sattelmayer, and Y. Matsumura, "Influence of boundary layer air injection on flashback of premixed hydrogen-air flames," in *Proceedings of the ASME Turbo Expo*, vol. 4A-2016, 2016.

[67] Baumgartner, G. and Sattelmayer, T., "Experimental investigation on the effect of boundary layer fluid injection on the flashback propensity of premixed hydrogen-air flames," in *Proceedings of The American Society of Mechanical Engineers Turbo Expo* (ASME, ed.), (San Antonio, TX, USA), ASME, Jun 2013.

[68] B. B. Breaux and S. Acharya, "The effect of elevated water content on swirl-stabilized ethanol/air flames," *Fuel*, vol. 105, pp. 90–102, Mar. 2013.

[69] DARPA, "Instant flame suppression phase ii - acoustic suppression," report, Harvard university, 2013.

[70] DARPA, "Instant flame suppression phase ii - electrostatics," report, Harvard university, 2013.

[71] K. Ogata, *Modern Control Engineering*. Upper Saddle River, NJ: Pearson, 5 ed., Aug. 2009.

[72] L. Ljung, "Black-box models from input-output measurements," vol. 1, pp. 138 – 146 vol.1, 06 2001.

[73] M. Verhaegen, *Filtering and system identification : a least squares approach*. Cambridge: Cambridge University Press, 2007.

[74] MATLAB, *MATLAB R2020a*. Natick, Massachusetts: The MathWorks Inc., 2020.

[75] K. J. Astrom and T. Hagglund, *PID controllers*. Research Triangle Park: ISA, 2 ed., June 1995.

[76] P. C. YOUNG and J. C. WILLEMS, "An approach to the linear multivariable servomechanism problem†," *International Journal of Control*, vol. 15, no. 5, pp. 961–979, 1972.

[77] S. Skogestad and I. Postlethwaite, *Multivariable Feedback Control: Analysis and Design*, vol. 2. JOHN WILEY and SONS, 01 2005.

[78] F. M. Dekking, C. Kraaikamp, H. P. Lopuhaa, and L. E. Meester, *A modern introduction to probability and statistics*. Springer Texts in Statistics, London, England: Springer, 1 ed., May 2005.

[79] F. Ritsma, *Advanced set bounding methods for fault detection*. Thesis, TU Delft, 2019.

[80] D. Miljković, "Fault detection methods: A literature survey.," in *Fault detection methods: A literature survey.*, pp. 750–755, 05 2011.

[81] R. Alur, C. Courcoubetis, N. Halbwachs, T. Henzinger, P.-H. Ho, X. Nicollin, A. Olivero, J. Sifakis, and S. Yovine, *The algorithmic analysis of hybrid systems*, vol. 138. 1995. Hybrid Systems.

[82] A. Muchta, "Understanding fuel injector working principle and diagram." https://www.autoexpose.org/2018/11/fuel-injector-working.html, 2018. Accessed: 01-06-2022.

[83] DATAQ instruments, "Di-2008 thermocouple and voltage data acquisition system." https://www.dataq.com/products/di-2008/. accessed at 8-3-2021.